NASA
Technical
Paper
2627

December 1986

Effects of Winglet on Transonic Flutter Characteristics of a Cantilevered Twin-Engine-Transport Wing Model

Charles L. Ruhlin,
Kumar G. Bhatia,
and K. S. Nagaraja

NASA

NASA Technical Paper 2627

1986

Effects of Winglet on Transonic Flutter Characteristics of a Cantilevered Twin-Engine-Transport Wing Model

Charles L. Ruhlin
Langley Research Center
Hampton, Virginia

Kumar G. Bhatia
and K. S. Nagaraja
Boeing Commercial Airplane Company
Seattle, Washington

National Aeronautics
and Space Administration

Scientific and Technical Information Branch

CONTENTS

SUMMARY

An experimental and analytical study was conducted to determine the effects of a winglet on the transonic flutter characteristics of a cantilevered model representative of a twin-engine-transport wing. Flutter tests were conducted in the Langley Transonic Dynamics Tunnel of a transonic model and a low-speed scaled model of this wing. Ten different transonic-model configurations were tested at Mach numbers up to 0.90. The basic transonic-model configuration variables were wing fuel loading (empty or full) and nacelle pylon stiffness (nominal or reduced). To separate the mass effect from the aerodynamic effect of the winglet, a basic configuration was tested with a nominal wingtip, a winglet (20° cant angle), and a nominal shaped wingtip ballasted to simulate the mass properties of the winglet. Also, a winglet with 0° cant angle was tested in one configuration. The low-speed model was tested to determine the effects of mass-density ratio (i.e., altitude) on subsonic flutter of a winglet-configured wing.

Flutter boundaries were measured for the transonic-model configurations. The addition of the winglet substantially reduced the flutter dynamic pressure of the wing over the transonic region. The winglet effect was configuration-dependent and was primarily due to winglet aerodynamics rather than winglet mass. Changing the winglet cant angle from 20° to 0° had only a slight effect on the transonic flutter characteristics.

Flutter analyses using modified strip-theory aerodynamics (experimentally weighted) were made for correlation with the experimental results. The analysis predicted reasonably well the test results through the transonic regime. The four transonic flutter mechanisms predicted by analysis were obtained in the tests. The analysis satisfactorily predicted the experimental effects of mass-density ratio obtained with the low-speed model, including a change in flutter mode. These correlations indicate that the flutter characteristics of a winglet-configured, twin-engine-transport wing can be satisfactorily predicted by existing conventional analytical methods. Additional flutter analyses were made to examine the flutter sensitivity to several parameters. These parameters included wing chordwise-bending mode frequency, aerodynamic terms, and theoretical doublet-lattice aerodynamics.

INTRODUCTION

The use of wingtip-mounted winglets can significantly improve the aerodynamic efficiency of aircraft by reducing drag at cruise conditions. (See ref. 1.) Winglets are particularly attractive for transport aircraft as fuel savers. (See refs. 2 and 3.) The published results on winglet effects on flutter (refs. 4 through 10) are reviewed in the section entitled "Background." These studies indicate that the addition of winglets to a wing generally causes a reduction in flutter speed, and the amount of the reduction is configuration-dependent. However, the results of two of these studies (refs. 5 and 6) raised concerns regarding the adequacy of conventional flutter analysis to predict the winglet effects on wings carrying pylon-mounted engines.

Therefore, a joint Boeing-NASA research program was undertaken to investigate the flutter aspects of the addition of winglets to a twin-engine-transport wing which

had the engines supported on flexible pylons. This program included (1) an aerodynamic, static-pressure, rigid-model test at transonic speeds, (2) a low-speed flutter-model test in a subsonic wind tunnel, (3) tests of a transonic flutter model and the low-speed flutter model in the Langley Transonic Dynamics Tunnel (TDT), and (4) correlation of flutter test results with analyses. One purpose of the pressure-model test was to provide spanwise distributions of aerodynamic data for use in the flutter analysis. In the flutter-model studies, a large number of configurations and parameters were tested subsonically with the low-speed model, from which a much smaller number of configurations were selected and tested transonically with the transonic model. The results of both model tests were correlated with flutter analyses employing modified strip-theory aerodynamic terms that were weighted by the pressure-model test data.

The low-speed and transonic flutter models were differently scaled versions of the twin-engine-transport wing design. Cantilevered wing flutter models were used because previous analyses and tests indicated that the characteristics of the airplane critical flutter modes were similar to those for the cantilevered wing and that the empennage and fuselage body effects could be accounted for by analysis. To separate the mass effect from the aerodynamic effect of the winglet, each flutter model was tested with three different wingtips: a nominal wingtip, a tip with a winglet, and a tip having a mass simulation of the winglet. Vibration surveys of representative model configurations were made and were compared with calculated vibration characteristics.

Some limited results of these flutter studies have been reported in reference 11. Reference 12 is a data report of these flutter studies that includes model physical properties in sufficient detail for independent flutter analysis. The present paper focuses on and reports the TDT flutter-test results and analysis correlations. Also included are pertinent data from the other portions of this program and the results of additional analyses to determine flutter sensitivity to several parameters.

SYMBOLS AND ABBREVIATIONS

a.c. aerodynamic center

BBL body buttock line, spanwise coordinate in fixed body (fuselage) axis system, in.

b semispan of exposed wing without winglet

C_{N_α} total normal-force curve slope, per degree angle of attack

C_{n_α} sectional normal-force curve slope, per degree angle of attack

C_{n_β} sectional normal-force curve slope, per degree angle of sideslip

C_{Y_β} total nacelle side-force curve slope, per degree angle of sideslip

c local wing streamwise chord

c.g. center of gravity

DRAS dynamic response actuated switch

E.A.	elastic axis
F	flutter
f, f_F	frequency of vibration mode or flutter mode, respectively, Hz
GVT	ground vibration test
g	structural damping coefficient
HR	high response
LD	low damping
M	Mach number
MAC	mean aerodynamic chord of exposed semispan wing without winglet
m	mass of exposed semispan of wing without nacelle or winglet
NF	no flutter
NR,NSB,NVB	vibration mode consisting predominantly of either nacelle roll, nacelle side bending, or nacelle vertical bending, respectively
q, q_F	dynamic pressure at test condition or flutter, respectively, psf
R	Reynolds number
T.E.	trailing edge
V	velocity, fps
WBL	wing buttock line, spanwise coordinate in wing reference plane
WBn	vibration mode consisting predominantly of wing bending where n = 1,2,... is mode identification in order of increasing frequency
WCB	vibration mode consisting predominantly of wing chordwise (fore-and-aft) bending
WRP	wing reference plane
WS	streamwise wing station, in.
WT	wingtip flutter mode
WT1	first predominantly wing torsion mode
η	normalized spanwise coordinate of wing or winglet, 1.0 at tip
$\Lambda_{c/4}$	sweep angle of wing quarter-chord line, deg

μ mass-density ratio, $\frac{m}{\pi\rho b(MAC/2)^2}$

ρ fluid density, slugs/ft^3

BACKGROUND

Literature Review

One of the first proposed applications of winglets was for the KC-135 airplane to obtain a potential drag reduction of about 6 percent. (See ref. 4.) The KC-135 winglet program was formulated to demonstrate the drag reduction by flight tests of a family of winglets. This program included a low-speed wind-tunnel flutter-model test and a flight flutter-test program. (See ref. 5.) Flight flutter tests of one winglet configuration (Cant angle = 0°, Incidence = -4°) were terminated at 6 percent below the test flight-speed goal of 395 knots (equivalent airspeed) because of unexpected low damping (g = 0.015) encountered in a 3.0-Hz wing structural mode. This low damping was not predicted by the flutter analysis. This lack of correlation was attributed to limitations of linear theory and to the inability to represent transonic effects in the analysis.

Winglets were also considered for use on the Boeing B-747 airplane as part of the NASA Energy Efficient Transport (EET) Program. (See ref. 6.) In low-speed, complete-airplane, flutter-model tests of the B-747 EET configuration with winglets, two flutter modes were obtained that were not present for the baseline (no winglets) airplane and were shown to result from the winglet aerodynamic effects rather than the mass effects. Flutter speeds of the winglet configuration were significantly lower than those of the baseline configuration. The flutter analysis did not correlate well with the test results. It was suggested (ref. 6) that the flutter mechanisms could be better predicted by incorporating the static-lift effects of the winglet similar to what is done in a T-tail flutter analysis.

Results of flight tests and low-speed wind-tunnel flutter-model tests of winglets on the DC-10 airplane are reported in references 7 and 8. These tests were also conducted under the NASA EET Program. Low-speed tests of a semispan Douglas DC-10 flutter model showed that the winglets generally caused a moderate decrease in flutter speed for the basic wing flutter mode and a large decrease in flutter speed for a higher frequency wing flutter mode. Consequently, for the flight tests of the DC-10 airplane with winglets, 500 lb of mass balance was installed near each wingtip to ensure adequate flutter safety margins.

Two transonic-model studies of winglet effects on flutter have been reported. (See refs. 9 and 10.) Simple flat-plate models were used in reference 9, whereas a more realistic, scaled model of an executive-jet transport wing with a supercritical airfoil was used in reference 10. In both studies, the model wings were cantilever-mounted and were without engines or stores. Good test-analysis correlation was obtained in each study. For the scaled executive-jet transport wing, the winglet reduced the flutter speed of the wing by about 7 percent over a Mach number range from 0.70 to 0.83, with over half the flutter-speed reduction attributed to the winglet mass effects. The analytical results of reference 9 also suggest comparable winglet mass effects on flutter. Thus, the winglet aerodynamic effects on flutter, although not negligible, were not large in these two transonic studies.

In summary, the aforementioned studies indicate that the addition of winglets to a wing generally causes a reduction in flutter speed, and the amount of the reduction is configuration-dependent. However, the results of the B-747 EET and KC-135 winglet programs raised concerns regarding the adequacy of conventional flutter analysis to predict the winglet effects on wings carrying pylon-mounted engines for which, at least for the B-747, the pylon flexibility had a significant effect on flutter.

Low-Speed Flutter Model Study

The low-speed flutter test was conducted in the Low-Speed Wind Tunnel, General Dynamics, Convair Division, San Diego, California. Details of the low-speed model properties, the flutter tests, and test-analysis correlations are reported in reference 12.

The primary low-speed test configurations and parameters are given in table I. Some sample results from this low-speed study (ref. 12) are reproduced in figure 1 to show the winglet effects on the flutter speed, the flutter modes, and the degree of test-analysis correlations. Figure 1(a) shows the critical flutter mode (i.e., the flutter mode having the lowest flutter speed) and associated flutter speed for six model conditions that were tested with each of the three wingtips. These six conditions consisted of nacelle on or off and variations in engine nacelle pylon stiffness and wing fuel loading. For the soft-nacelle configuration, the engine pylon had a reduced (from nominal) vertical-bending stiffness. The results for the 50- and 75-percent fuel conditions, which were also tested, were essentially the same as those presented for the 0-percent fuel condition. The simulator wingtip simulated the mass, center of gravity (including vertical offset), and inertia properties of the winglet. The isolated mass and aerodynamic effect of the winglet were established from data comparisons of nominal tip with simulator tip (mass effect) and of simulator tip with winglet (aerodynamic effect). Figure 1(b) gives a percentage measure of the test-analysis flutter-speed correlations.

The significant conclusions from the low-speed model study (ref. 12) are summarized as follows:

1. Four different flutter modes were identified (described subsequently in this report). A change in flutter mode often resulted from a change in wingtip configuration.

2. Typically, the results for the full-fuel conditions (100 percent) were different from those for the less-than-full fuel conditions (0, 50, and 75 percent).

3. In every case, the effect of the winglet was to sizeably reduce the wing flutter speed. This reduction was due primarily to the winglet-associated aerodynamic effects.

4. The addition of the winglet mass (simulator tip cases, no aerodynamic surface) caused either an increase or decrease in the wing flutter speed, but the speed increments were usually small compared with the winglet aerodynamic effects.

5. Variations in the model static-lift (angle of attack) and yaw angle only slightly affected the flutter-test results.

6. Increasing the winglet cant angle from 0° to 20° caused only a small decrease in flutter speed.

7. The analysis accurately predicted the test flutter modes, frequencies, and speeds. The differences between analytical and test flutter speeds ranged from +8 percent (analytical speed higher than test) to -4 percent. (See fig. 1(b).) About the same degree of correlation was obtained for the configurations with the winglet as for those without the winglet.

8. Analysis indicated that the aerodynamics on the winglet surface itself was a primary driver in winglet flutter, rather than the winglet interference effects on the wing aerodynamics. This was determined by comparing results for a winglet-on case with those for the same case but for which the aerodynamics on the winglet surface were neglected.

9. For some configurations, analysis indicated that variations in model structural damping values caused changes in the critical flutter mode and speeds. These trends were verified by limited test results.

TDT Test Configurations

The objectives of the transonic-model test in the TDT were to determine winglet effects on transonic flutter of representative airplane configurations and, if practical, to determine the effects of Mach number on each of the flutter modes encountered in the low-speed tests. The configurations listed in table II were selected for testing in the TDT. The transonic-model variables consisted of wingtip configuration, wing fuel, nacelle pylon vertical-bending stiffness, and winglet cant angle. The nacelle stiffness was varied because a change in the vertical-bending stiffness could result in a change in flutter mode. Two low-speed model configurations (table II) were tested to verify that mass-density ratio μ effects could be analytically predicted at low speeds where Mach number effects would be negligible. This particular winglet-on configuration was tested because analysis had indicated a change in flutter mode due to a change in mass-density ratio.

DESCRIPTION OF MODELS TESTED IN TDT

Transonic Flutter Model

General

Photographs of the transonic flutter-model wing and winglet are presented in figure 2, and pertinent model dimensions are given in figure 3. The semispan model was a dynamically and elastically scaled version of an advanced twin-engine-transport aircraft wing and winglet design. The model was scaled for transonic testing in Freon.[1] The wing had an aspect ratio of 7.88 and a sweep angle of the quarter-chord line of approximately 31°. The transonic flutter-model wing had a built-in twist distribution, so that at simulated cruise conditions the flutter-model wing matched the wing design twist distribution. The winglet extended over the full wingtip chord. The area and weight of the winglet were about 3.6 percent and 1.6 percent, respectively, the area and weight of the exposed semispan wing (empty wing with nacelle).

---

[1]Registered trademark of E. I. du Pont de Nemours & Co., Inc.

Construction

The model was constructed primarily of fiberglass sandwich elements with ribs, spars, and stressed skins representative of a modern transport wing. The wing had a front and rear primary spar and was formed with an integral root fitting block. In mounting the wing, the wing root block was attached to the aerodynamic force balance with a relatively rigid mounting adapter.

The wing was built with integral wet fuel cells. Fuel loadings were simulated with water that was pumped into and evacuated from the fuel cells through a tubing system. Three simulated flap-track fairings were located on the wing lower surface. The wing was equipped with an aileron that was locked in an undeflected position. A flowthrough, simulated engine nacelle was attached to the wing lower surface by a spring beam (nacelle strut) that was enclosed within a pylon-shaped fairing. Two nacelle struts were used; one had nominal stiffnesses, and one had a soft (reduced) vertical-bending stiffness and a nominal side-bending stiffness.

The wingtip configurations were constructed so that they were similar to the wing. Each wingtip assembly was attached to two hard points in the wingtip structure. The winglet was mounted to the wing with brackets. Two sets of brackets were constructed to allow a winglet cant angle of either 20° (nominal) or 0°.

Instrumentation

Twenty accelerometers and six strain-gage bridges were used to monitor the model static loads, dynamic loads, and dynamic responses during the test. The strain-gage bridges were mounted on the wing spars, winglet attachment bracket, and nacelle strut, and the accelerometers were mounted in the wing and winglet as shown in figure 3(c).

Physical Properties

Calculated individual-panel and total mass properties of the various model components are given in reference 12, along with calculated wing spanwise distributions of the torsional stiffness, vertical-bending stiffness, and fore-and-aft bending stiffness. Measured total component weights are as follows: Empty wing = 16.45 lbm; Full wing = 33.52 lbm; Nacelle pod = 10.73 lbm; Nacelle strut = 3.56 lbm. The measured mass properties of the three wingtip configurations are given in table III. Of all the winglet mass and inertial properties, the total mass and chordwise c.g. locations were considered to have the most important effects on flutter. By closely matching these two parameters for the ballasted tip with those of the winglet, the separate effects of the winglet mass and aerodynamics could be isolated by comparing the flutter-test data for the different wingtips.

Low-Speed Flutter Model

General

A photograph of the low-speed model wing with winglet is shown in figure 2(a). The model was a dynamically and elastically scaled version of the wing/winglet design from which the transonic model was scaled, but it was only 60 percent of the size of

the transonic model. The model was scaled for testing in atmospheric air at low speeds. The low-speed model was mounted in the TDT in the same manner as the transonic model. There was no built-in twist in the low-speed wing tested in the TDT.

Construction

The model wing was of a conventional single-spar and pod construction with wing sections perpendicular to the spar elastic axis. The wing sections, flowthrough nacelle, and pylon strut were obtained from an existing model. A new wing spar was built to scale the stiffness level and distribution of the transonic model. The model was provided with a nominal tip and a winglet. The winglet was constructed as a single surface and was attached to the wing by a stiff bracket arrangement.

Instrumentation

The model was equipped with strain-gage bridges and accelerometers on the wing, nacelle, and winglet to monitor steady and dynamic loads and dynamic responses during the test.

Physical Properties

The wing consisted of 11 wing sections that were mass ballasted to match the required fuel condition. Model dimensions and mass and stiffness distributions are given in reference 12.

Model Differences

Two differences between the flutter models are noteworthy. On the low-speed model, the winglet mass was simulated by a lumped mass offset from the wing and exposed to the airflow. On the transonic model, ballast weights for the winglet mass simulation (ballasted-tip configuration) were incorporated inside the wing contour and resulted in a wingtip aerodynamically similar to the nominal tip. The second difference was that the inboard wing sections of the low-speed model were heavier (proportionately) than those of the transonic model. Consequently, the ratio of winglet-to-wing (empty) weight for the low-speed model is 0.012, compared with 0.016 for the transonic model. All differences were accounted for in the analyses.

ANALYSIS PROCEDURES

Vibration-Mode Analysis

Transonic Model

The vibration characteristics of the transonic flutter model were calculated using the ATLAS computer program. (See ref. 13.) In this program, the exposed wing was divided into 33 mass panels composed of 3 chordwise panels in each of 11 spanwise strips, and the winglet was divided into 5 mass panels composed of full-chord panels in each of 5 spanwise strips. The wing was structurally represented by finite-beam elements and was reduced to an equivalent single-spar construction with an elastic

axis. The wing was cantilevered 9.80 in. inboard from the exposed wing root. (See fig. 3(b).) In this region, the wing was assumed to be massless but with a stiffness approximately equal to that of the inboard exposed wing section. The nominal tip, ballasted tip, and winglet were each represented as a separate substructure using branch mode representation. The measured frequencies and mode shapes of the cantilevered nacelle strut and winglet were input as assumed component modes. The calculated total mass and inertias of assembled components were verified with measured values. The mass-inertia properties used for the nominal and ballasted tip were measured values. Measured model stiffness properties were used to improve the modeling of the finite-beam elements.

The mathematical structural model at the wing root was adjusted to account for balance flexibilities. To improve the correlation between the calculated and measured vibration data, the analytical stiffness representation of the basic wing structure was modified as described in appendix A. Briefly, for the basic wing (no nacelles/empty wing/nominal wingtip), it was assumed that the analytical mode shapes exactly matched the test mode shapes, and the analytical stiffness matrix was modified based on matching the test frequencies. This modified stiffness matrix was used for all the transonic-model configurations.

Low-Speed Model

The vibration analysis procedure used for the low-speed model was similar to that used for the transonic model, with the following exceptions. The calculated mass-inertia distributions of the wing spar were verified with measured total spar values. The mass-inertia properties of the wing and winglet surface sections were measured values. Measured wing-spar stiffnesses were used to adjust the mathematical structural model. Because of the reasonable agreement between the calculated and measured vibration characteristics, no modifications to the stiffness matrix or modifications to account for balance flexibilities in the mathematical model were deemed necessary.

Flutter Analysis

Transonic Model

A flutter analysis of each test configuration was made for M = 0.40, 0.65, 0.80, 0.88, and 0.91. The analysis employed the calculated values for the vibration mode shapes, frequencies, and generalized masses, with the exception that the WCB mode frequencies were measured values. The ATLAS AF1 Aerodynamics Program (ref. 13) was used to generate the unsteady aerodynamic terms. The aerodynamic representation was based on strip-theory aerodynamics using 14 streamwise wing strips, 5 winglet strips, and 2 nacelle strips (cruciform horizontal and vertical strips). Wing sectional static aerodynamic data (i.e., C_{n_α} and a.c. location) were available from the pressure model test for each of the five Mach numbers analyzed. (See appendix B, which contains measured total wing/winglet data (fig. 17) and measured distributed wing/winglet data (figs. 18 through 20).) These steady-state data are input to the AF1 program, which then computes a three-dimensional static induction matrix and equivalent slopes of the two-dimensional normal-force curves using lifting-line theory. The slopes of the two-dimensional normal-force curves and specified aerodynamic-center locations are used to calculate unsteady aerodynamic coefficients for each strip. The induction effects are then utilized to calculate generalized

aerodynamic matrices. The nacelle was aerodynamically represented as a cruciform plate with the horizontal plate located 6.87 in. below the WRP. (See fig. 3(b).) The measured nacelle C_{N_α} and C_{Y_β} values were 0.052 and 0.042 per degree, respectively, at $M = 0.40$. These nacelle values were used for all Mach numbers because they changed very little at the higher Mach numbers. At each Mach number, flutter solutions were obtained at five different density values for each configuration. Matched-point solutions were determined for each flutter mode for structural damping values g of 0.0 and 0.03. (A matched-point solution is defined as a solution in which the test velocity at a specific M is exactly matched in the analysis.)

The steady-state aerodynamic data used in the flutter analyses were measured on the pressure model that had the same cruise wing-twist distribution as the transonic flutter model. No attempt was made to adjust these aerodynamic data for aeroelastic effects.

As part of an analytical parameter sensitivity study, theoretical generalized aerodynamic matrices were calculated using the ATLAS DUBLAT program (ref. 13), which employs doublet-lattice theory. These data were used in one analytical case.

Low-Speed Model

The flutter-analysis procedure for the low-speed model was similar to that for the transonic model, with the following exceptions. The frequencies used in the analysis were those measured in the TDT. (When measured rather than calculated frequencies were used in a sample analysis, the results indicated a 1.5-knot increase in flutter speed.) Flutter solutions were obtained at density values that matched test values. Only aerodynamic data for $M = 0.40$ were used. Structural damping g values of 0.015 and 0.005 were used in the flutter solutions for the nacelle vertical-bending mode and wing second-bending mode, respectively. No attempt was made to adjust the steady-state aerodynamic data used in the flutter analysis for either aeroelastic effects or the pressure-model built-in twist effects.

VIBRATION CHARACTERISTICS

Transonic Flutter Model

Data Presentation

The measured and calculated frequencies of the natural vibration modes for various transonic-model configurations are given in table IV. Measured vibration frequencies for the cantilevered nacelle and winglet are given in table V. Comparisons of measured and calculated node line patterns associated with the vibration modes for selected model configurations are shown in figures 4 through 6. Each vibration mode is identified as either primarily a wing or nacelle mode.

A ground vibration test (GVT) was made of several model configurations prior to the TDT test in the Boeing Structural Dynamics Lab (SDL), and frequency, node lines, and structural damping of the primary vibration modes were measured. Typically, the GVT data were measured with the model mounted to the balance, which was supported on

a rigid mounting block (strong back). In the TDT tests, the model was mounted to the balance, which was mounted to the sidewall turntable. Before and after each test in the TDT, the vibration frequencies were measured by a hammer rap test and compared with the GVT or analytical data to verify the structural integrity of the model. (In a rap test, the model is struck with an instrumented hammer. The resulting hammer signal and the response from a model accelerometer are input to a frequency analyzer, which calculates and displays a transfer function plot from which the vibration mode frequencies are identified.)

Vibration data for the basic wing of the transonic model (no nacelle/empty wing/ nominal tip) are included in table IV to demonstrate the effects of the balance flexibilities (shown by comparison of GVT data obtained on a rigid steel plate and on the balance) and the analytical frequency corrections due to the analytical stiffness modification. The GVT data for the low-speed model were measured only with the wing mounted on the steel plate.

Discussion

Differences between the GVT and the TDT rap frequencies are attributed to installation variations, to frequency measurement scatter, and to possible TDT turntable flexibilities. Winglet flexibility was assumed to have no effect on the flutter-test results because the fundamental cantilevered winglet mode frequency at 93 Hz (table V) was much higher than the flutter mode frequencies. The vibration mode frequencies identified as predominantly nacelle modes (table IV) appeared to be nearly independent of wingtip configuration and wing fuel. Replacing the nominal wingtip with a ballasted tip or winglet reduced the wing mode frequencies about 10 percent (average) with considerable variance in the individual mode reductions (table IV).

The modal correlation between the analytical and GVT results was good. One significant difference in the modal correlation was found to be in the wing chordwise-bending (WCB) mode for the nominal-nacelle/full-wing/winglet (20°) configuration. For this mode, the wing fore-aft motion is dominant with significant coupling of outboard wing bending and torsion. The analytical frequency is about 2 Hz higher than the 20.7 Hz obtained in the TDT rap test. This difference was found by analysis to be significant for some flutter modes.

Although the fuselage was independently suspended from the TDT turntable, an attempt was made to ascertain whether any fuselage vibration modes influenced the wing vibration characteristics. Vibration data were measured with the fuselage on and off for a sample model configuration, but there was no appreciable effect of the fuselage.

Low-Speed Model

The measured and calculated frequencies of the natural vibration modes for the tested low-speed model configuration (with winglet) are included in table IV. The agreement between calculated and measured vibration data was satisfactory. The measured TDT rap frequencies were used in the flutter analysis.

TEST APPARATUS AND PROCEDURE

Test Facility

The TDT is a return-flow, variable-pressure, slotted-throat wind tunnel which has a 16-ft-square test section with cropped corners. It is capable of operation at stagnation pressures from near vacuum to near atmospheric pressures and at Mach numbers from 0 to 1.20 using air or Freon as the test medium. Mach number and dynamic pressure can be varied independently. The tunnel is equipped with four quick-opening bypass valves which can be opened to rapidly reduce the dynamic pressure and Mach number in the test section when flutter occurs.

Model Mounting and Fueling Arrangement

The model was cantilevered from a five-component strain-gage balance mounted to the TDT sidewall turntable. Enclosing the balance and wing root was a half-fuselage-shaped aerodynamic fairing that was attached to the turntable independently of the balance and wing. (See fig. 2(a).) The fairing allowed the exposed wing root to be located outside the boundary layer of the tunnel wall. The turntable was remotely controlled and was capable of rotating the model and fuselage body through a wide angle-of-attack range.

The full-fuel condition on the transonic model was simulated by pumping water from an external reservoir into the wing fuel cells. Fuel changes were remotely controlled and were made only during wind-off conditions. The pumping system included a device for measuring the weight of the water that was added or removed from each fuel cell.

Test Procedure

The test procedure in a tunnel "run" was to select a stagnation pressure and slowly increase Mach number (and consequently dynamic pressure) until one of the following conditions was reached: (1) Onset of flutter, (2) $M = 0.91$, (3) $q \approx 200$ psf, or (4) Model response amplitudes due either to buffet or low damping becoming large enough to be safety concerns. At severe flutter, the tunnel bypass valves were opened, and the flutter quickly subsided. Flutter was easily observed visually from the control room.

The results of pretest analyses were used to guide the tunnel runs. An attempt was made to repeat the same stagnation pressure H level runs (H = 300, 400, and 600 psf) with each different transonic-model configuration.

During each run, a printout of selected reduced test data and tunnel flow parameters was obtained at selected test conditions and at the flutter points. The model responses were monitored by strip-chart traces and reduced to power spectra and "damping-indicator" plots. The power spectrum of the response from either the wingtip vertical and/or fore-aft accelerometers was displayed in real time with updates every second. The inverse of the amplitude of each of the three highest spectrum peaks (within the range of potential flutter frequencies) for the wingtip vertical accelerometer was automatically plotted, also in real time, versus Mach number. This was called a damping-indicator plot. Each inverse-amplitude plot was tracked to determine its proximity to and approach to a zero value (flutter point).

Two Boeing developed DRAS (dynamic response actuated switch) units were employed during the test. A DRAS unit provided a measure of the amplitude and duration of the oscillatory response of a model motion sensor. One unit was set to detect the flutter onset. The second unit acted as a safety system and was set to detect a higher amplitude, severe flutter condition which would automatically activate the tunnel bypass valves. After some initial adjustments, the system worked well and provided a consistent flutter-response amplitude level at which a tunnel run could be ended. High-speed movie cameras were activated at each flutter or high-response condition to provide a visual record of the model response.

RESULTS AND DISCUSSION

Data Presentation

The TDT flutter-test results are compiled in table VI. The response conditions in the column "Model Behavior" are defined in this section. Flutter (F) is characterized by high-amplitude, sinusoidal oscillations at a specific frequency that are sustained long enough to be considered continuous. Low damping (LD) is a response condition of sinusoidal oscillations at a specific frequency in which the oscillations are not fully sustained but increase in both amplitude and duration as q and M are increased. A high-response (HR) condition is characterized by a high-amplitude response that appears to be a multimode response to broadband turbulence rather than a lack of damping in any specific mode. No-flutter conditions are indicated by NF in table VI.

General Remarks

The flutter conditions were obtained with the models at a near-zero lift condition. This condition corresponded to a fuselage angle of attack of approximately -2°. A series of runs were made with the transonic-model (nominal nacelle/empty wing/winglet (20°)) in a search for single degree-of-freedom instabilities induced by angle of attack. In these runs the model was tested through an angle-of-attack range at discrete test points within the scaled airplane flight envelope. The test angle of attack corresponded to a wing loading that was varied from approximately 80 lbm download (-0.5g load) to 180 lbm upload (+1.0g load). A similar search had been made with a nominal-tip configuration in a previous test of the transonic model. No single degree-of-freedom instability was encountered in either test.

Flutter-Mode Descriptions

The four flutter modes encountered for the transonic model were similar to those for the low-speed model. The flutter mode was more clearly identifiable for the low-speed model than for the transonic model. Therefore, the phase relationships for the different flutter modes were established from the responses of the low-speed model in the Convair tunnel tests and are considered to be applicable to the transonic model. The response frequency was the primary means of identifying the flutter mode of the transonic model. Model deflections are defined as positive for wing vertical bending up, wing chordwise bending aft, wing twisting leading edge up, nacelle vertical bending up, and nacelle side bending outboard. The four flutter modes are described as follows:

1. The nacelle vertical-bending (NVB) flutter mode was characterized by relatively large nacelle and wingtip vertical motions. The nacelle motion led the wingtip motion generally by about 200° to 270°.

2. The second wing-bending (WB2) flutter mode was characterized by large wingtip vertical motion with less nacelle motion than in the NVB mode. With the winglet, the wingtip chordwise motion led the wingtip vertical motion by about 200° and appeared to be distinctly harmonic with and of similar amplitude as the wingtip vertical motion. For the nominal and ballasted-tip configurations, the wingtip chordwise motion was not evident.

3. The wingtip (WT) flutter mode was characterized by a high frequency and sudden flutter onset. It was a classic type of flutter mode, where the wing-bending and first torsion modes coalesce into a mode with rapidly reducing damping level and frequency. Therefore, the flutter frequency of this mode depended upon the level of response at which the tunnel was stopped. For most configurations, there was some wingtip chordwise motion, and the chordwise motion was almost in phase with the wingtip vertical motion.

4. The wing chordwise-bending (WCB) flutter mode was characterized by a slow coalescence of the predominant wing chordwise mode with a higher frequency wing-bending mode. The wingtip chordwise motion appeared to lead the wingtip vertical motion by either about 250° or 0° (in phase).

TDT Low-Speed Model Results

The purpose of the low-speed model test in the TDT was to verify that the analysis could predict the effects of μ on flutter for a winglet-configured wing, in particular the change in flutter mode predicted at low values of μ. The experimental variations of q_F versus μ obtained for the two test configurations are shown in figure 7(a) and are considered typical. A change in flutter mode was obtained experimentally for the winglet configuration at low values of μ. Analytical results are shown only for the winglet configuration in the lower μ range ($\mu < 50$). Comparison indicates that the analysis predicted both the experimental q_F level and μ trend fairly well for the NVB mode. However, analysis predicted a higher q_F than experiment but showed a reasonable μ trend for the WB2 mode. The test-analysis correlations are also shown in terms of the flutter speed and frequency variations with μ in figure 7(b). The change in flutter mode occurred at a higher μ value in the test than was predicted by analysis. Comparison of the data shows that only a small drop in the analytical flutter-speed level for the WB2 mode would be necessary to match the experimental results. The flutter-mode frequencies predicted by analysis were in good agreement with the test frequencies. Thus, these results indicate that the effects of mass-density ratio can be predicted adequately by the present flutter analytical technique.

Transonic-Model Results

Experimental Results

The transonic-model test results are plotted in figure 8. The separate effects of the winglet addition on the wing flutter dynamic pressure are obtained by comparisons in figures 8(a) through 8(c) of data for the following wingtip configurations:

(1) total winglet effect; winglet versus nominal tip, (2) winglet mass effect; ballasted tip versus nominal tip, and (3) winglet aerodynamic effect; winglet versus ballasted tip. For all tested configurations, the addition of the winglet significantly reduced the q_F of the wing over the transonic range. At the higher Mach numbers, this reduction was due primarily to winglet aerodynamic effects, because the winglet mass effects were relatively small. Changing the winglet cant angle from 20° to 0° had only a small effect on q_F. (See fig. 8(d).)

The winglet impact on the wing flutter design is most important in the Mach number region where the flutter dynamic pressure is lowest. For all tested configurations, this flutter-critical M was about 0.88. Considering the nominal-nacelle configurations with empty- and full-wing conditions as the airplane flutter-design configurations, the effect of the winglet addition to these configurations is shown in figures 8(a) and 8(b). For the nominal wingtip at $M = 0.88$, the lowest q_F was obtained with the empty-fuel condition at about 120 psf. For the winglet at $M = 0.88$, the lowest q_F was obtained with the full-fuel condition at about 85 psf. Based on these data, the reduction in the critical wing flutter speed due to the winglet addition is roughly 15 percent $(1 - \sqrt{85/120})$.

Test-Analysis Correlation

Test-analysis comparisons for the transonic model are shown in figures 9 through 12. In general, the agreement between calculated and measured frequencies of the various flutter modes was good. The test-analysis correlation for each configuration is discussed in the following sections.

Nominal nacelle/empty wing/different wingtips.- For all three wingtip configurations (figs. 9(a) through 9(c)), the NVB mode was found experimentally and analytically to be the critical flutter mode. The analysis predicted the WB2 mode as the next critical flutter mode. The analysis also indicated that the q_F levels of both these modes were sensitive to structural damping and that the degree of sensitivity varied with Mach number and wingtip configuration. For the winglet configuration (fig. 9(c)), the experimental flutter point at $M = 0.66$ had high-amplitude responses in the NVB mode (17.6 Hz) and the WB2 mode (22.3 Hz) and was interpreted as flutter onset in each mode.

The analytical flutter boundaries for the NVB mode had shapes similar to the test boundaries, but the correlation in q_F level varied with wingtip configuration. For the nominal-tip configuration, the predicted q_F levels were somewhat conservative, whereas, for the other two wingtips, the predicted q_F levels were in good agreement with test results. Past experience has indicated that, in general, q_F levels of damping-sensitive modes are not predicted very accurately. Comparison of the data for the nominal tip with those for the ballasted tip shows that the analysis predicted the winglet mass effect to be stabilizing; the tests, however, showed a slight destabilizing effect (fig. 8(a)).

Nominal nacelle/full wing/different wingtips.- For the full-wing condition (figs. 10(a) through 10(c)), the analysis predicted (1) the WCB mode as the flutter-critical mode for all wingtip configurations, (2) the NVB mode as equally critical for the winglet configuration, (3) the WT mode as the next critical mode for two wingtip configurations, and (4) the WCB and NVB modes as very sensitive to g level and the WT mode as less g sensitive. For the nominal-tip configuration

(fig. 10(a)), only one flutter point was obtained experimentally, and that occurred in the WT mode at a high q_F that was in good agreement with the predicted level. For the ballasted-tip configuration (fig. 10(b)), no flutter was obtained in the test, although high-amplitude responses were observed. Because predicted q_F levels were never attained in the test, the test-analysis correlation for this configuration is unresolved.

For the winglet configuration (fig. 10(c)), it was difficult to distinguish the experimental flutter mode at the higher Mach numbers (M = 0.86 and 0.79), because there was a distinct beating between the NVB (18.5 Hz) and WCB (19.1 Hz) modes. At the lower Mach numbers (M = 0.73 and 0.64), flutter occurred experimentally in the WT mode. Comparison of the test and analytical results indicate that the analytical q_F predictions for the WCB (or NVB) mode are unconservative at $M = 0.86$ and conservative at $M = 0.79$. At the lower Mach numbers, the predicted q_F levels for the WT mode are considerably unconservative.

In summary, the test-analysis q_F correlations for these configurations were mixed. The analytical q_F sensitivity to damping level for the WCB and NVB modes makes q_F correlations difficult. However, the winglet effects on flutter are predicted satisfactorily at the higher Mach numbers where the q_F values are lowest and most critical. Considerable analytical effort was devoted to understanding the sensitivities of the WCB and WT modes as discussed in the section "Analytical Transonic Parameter Sensitivities."

Soft nacelle/empty wing/different wingtips.- For these configurations (figs. 11(a) through 11(c)), the analysis predicted: (1) the NVB mode as the critical flutter mode at the higher Mach numbers with a closed region of instability ($g = 0$), (2) the next critical mode as the WB2 mode, (3) a third potential flutter mode (WT mode) for the ballasted tip at the higher Mach numbers, and (4) only the WB2 mode as relatively insensitive to structural damping. Experimentally, low damping in the NVB mode (primarily) and WB2 mode was experienced at the higher Mach numbers with the nominal-tip and ballasted-tip configurations. In the winglet configuration tests at the higher Mach numbers, high-amplitude responses in both the NVB and WB2 were obtained, which again made it difficult to establish a specific flutter mode. At the lower Mach numbers, the test flutter mode was more clearly defined as the WB2 mode for all wingtip configurations.

Overall, the test-analysis correlations were considered satisfactory. The analytical q_F values were, in general, slightly unconservative for the WB2 mode, but the flutter boundary shapes were similar to those obtained experimentally. The analysis was used to predict the potential flutter areas for the WCB mode which were verified by the test results (NVB low damping points and combined NVB and WCB flutter points).

Nominal nacelle/empty wing/winglet (0°).- The test-analysis correlation of the 0° canted-winglet configuration was satisfactory. (See fig. 12.) The analysis predicted a somewhat higher q_F than was obtained experimentally at $M = 0.64$, where the specific flutter mode was again difficult to identify because of the high responses in both the NVB and WB2 modes. Experimentally, changing the winglet cant angle from 20° to 0° caused only a small decrease in q_F over the Mach number range. (See fig. 8(d).) Analytically (compare figs. 9(c) and 12), the cant-angle change was predicted to increase q_F slightly for the $g = 0$ solutions. However, the analytical sensitivity to structural damping for both flutter modes was also affected. As a result, the 0° canted winglet was indicated to have a somewhat harder NVB flutter

mode, which increased the likelihood of obtaining flutter in this mode at a lower q_F than the 20° canted winglet.

Analytical Winglet Effects

The aforementioned analytical and test results for the transonic model include the combined effects of M and μ. To eliminate μ effects, an analysis was made at a single density value (ρ = 0.00111 slug/ft^3) of the nominal-nacelle/empty-wing configuration with each of the three wingtips. The results for the flutter-critical modes are presented in figure 13. The following comments are limited to the $g = 0.03$ cases. For the NVB mode at $M = 0.88$, the effect of the tip weight is to increase q_F by 7 percent relative to the nominal tip. The aerodynamic effect of the winglet is to reduce q_F by 14 percent relative to the ballasted-tip configuration. Thus, the net reduction in the analytical q_F due to the combined effect of winglet mass and aerodynamics is relatively small (7 percent) for the conditions cited. However, the effects of the winglet weight and aerodynamics are expected to be different for different wing configurations or different modes. A comparison of these data (fig. 13) with the analytically matched test-velocity results (fig. 9) shows that the M effects and winglet effects on q_F appear much larger when μ effects are present, as in the matched test-velocity solutions.

Analytical Transonic Parameter Sensitivities

Parameter Survey

An analytical sensitivity study of the transonic model was conducted to evaluate the effect on flutter of selected parameters. The primary configuration for the sensitivity study was the nominal nacelle/full wing/winglet (20°). This configuration was selected because three different flutter mechanisms were observed.

The flutter speeds were found to be sensitive to the following parameters:

1. Structural parameter (wing chordwise-bending stiffness).

2. Aerodynamic parameters (spanwise distributions of static-lift-curve slope and aerodynamic center).

The following parametric variations and procedures had little or no effect on the flutter results:

1. The wing elastic axis (E.A.) location was moved aft over the outboard spanwise portion of the wing. This aft E.A. was a straight line extending from the original E.A. wing-root location to a streamwise wingtip location that was 0.91 in. aft (or 10 percent of tip chord) of the original E.A. tip location. (See fig. 3(b).)

2. The number of aerodynamic strips in the flutter analysis was varied.

3. The static-lift effect in the vicinity of the winglet was included in the flutter analysis (SLOAEF program of ref. 13, which is based on the analysis used in ref. 14).

4. The stiffness matrix was modified (appendix B).

Some results from this analytical sensitivity study are presented in table VII and are plotted in figures 14 and 15. These data were calculated for $M = 0.40$ ($\rho = 0.00111$ slug/ft^3), $M = 0.65$ ($\rho = 0.00350$ slug/ft^3), $M = 0.80$ ($\rho = 0.00150$ slug/ft^3), and $M = 0.88$ ($\rho = 0.00111$ slug/ft^3), which were representative of test conditions. The reference analysis (table VII) was that used in the test-analysis correlations. The base case for the sensitivity study differed from the reference analysis in chordwise-bending stiffness level and distribution. The individual parametric effects are examined (fig. 14) by comparisons of q_F versus M for each of the three significant flutter modes. Only the most conservative ($g = 0$) results are compared in figure 14. The analytical q_F for some flutter modes was very sensitive to structural damping level, as indicated by the q_F variations (table VII) for a change in g from 0.00 to 0.03. This sensitivity to damping may exaggerate the effects of some parametric changes on q_F, particularly for the NVB mode.

Wing Chordwise-Bending Sensitivity

The flutter sensitivity to wing chordwise bending is attributed to the combined effects of the addition of both the winglet mass and wing fuel to the outboard wing region. The importance of the frequency of the WCB vibration mode is demonstrated in figure 15. The analysis was conducted at $M = 0.65$ ($\rho = 0.00350$ slug/ft^3) and at $M = 0.88$ ($\rho = 0.00111$ slug/ft^3). The WCB mode frequency appreciably affects the q_F of both the NVB and WT flutter modes as well as the q_F of the WCB flutter mode. The WCB vibration mode has a significant wingtip vertical-motion component (fig. 6(a)), which accounts for its effect on flutter speeds.

The chordwise-bending stiffness was modified to evaluate the effect of change in stiffness distribution. The modification probably gave a better representation of the actual model than the nominal-stiffness distribution when compared with typical airplane distributions. Roughly, the chordwise stiffnesses were increased by a factor of about 5 inboard of the side-of-body spanwise location and decreased by factors varying from about 0.9 to 0.3 over the remaining semispan. This change in chordwise-bending stiffness had a sizeable effect on the frequencies of the wing chordwise and torsion modes. The resulting wing chordwise-bending and torsion frequencies for the nominal-nacelle/full-wing/winglet (20°) configuration were 20.3 Hz and 40.3 Hz, respectively. The corresponding frequencies for the reference analysis were 22.87 Hz and 41.89 Hz. (See fig. 6.) The corresponding measured (TDT installation) frequencies were 20.7 Hz and 42.8 Hz. Thus, the modification to the wing chordwise-bending stiffness improved the frequency correlation for the chordwise-bending mode with some deterioration for the torsion mode.

The effect of the chordwise-bending stiffness change is examined in figure 14(a) by comparing the results for the reference and base analytical cases. The stiffness modification (base case) increased the q_F for the WCB flutter mode, so that the NVB mode became the most critical flutter mode at the higher Mach numbers. However, the WCB mode remained the critical flutter mode at the lower Mach numbers.

The effect of the change in the mode shape as a result of this stiffness modification may also be significant, because there is considerable wing bending and torsion motion in the WCB mode for this configuration. An attempt to use the experimentally measured mode shape was initiated; however, it was found that the wing twist could not be reliably determined, because it was dependent on small differences in accelerometer readings which were within the measurement error band.

Sensitivity to Other Parameters

Case 1 was analyzed to show the effect of "tuned" frequencies; that is, all vibration-mode frequencies used in the analysis were measured GVT values. Comparison with the base case shows that frequency tuning (fig. 14(b)) does not have a significant effect on the critical flutter mode q_F values. The q_F values for the WT flutter mode are increased, primarily as a result of the wing-torsion-mode frequency change from 40.3 Hz to 42.8 Hz.

Case 2 was similar to case 1 except that the wing C_{n_α} values were increased 10 percent at semispan stations η from 0.538 to 1.0. The increase in C_{n_α} caused an appreciable drop in q_F for all three flutter modes. (See fig. 14(c).)

The effect of moving the wing a.c. forward by 0.05c and 0.10c (at η = 0.538 to 1.0) is also shown to be significant by a comparison of the q_F results for cases 3 and 4 with those for case 2. (See fig. 14(d).) As expected, the q_F values decrease for all three flutter modes as the a.c. moves forward.

The effect of including the stiffness matrix modification is seen by comparison of the results for case 5 with those for case 4. (See fig. 14(e).) The stiffness modification caused a small drop in q_F for the NVB and WCB flutter modes. Both analyses employed the same (tuned) frequencies for the vibration modes, but there are some differences in the calculated vibration-mode shapes which, although expected to be relatively minor, could have resulted in these q_F reductions. However, these differences in mode shapes were not investigated.

The effect of using a doublet-lattice aerodynamics program (DUBLAT) rather than the strip-theory program (AF1) was evaluated. No empirical corrections were made to the theoretical DUBLAT aerodynamic data. The C_{n_α} values from DUBLAT are roughly 10 percent higher than the test data at $M = 0.40$ and 0.65 as an average over the outboard wing span. (See figs. 18(a) and 18(b).) At $M = 0.80$, the test and theoretical C_{n_α} distributions are roughly similar (fig. 18(c)), whereas at $M = 0.88$, the DUBLAT C_{n_α} distribution is lower than test data over the entire span (fig. 18(d)). Based simply on comparable C_{n_α} levels, the q_F values calculated using DUBLAT based terms should be comparable to the case-2 results at $M = 0.40$ and 0.65 and to the case-1 results at $M = 0.80$. The actual results (fig. 14(f)) are somewhat inconsistent relative to the expected trends, and the reasons for these discrepancies are not known.

Compressibility C_{N_α} Correction

The application of an empirical compressibility factor correction, or "C_C correction," was evaluated by comparison of the transonic flutter boundaries formed using the C_C correction with those calculated using the experimentally weighted AF1 program. The correction factor is derived as follows. It is assumed that q_F is inversely proportional to the steady normal-force curve slope of the total semispan wing, or

$$q_F \approx 1/C_{N_\alpha}$$

The q_F at any Mach number $(q_F)_M$ can therefore be related to the q_F at any other Mach number $(q_F)_{M_1}$ as follows:

$$(q_F)_M = \frac{\left(C_{N_\alpha}\right)_{M_1}}{\left(C_{N_\alpha}\right)_M} (q_F)_{M_1} = C_C^2 (q_F)_{M_1}$$

The quantity C_C^2 was determined from wind-tunnel test data (fig. 17). The reference $(q_F)_{M_1}$ was the q_F calculated by analysis at the incompressible Mach number of 0.40. Figure 16 shows the comparisons of the two methods for the nominal-nacelle/empty wing with the nominal wingtip and with the winglet. The data were obtained at a density value ρ of 0.00111 slug/ft^3 and for $g = 0$ and $g = 0.03$ solutions. For the wing with nominal tip (figs. 16(a) and (b)), the C_C correction resulted in slightly higher q_F values at transonic Mach numbers below 0.90 for both flutter modes. For the winglet configuration (figs. 16(c) and (d)), the C_C correction agreed closely with the analytical results. These comparisons have been made for specific configurations and altitude ρ. Only one general conclusion is warranted. The C_C correction approach may give results different from the actual calculated Mach number boundary and may not always be conservative. Nevertheless, this simple approach provides an estimate of Mach number effects on the flutter dynamic pressure instead of making a large number of flutter calculations over the Mach number range, and is useful for preliminary evaluation of test configurations for the purpose of planning the test.

SUMMARY OF RESULTS

An experimental and analytical study was conducted to determine the effects of a winglet on the flutter characteristics of cantilevered models representative of a twin-engine-transport wing. Flutter tests were conducted in the Langley Transonic Dynamics Tunnel of both a transonic and a low-speed scaled model of this wing. The low-speed model tests were conducted at low subsonic Mach numbers ($M < 0.45$) to obtain mass-density-ratio effects for a specific configuration with a winglet on or off.

Ten different transonic-model configurations were tested at Mach numbers up to 0.90. These included three different wingtips (a nominal tip, a winglet with 20° cant angle, and a nominal-shaped wingtip ballasted to simulate the winglet mass properties) on each of the following conditions: (1) nominal nacelle/empty wing, (2) nominal nacelle/full wing, and (3) soft nacelle/empty wing. The tenth configuration consisted of a winglet with 0° cant angle with a nominal-nacelle/empty-wing condition. Flutter analyses were made for correlation with experiment and to examine the flutter sensitivity to several parameters. The flutter analyses generally employed vibration modes and frequencies calculated using a finite-element-beam structural simulation of the flutter models and modified strip-theory unsteady aerodynamics that were experimentally weighted.

The four flutter mechanisms (modes) predicted by analysis were obtained in the transonic-model tests. For all tested configurations, the addition of the winglet

substantially reduced the flutter dynamic pressure of the wing over the transonic Mach number range. The winglet effect was configuration-dependent and was primarily the result of winglet aerodynamics rather than winglet mass. Changing winglet cant angle from 20° to 0° had only a slight effect on the transonic flutter characteristics.

The mass-density effects on flutter obtained with the low-speed model, including a change in flutter mode, were predicted satisfactorily by analysis. The analytical results correlated reasonably well with test results through the transonic regime. It was concluded that the transonic flutter characteristics of a twin-engine-transport wing with a winglet can be satisfactorily predicted by the present conventional method.

Using a correction factor based on the measured variation of the slope of the normal-force curve with Mach number appeared useful as a first approximation to determine Mach number effects on the flutter dynamic pressure for certain flutter modes. The analysis indicates that the wing chordwise-bending mode, which had significant wing-bending and torsion motion components, is important to flutter for the one winglet configuration studied.

NASA Langley Research Center
Hampton, VA 23665-5225
October 2, 1986

APPENDIX A

PROCEDURE FOR MODIFYING STIFFNESS MATRIX

Comparison of the vibration data for the basic clean wing (no nacelle/empty wing/nominal tip) in table IV indicates that there are small differences between the measured and calculated (before-modification analysis) frequencies. These frequency differences are attributed mainly to inaccuracies in the wing stiffness modeling that result from the difficulties in (1) defining the stiffnesses near the wing-root support and (2) representing the wing analytically as an elastic-axis beam structure. Therefore, the wing stiffness matrix was targeted for modification to obtain a better correlation of the test-analysis vibration data. The modification was made because the wing stiffness matrix was a primary element in determining the stiffness matrices for the wing/nacelle and wing/nacelle/winglet configurations formed from the component vibration test data for the nacelle and winglet.

The procedure for modifying the wing stiffness matrix was based on the following assumptions:

1. The analytical mode shapes exactly matched the test mode shapes.

2. The test frequencies for the vibration modes $m + 1$ through n matched the corresponding analytical mode frequencies where m lowest frequency modes were those measured in the GVT and where n was the total number of degrees of freedom in the analytical model.

The modification procedure is summarized as follows:

Let K and M be the $n \times n$ wing stiffness and mass matrices, respectively. The wing frequencies and mode shapes are calculated from

$$(K - \lambda_i M) q_i = 0 \qquad (i = 1, n) \qquad (1)$$

where $\lambda_i = \omega_i^2$ is the ith eigenvalue,

ω_i = the ith frequency, rad/sec, and

q_i = the ith eigenvector, $n \times 1$

Let the eigenvectors be arranged in an $n \times n$ model matrix Φ as follows:

$$\Phi = \left[\Phi_m \mid \Phi_\ell\right] = \left[q_1\ q_2 \cdots q_m \mid q_{m+1} \cdots q_n\right] \qquad (m + \ell = n) \qquad (2)$$

Since the eigenvectors are orthogonal with respect to K and M,

$$\Phi^T M \Phi = I \qquad (3a)$$

and

$$\Phi^T K \Phi = K_{g_n} = \begin{bmatrix} K_{g_m} & 0 \\ 0 & K_{g_\ell} \end{bmatrix} \tag{3b}$$

where

I	$n \times n$	identity matrix
K_{g_n}	$n \times n$	diagonal matrix of eigenvalues
K_{g_m}	$m \times m$	partition of K_{g_n}
K_{g_ℓ}	$\ell \times \ell$	partition of K_{g_n}

Equation (3b) can be rewritten as

$$\Phi^T K \Phi = (\Phi^T M \Phi)^T K_{g_n} (\Phi^T M \Phi)$$

or

$$K = M^T \Phi K_{g_n} \Phi^T M \tag{4}$$

Separating equation (4) into m and ℓ partitions,

$$K = M^T \Phi_m K_{g_m} (\Phi_m)^T M + M^T \Phi_\ell K_{g_\ell} (\Phi_\ell)^T M \tag{5}$$

Based on the assumptions outlined at the beginning, a modified stiffness matrix K^* can be expressed as

$$K^* = M^T \Phi_m K^*_{g_m} (\Phi_m)^T M + \left[K - M^T \Phi_m K_{g_m} (\Phi_m)^T M \right] \tag{6}$$

where $K^*_{g_m}$ is the $m \times m$ generalized stiffness matrix based on the test data, where

$$\left(K^*_{g_m}\right)_i = (2\pi f_T)^2_i \qquad (i = 1, m) \tag{7}$$

and where f_T is the test frequency in Hz.

If $(f_A)_i$ is the ith analytical frequency,

$$K^* = K + (2\pi)^2 M^T \Phi_m \left[\left((f_T)_i^2 - (f_A)_i^2 \right) \right] (\Phi_m)^T M \tag{8}$$

It is shown in equation (8) that the modification to the analytical stiffness matrix is based upon the difference between the test and analytical frequencies of the first lowest m modes. The modified wing stiffness was used in all transonic-model analyses except for several analytical cases in the flutter sensitivity study.

APPENDIX B

AERODYNAMIC DATA

The aerodynamic data given herein were used in the flutter calculations discussed in this report and include both measured and calculated data. All wing data are for the nacelle attached to the wing, and all winglet data are for the winglet mounted to the wing. The sectional normal force is defined as the force acting normal to the surface local chord.

Measured

The experimental data were measured in tests of a pressure model that were conducted in the Boeing Transonic Wind Tunnel (BTWT). The model consisted of a cantilevered wing and half-body that were tested mounted to the tunnel floor. The model was equipped with a flow-through simulated engine nacelle and a winglet. The model was instrumented to measure the chordwise distribution of static pressures at several spanwise stations on both the wing and winglet.

Static-pressure data were collected over an angle-of-attack range at selected test Mach numbers. Configurations investigated included the winglet on or off the wing with nacelle and winglet cant angles of 20°, 10°, and 0°. The tests included variations in wing sweep angle of ±5° from nominal to approximate the effects of sideslip angle β as in simple wing theory. (The sideslip angle was equivalent to an angle of attack for the winglet.)

The pressure data were reduced to sectional data. The wing sectional data were linearized with respect to angle of attack to obtain sectional normal-force curve slope C_{n_α} and were corrected to remove the effect of the model wing flexibility. The winglet sectional data were also linearized with respect to the wing sweep angle to obtain C_{n_β}, but they were not corrected for model flexibility effects. Figure 17 shows the measured Mach number variation of the total lift curve slope C_{N_α} of the wing (with nacelle) with and without winglet. Measured spanwise variations at several Mach numbers of normal-force slope C_{n_α} over the wing and C_{n_α} over the winglet are given in figures 18 and 19, respectively. Measured spanwise distributions of the a.c. location over the wing and winglet are shown in figure 20. More extensive data are presented in reference 12.

Calculated

Calculated spanwise distributions of the normal-force curve slopes are included in figures 18 and 19, and calculated a.c. distributions at $M = 0.40$, 0.80, and 0.88 are given in figure 21. These data were generated using the DUBLAT program of reference 13.

REFERENCES

1. Whitcomb, Richard T.: A Design Approach and Selected Wind-Tunnel Results at High Subsonic Speeds for Wing-Tip Mounted Winglets. NASA TN D-8260, 1976.

2. Flechner, Stuart G.; Jacobs, Peter F.; and Whitcomb, Richard T.: A High Subsonic Speed Wind-Tunnel Investigation of Winglets on a Representative Second-Generation Jet Transport Wing. NASA TN D-8264, 1976.

3. Flechner, Stuart G.; and Jacobs, Peter F.: Experimental Results of Winglets on First, Second, and Third Generation Jet Transports. NASA TM-72674, 1978.

4. Ishimitsu, K. K.: Aerodynamic Design and Analysis of Winglets. AIAA Paper 76-940, Sept. 1976.

5. Kehoe, Michael W.: KC-135A Winglet Flight Flutter Program. KC-135 Winglet Program Review, NASA CP-2211, 1982, pp. 171-188.

6. Staff, Boeing Commercial Airplane Co.: Selected Advanced Aerodynamics and Active Controls Technology Concepts Development on a Derivative B-747 Aircraft - Final Report. NASA CR-3164, 1980.

7. Shollenberger, Carl A.; Humphreys, John W.; Heiberger, Frank S.; and Pearson, Robert M.: Results of Winglet Development Studies for DC-10 Derivatives. NASA CR-3677, 1983.

8. Staff, Douglas Aircraft Co.: DC-10 Winglet Flight Evaluation. NASA CR-3704, 1983.

9. Doggett, Robert V., Jr.; and Farmer, Moses G.: Preliminary Study of Effects of Winglets on Wing Flutter. NASA TM X-3433, 1976.

10. Ruhlin, Charles L.; Rauch, Frank J., Jr.; and Waters, Catherine: Transonic Flutter Model Study of a Supercritical Wing and Winglet. J. Aircr., vol. 20, no. 8, Aug. 1983, pp. 711-716.

11. Bhatia, Kumar G.; Nagaraja, K. S.; and Ruhlin, Charles L.: Winglet Effects on the Flutter of Twin-Engine Transport-Type Wing. J. Aircr., vol. 22, no. 7, July 1985, pp. 587-594.

12. Bhatia, Kumar G.; and Nagaraja, K. S.: Flutter Parametric Studies of Cantilevered Twin-Engine-Transport Type Wing With and Without Winglet. Volumes I and II. NASA CR-172410, 1984.

13. Dreisbach, Rodney L., ed.: ATLAS - An Integrated Structural Analysis and Design System - ATLAS User's Guide. NASA CR-159041, 1979.

14. Jennings, W. P.; and Berry, M. A.: Effect of Stabilizer Dihedral and Static Lift on T-Tail Flutter. J. Aircr., vol. 14, no. 4, Apr. 1977, pp. 364-367.

TABLE I.- PARAMETERS INVESTIGATED IN LOW-SPEED MODEL STUDY

Primary test parameters (with analysis correlation)	Other parameters analyzed
1. Wingtip configuration: nominal tip, simulator tip, winglet 2. Wing fuel condition: 0% (empty), 50%, 75%, 100% (full) 3. Nacelle: on, off 4. Nacelle pylon stiffnesses: nominal, soft in vertical bending, soft in side bending 5. Winglet/simulator-tip cant angle: 20° (nominal), 10°, 0° 6. Winglet/simulator-tip attachment-to-wing stiffness: nominal, soft 7. Model angle of attack 8. Model yaw angle	1. Variations in winglet and simulator-tip mass 2. Variations in chordwise location of simulator-tip c.g. 3. No winglet aerodynamics

TABLE II.- MODEL CONFIGURATIONS TESTED IN LANGLEY TRANSONIC DYNAMICS TUNNEL

Nacelle pylon stiffness	Wing fuel	Wingtip	Test medium
Transonic flutter model			
Nominal ↓	Empty/full ↓ Empty	Nominal Ballasted Winglet (20° cant) Winglet (0° cant)	Freon ↓
Soft ↓	Empty ↓	Nominal Ballasted Winglet (20° cant)	
Low-speed flutter model			
Nominal Nominal	Empty Empty	Nominal Winglet (20° cant)	Air Air/Freon

TABLE III.- MASS PROPERTIES OF MODEL WINGTIPS

(a) Wingtip mass and c.g. location

Wingtip	Weight, lbm	c.g.[1] relative to wingtip leading edge, in.	
		Aft	Outboard
Nominal[2]	0.0198	3.96	0.30
Ballasted[2]	.350	5.00	.40
Winglet (plus bracket)	.359	5.44	1.44

(b) Wingtip c.g. location and inertia properties

Wingtip[3]	Weight, lbm	c.g. location[4]			Inertia about component c.g.		
		u, in.	v, in.	w, in.	$I_{uu'}$, lb-in^2	$I_{vv'}$, lb-in^2	$I_{ww'}$, lb-in^2
Nominal	0.0198	3.96	0.30	0.60	0.001	0.079	0.079
Ballasted	.3503	5.00	.40	.60	.027	.286	.285
Winglet	.2586	5.87	4.35	.19	3.075	.855	3.906
Winglet bracket	.100	4.33	.50	.00	.045	.129	.097

[1]Dimensions are in wing reference plane.

[2]Half-body streamlined fairing was used for wingtip closure structure.

[3]For nominal tip and ballasted tip, dimensions are measured in WRP with origin at intersection of wing leading edge and wingtip streamwise chord. For winglet, coordinate dimensions are measured in winglet chord plane with origin at intersection of winglet leading edge and winglet root chord.

[4]u, v, and w are streamwise (positive aft), spanwise (positive outboard), or vertical (positive up), respectively, coordinates of wingtip center of gravity.

TABLE IV.- VIBRATION-MODE FREQUENCIES OF MODEL CONFIGURATIONS

Method	Configuration			Wing mode frequency, Hz							Nacelle mode, Hz			Comments
	Nacelle	Wing fuel	Wingtip	WB1	WB2	WCB	WB3	WT1	Higher frequency modes		NSB	NVB	NR	
Transonic-model configuration used for analytical stiffness modification														
GVT	None	Empty	Nominal	7.81	25.00	34.00	52.68	58.42	86.71	96.10	None			On steel plate
GVT				7.80	24.70	32.02	52.12	58.08	85.88	94.12				On balance
Analysis				7.61	23.93	34.90	52.61	57.07	90.83	95.91				Before modification
Analysis				7.80	24.70	32.02	52.12	58.08	85.88	94.12				After modification
Transonic-model test configurations														
Analysis	Nominal	Empty	Nominal	7.76	24.15	32.07	42.76	57.19	-	-	15.26	18.60	29.80	
GVT			Nominal	7.72	24.02	30.47	43.75	55.55	-	-	15.14	19.82	29.49	
Rap			Nominal	7.5	23.5	-	42.2	54.13	-	-	15.0	19.2	27.8	
Analysis			Ballasted	6.84	21.80	27.92	40.58	55.2	-	-	15.20	18.56	30.08	
Rap			Ballasted	6.8	21.3	27.0	40.3	52.6	-	-	15.0	19.2	28.2-31.0	
Analysis			Winglet (20°)	6.72	21.08	26.64	38.91	47.01	-	-	15.19	18.54	29.98	
GVT			Winglet (20°)	6.84	21.09	27.64	40.33	46.88	-	-	15.23	19.82	29.69	
Rap			Winglet (20°)	6.6	20.7	26.7	39.1	46.7	-	-	14.8	19.1	28.0	
Analysis		Full	Nominal	6.06	16.80	25.20	32.41	46.63	-	-	14.98	19.06	29.93	
GVT			Nominal	6.06	17.19	22.36	32.03	46.39	-	-	15.04	19.14	29.20	
Rap			Nominal	6.0	16.9	-	31.2	45.8	-	-	14.8	18.5	27.7	
Analysis			Ballasted	5.64	14.28	23.39	39.37	46.15	-	-	15.86	18.71	30.56	
Rap			Ballasted	5.7	14.8	21.5	28.1	43.9	-	-	15.8	18.8	29.8	
Analysis			Winglet (20°)	5.59	14.04	22.87	28.73	41.89	-	-	15.75	18.65	30.26	
GVT			Winglet (20°)	5.66	14.45	21.48	28.61	43.06	-	-	15.62	19.04	29.68	
Rap			Winglet (20°)	5.5	14.3	20.7	27.5	42.8	-	-	15.5	18.8	28.5	
Analysis	Soft	Empty	Nominal	7.5	23.0	30.0	38.8	54.5	-	-	14.5	15.4	31.5	
Rap			Nominal	7.5	23.5	27.6	40.8	53.5	-	-	14.5	15.4	28.7	
Analysis			Ballasted	6.8	21.5	27.9	37.9	53.2	-	-	14.1	15.3	30.1	
Rap			Ballasted	6.8	21.1	26.2	38.5	50.3	-	-	14.4	15.3	27.8	
Analysis			Winglet (20°)	6.7	20.8	26.6	36.7	46.6	-	-	14.1	15.3	30.0	
Rap			Winglet (20°)	6.8	20.7	26.8	38.4	46.3	-	-	14.5	15.5	31.6	
Low-speed model test configuration														
Analysis	Nominal	Empty	Winglet (20°)	3.78	11.93	12.40	31.73	-	22.85	25.6	7.83	9.13	17.88	No balance effects
GVT	Nominal	Empty	Winglet (20°)	3.93	12.19	11.74	27.00	-	23.46	23.80	-	9.45	17.88	On steel plate
Rap	Nominal	Empty	Winglet (20°)	4.0	13.0	13.5	26.6	-	24.6	24.2	8.0	9.5	-	

TABLE V.- MEASURED VIBRATION FREQUENCIES OF CANTILEVERED PYLON-NACELLE AND WINGLET

Cantilevered vibration mode	Frequency, Hz	
	Transonic model	Low-speed model
Nacelle side bending	15.74	8.15
Nacelle vertical bending (nominal)	24.70	11.72
Nacelle vertical bending (soft)	15.99	-
Nacelle roll	28.97	17.96
Winglet first bending	93.0	30.1

TABLE VI.- COMPILATION OF TEST RESULTS

Nacelle pylon stiffness	Wing fuel	Wingtip configuration	Run-point number	Model behavior	Flutter		M	q, psf	V, fps	ρ, slug/ft^3	R, per ft
					Frequency, Hz	Predominant mode(s)					
Transonic model, tested in Freon only											
Nominal	Empty	Nominal	9-32	LD	16.0	NVB	0.890	120.6	441.4	0.001228	2.13×10^6
		Nominal	10-48	F	17.5	NVB	.830	140.0	411.8	.001633	2.64
		Nominal	11-61	F	18.0	NVB	.780	169.3	385.6	.002244	3.37
		Winglet (20°)	2-30	F	17.5	NVB	0.770	124.4	381.0	0.001714	2.55×10^6
		↓	3-37	F	22.0/17.5	WB2/NVB	.660	157.0	330.3	.002878	3.64
			4-48	HR/NF	-	-	.900	85.1	443.4	.000866	1.53
			5-60	F	17.5	NVB	.828	105.6	411.3	.001248	2.01
		Ballasted	6-74	LD	14.5/17.0	- /NVB	0.900	122.5	446.4	0.001229	2.16×10^6
		Ballasted	7-93	F	16.0	NVB	.820	138.5	406.8	.001674	2.67
		Ballasted	8-104	F	17.5	NVB	.745	163.5	368.3	.002411	3.45
	Full	Nominal	12-71	HR/NF	-	-	0.900	158.0	442.3	0.001596	2.82×10^6
		Nominal	13-82	F	23.5	WT	.840	206.2	411.4	.002350	3.79
		Winglet (20°)	14-91	F	19.5/18.5	WCB/NVB	0.856	97.2	420.6	0.001077	1.79×10^6
		↓	15-103	LD	20.0/19.5	WCB/NVB	.790	128.5	392.9	.001648	2.53
			16-109	F	24.5	WT	.730	161.7	350.0	.002428	3.30
			17-115	F	26.0	WT	.640	171.7	320.3	.003287	4.05
		Ballasted	18-128	HR/NF	-	-	0.864	164.1	422.3	0.001812	3.10×10^6
		Ballasted	19-134	HR/NF	-	-	.820	189.7	406.8	.002258	3.62
	Empty	Winglet (0°)	36-313	NF/HR	-	-	0.860	79.8	426.6	0.000870	1.45×10^6
	↓	↓	37-320	F	18.0	NVB	.815	106.0	404.8	.001283	2.03
			38-326	F	18.0	NVB	.760	122.0	374.1	.001685	2.44
↓			39-331	F	17.8/20.0	NVB/WB2	.640	154.0	322.3	.002915	3.60
Soft	Empty	Nominal	27-240	LD	13.0	NVB	0.900	86.5	443.4	0.000873	1.54×10^6
	↓	↓	28-250	LD/HR	13/17.4/14	NVB/WB2/NSB	.890	122.6	441.3	.001248	2.17
			29-256	LD/HR	20.5/13.2/16	WB2/NVB/NSB	.865	139.9	423.1	.001509	2.50
			30-266	F	21.5/17.0	WB2/NVB	.823	161.0	398.2	.001906	2.95
			31-273	F	23.0	WB2	.782	190.0	398.5	.001893	2.93
		Winglet (20°)	23-211b	F	14.0/22.7	NVB/WB2	0.890	85.3	425.0	0.000890	1.53×10^6
		↓	24-218	F	17.5/19.0	NVB/WB2	.844	107.7	417.2	.001227	2.02
			25-224	F	21.0/14.0	WB2/NVB	.778	136.1	385.8	.001807	2.73
			26-231	F	23.0	WB2	.710	153.6	353.7	.002422	3.32
		Ballasted	32-282	LD	13.0	NVB	0.870	131.0	428.8	0.001414	2.41×10^6
		↓	33-289	F	16.5	WB2	.820	153.0	408.7	.001815	2.88
			34-294	F	19.0	WB2	.737	169.0	349.5	.002454	3.31
↓			34R-298	F	19.0	WB2	.750	173.0	373.7	.002443	3.54
Low-speed model tested in air (runs 40-52) and Freon (runs 53-55)											
Nominal	Empty	Winglet (20°)	40-335	F	8.8	NVB	0.348	22.8	384.9	0.000307	0.30×10^6
	↓	↓	42-344	F	8.8	↓	.395	22.2	435.1	.000235	.28
			43-348	F	8.7		.350	22.3	386.0	.000299	.30
			44-353	F	8.9		.305	23.0	336.4	.000407	.36
			45-	F	8.8		.250	23.5	275.8	.000618	.45
			46-	F	8.8		.190	24.4	209.6	.001111	.61
			47-	F	8.8		.16	24.3	176.5	.001560	.73
			48-	F	9.0		.14	24.2	154.4	.002030	.83
			49-	F	9.0		.13	24.3	143.4	.002363	.89
		Nominal	50-360	F	8.8	NVB	0.454	25.7	498.6	0.000207	0.28×10^6
		Nominal	51-373	F	9.0	NVB	.198	26.6	218.7	.001113	.66
		Nominal	52-383	F	9.0	NVB	.139	27.8	153.9	.002349	.98
		Winglet (20°)	53-392	F	9.0	NVB	0.292	25.6	142.2	0.002489	1.44×10^6
		Winglet (20°)	54-402	F	12.1	WB2	.231	28.2	112.7	.004316	1.96
↓		Winglet (20°)	55-410	F	12.1	WB2	.180	29.2	87.6	.007301	2.57

TABLE VII.- ANALYTICAL FLUTTER SENSITIVITY RESULTS FOR TRANSONIC-MODEL CONFIGURATION

[Nominal nacelle/full wing/winglet (20°)]

Parameters			Analytical case															
			Reference		Base		1		2		3		4		5		6	
Stiffness matrix modification			Yes		No		No		No		No		No		Yes		No	
WCB stiffness distribution			Nominal		Adjusted		Adjusted		Adjusted		Adjusted		Adjusted		Adjusted		Adjusted	
Vibration frequencies			Tuned WCB		Untuned WCB		Tuned WCB		Tuned WCB		Tuned WCB		Tuned WCB		Tuned WCB		Tuned WCB	
C_{n_α} distribution			Test		Test		Test		10% increase		10% increase		10% increase		10% increase		Theoretical	
a.c. distribution			Test		Test		Test		Test		0.05c forward		0.10c forward		0.10c forward		Theoretical	
Aerodynamic program			Strip (AF1)		Strip (AF1)		Strip (AF1)		Strip (AF1)		Strip (AF1)		Strip (AF1)		Strip (AF1)		DUBLAT	
Mach number	Density, slug/ft^3	Flutter mode	Calculated q_F, psf, for g of -															
			0.00	0.03	0.00	0.03	0.00	0.03	0.00	0.03	0.00	0.03	0.00	0.03	0.00	0.03	0.00	0.03
0.40	0.00111	NVB	-	-	209	-	-	-	-	-	170	-	143	153	134	148	275	372
		WCB	153	172	198	209	198	220	187	193	176	177	160	167	148	162	148	182
		WT	275	-	257	266	275	288	247	256	221	235	204	-	209	-	207	227
0.65	0.00350	NVB	511	-	-	-	437	496	422	575	375	543	161	-	152	-	-	-
		WCB	152	174	202	217	207	232	183	202	169	183	161	165	144	161	152	192
		WT	248	259	238	248	259	270	227	237	207	209	190	197	183	197	222	238
0.80	0.00150	NVB	115	125	130	146	130	-	115	-	106	-	97	106	93	106	340	370
		WCB	106	118	130	141	135	146	115	123	111	123	106	114	97	111	146	168
		WT	174	192	163	168	174	183	157	163	141	149	130	138	130	143	212	221
0.88	0.00111	NVB	109	117	123	130	125	128	109	-	101	109	91	97	89	93	-	-
		WCB	97	113	130	136	134	141	115	117	107	117	103	117	93	-	148	160
		WT	165	185	155	162	-	-	148	153	134	141	125	130	125	139	204	237

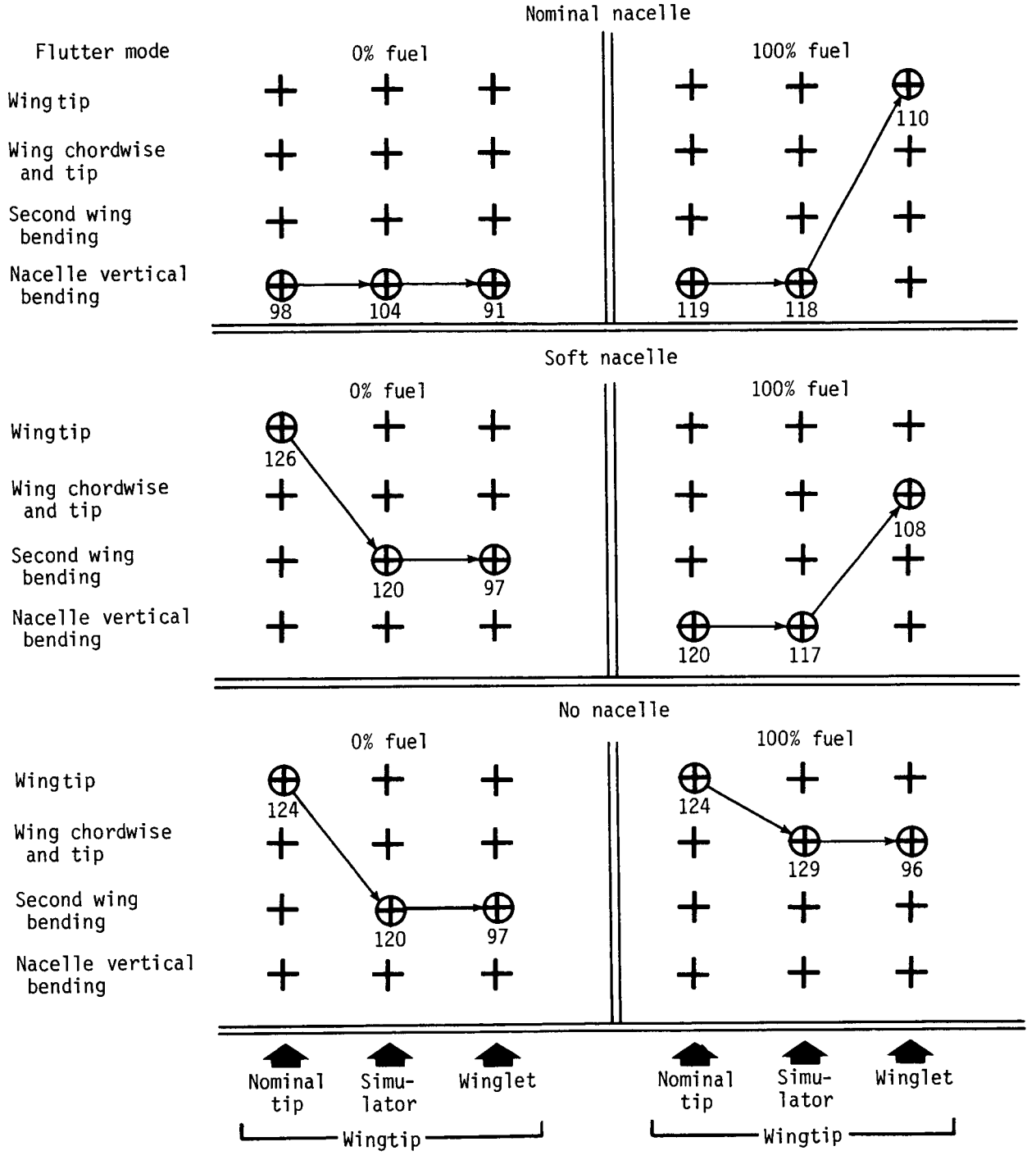

(a) Critical test flutter modes and speeds. (Numbers are test flutter speeds in knots true airspeed.)

Figure 1.- Representative results from low-speed model study.

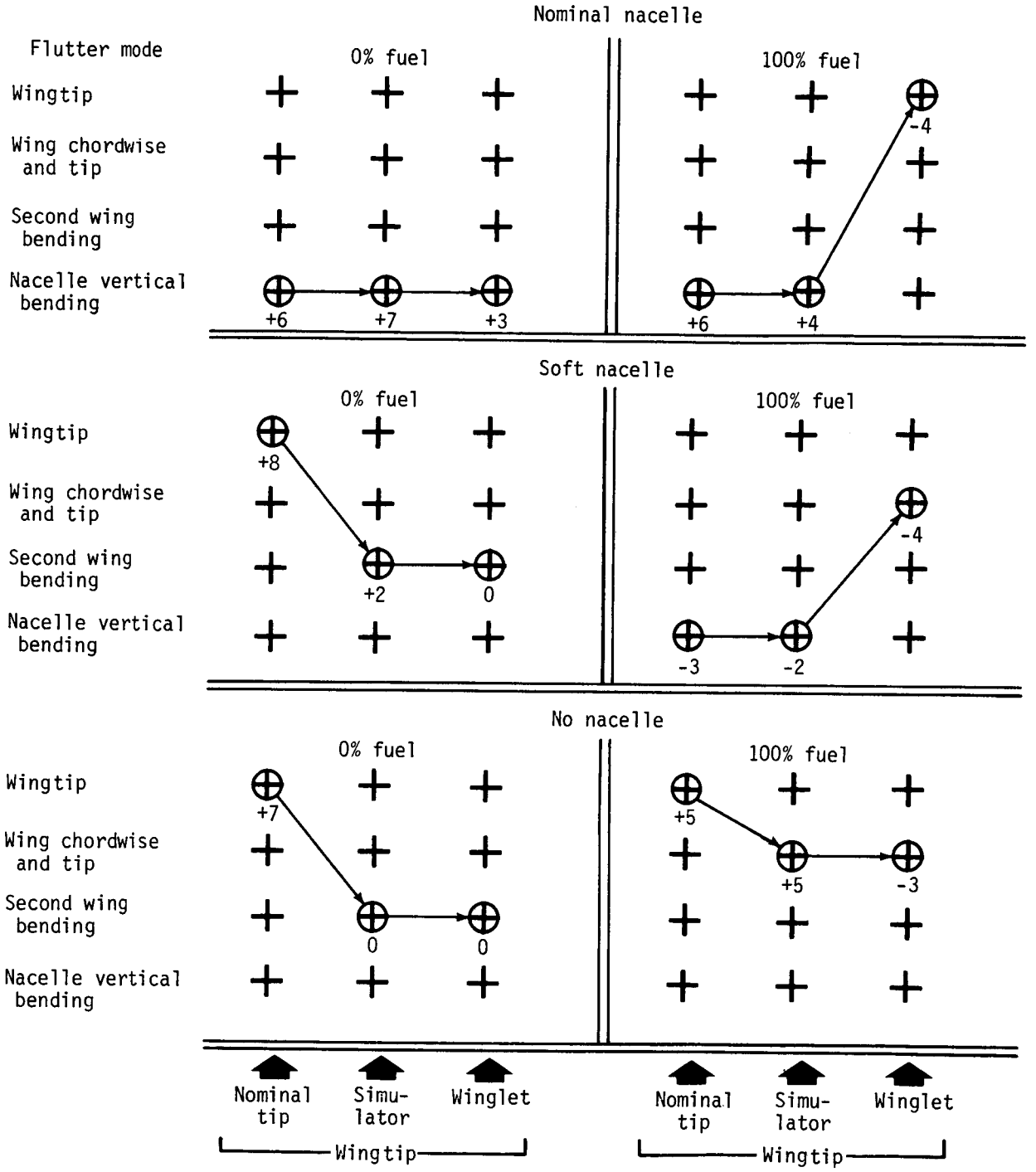

(b) Analysis test flutter speed correlation. (Numbers are percent deviation of predicted flutter speeds from test speeds.)

Figure 1.- Concluded.

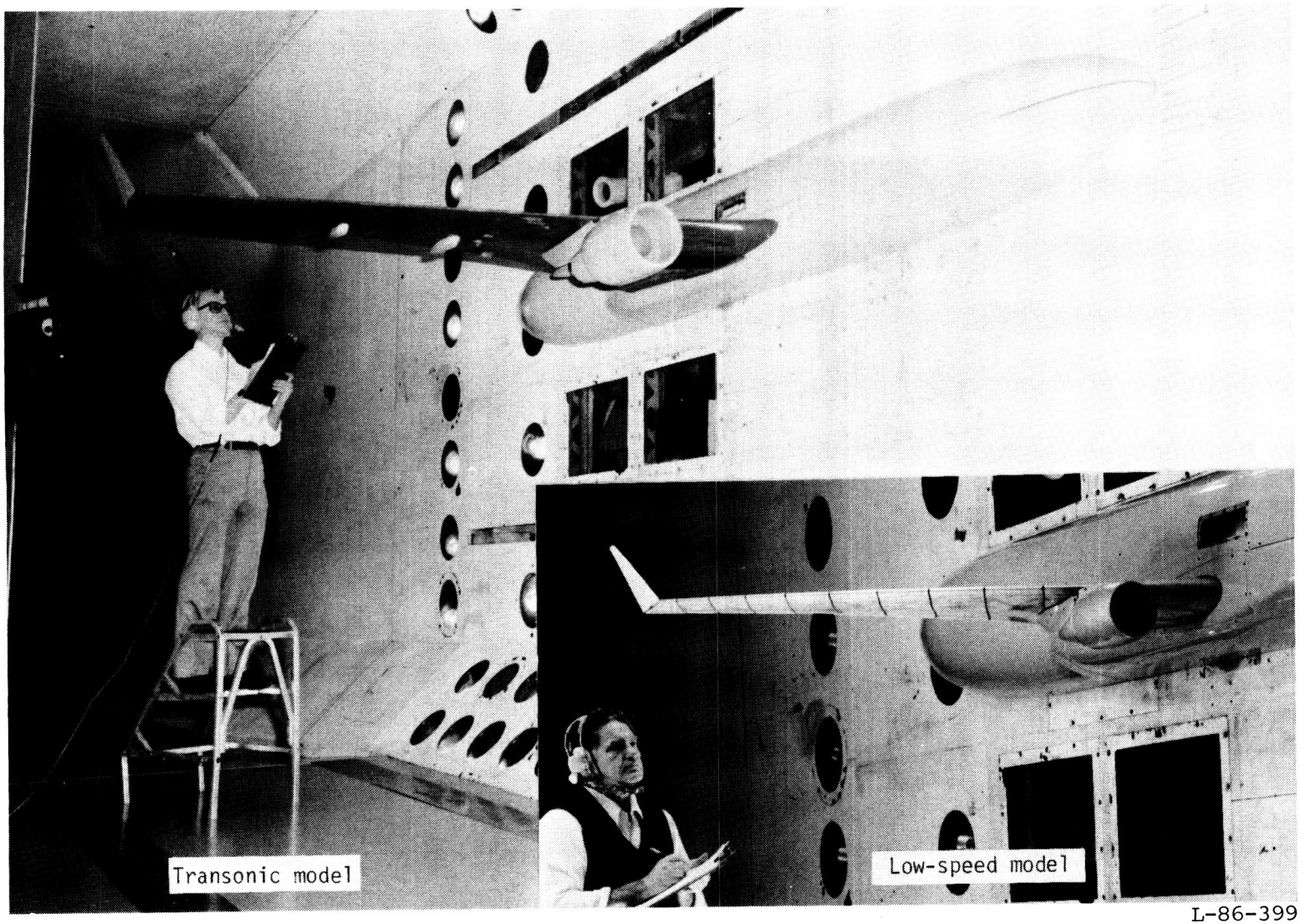

(a) Front-side view of models with winglet.

Figure 2.- Photographs of models tested in Langley Transonic Dynamics Tunnel (TDT).

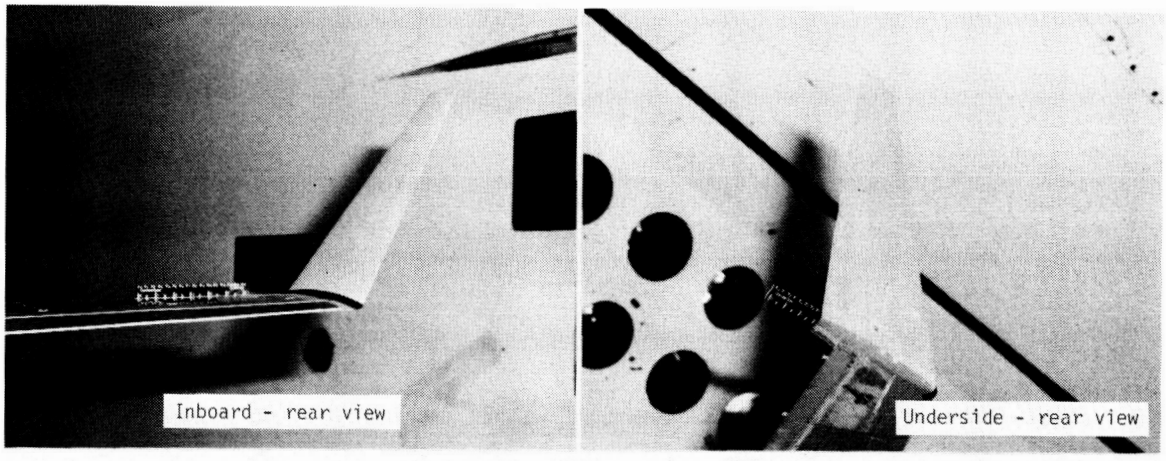

Wingtip with winglet

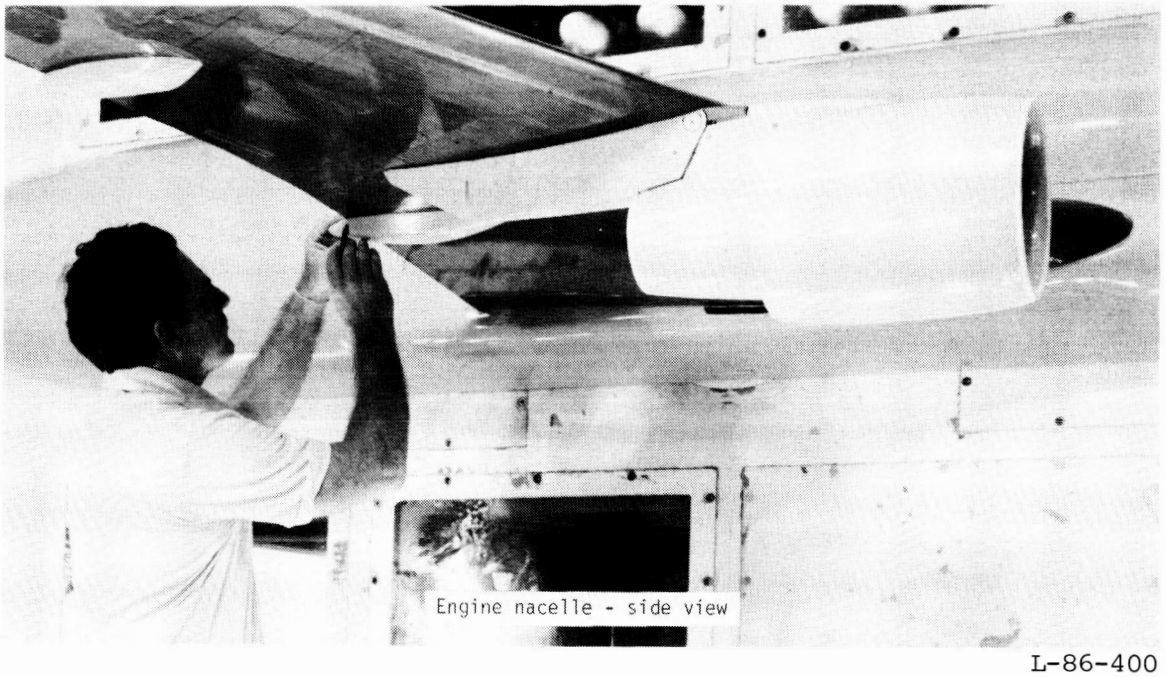

L-86-400

(b) Transonic-model components.

Figure 2.- Concluded.

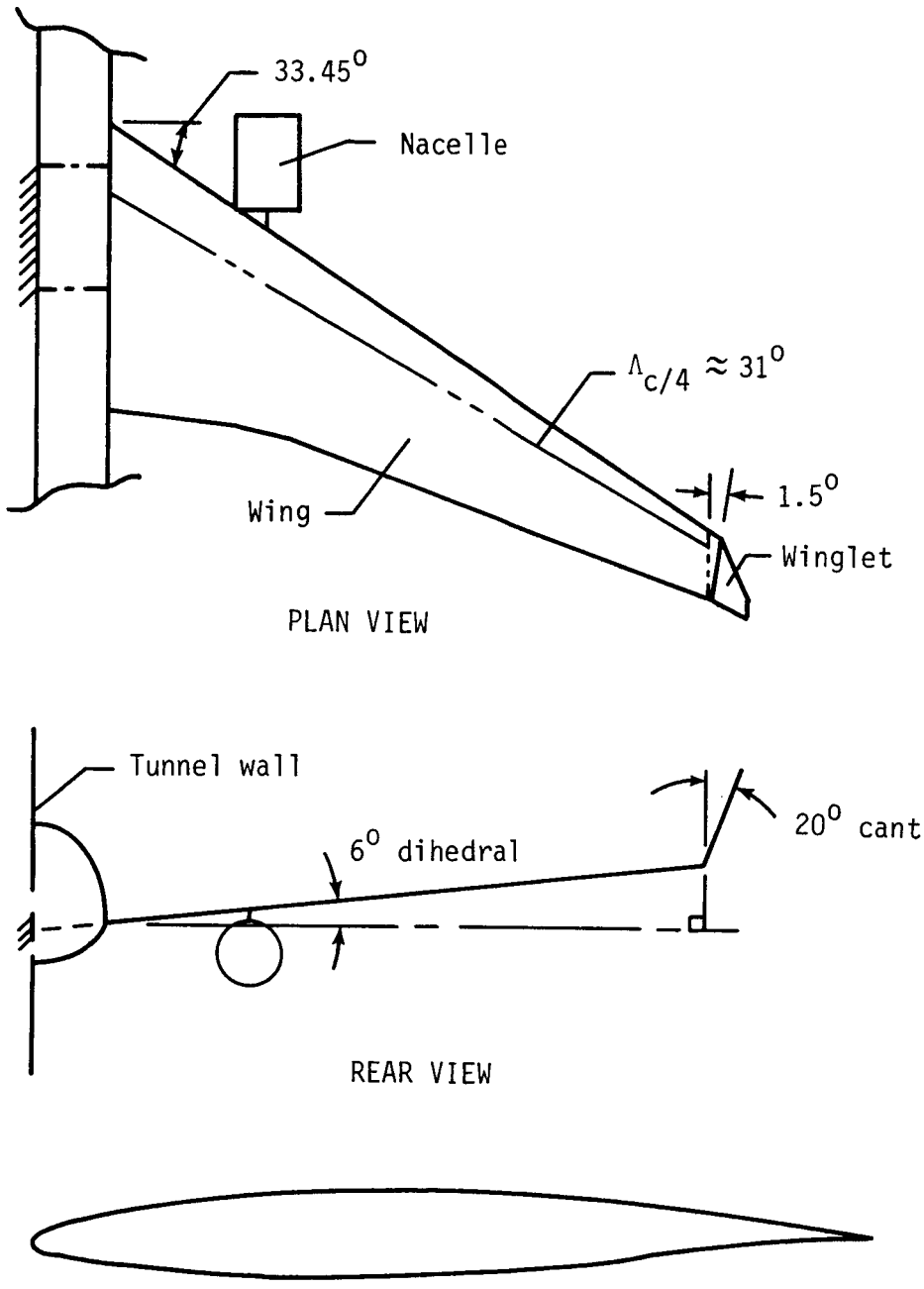

(a) Transonic flutter model installation in TDT and wing airfoil section.

Figure 3.- Sketches of transonic flutter model showing selected dimensions, TDT installation, and instrumentation.

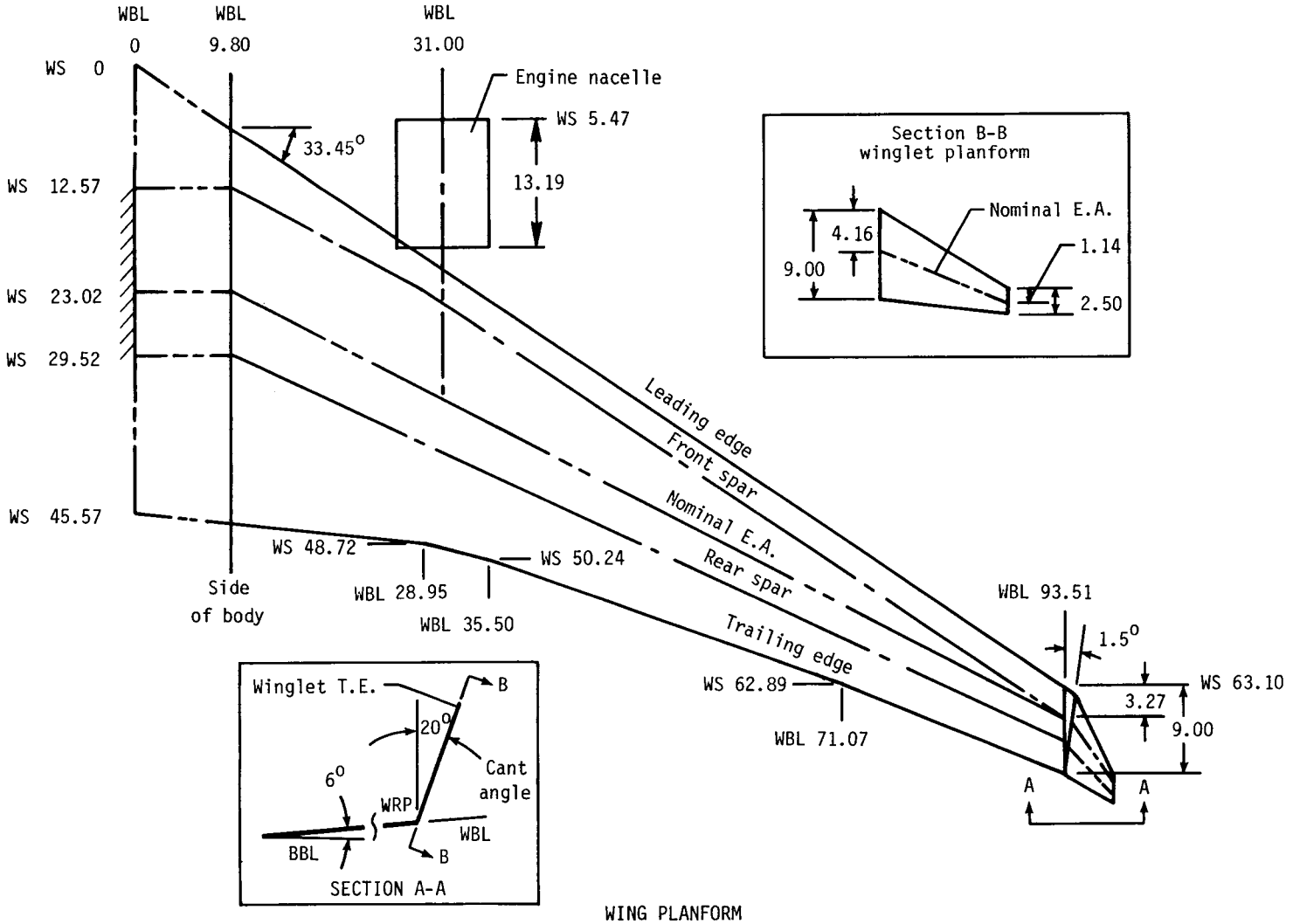

(b) Planform and selected dimensions of transonic-model components. Linear dimensions are in inches. Nacelle aerodynamically represented as cruciform with horizontal plate located 6.87 in. below WRP.

Figure 3.- Continued.

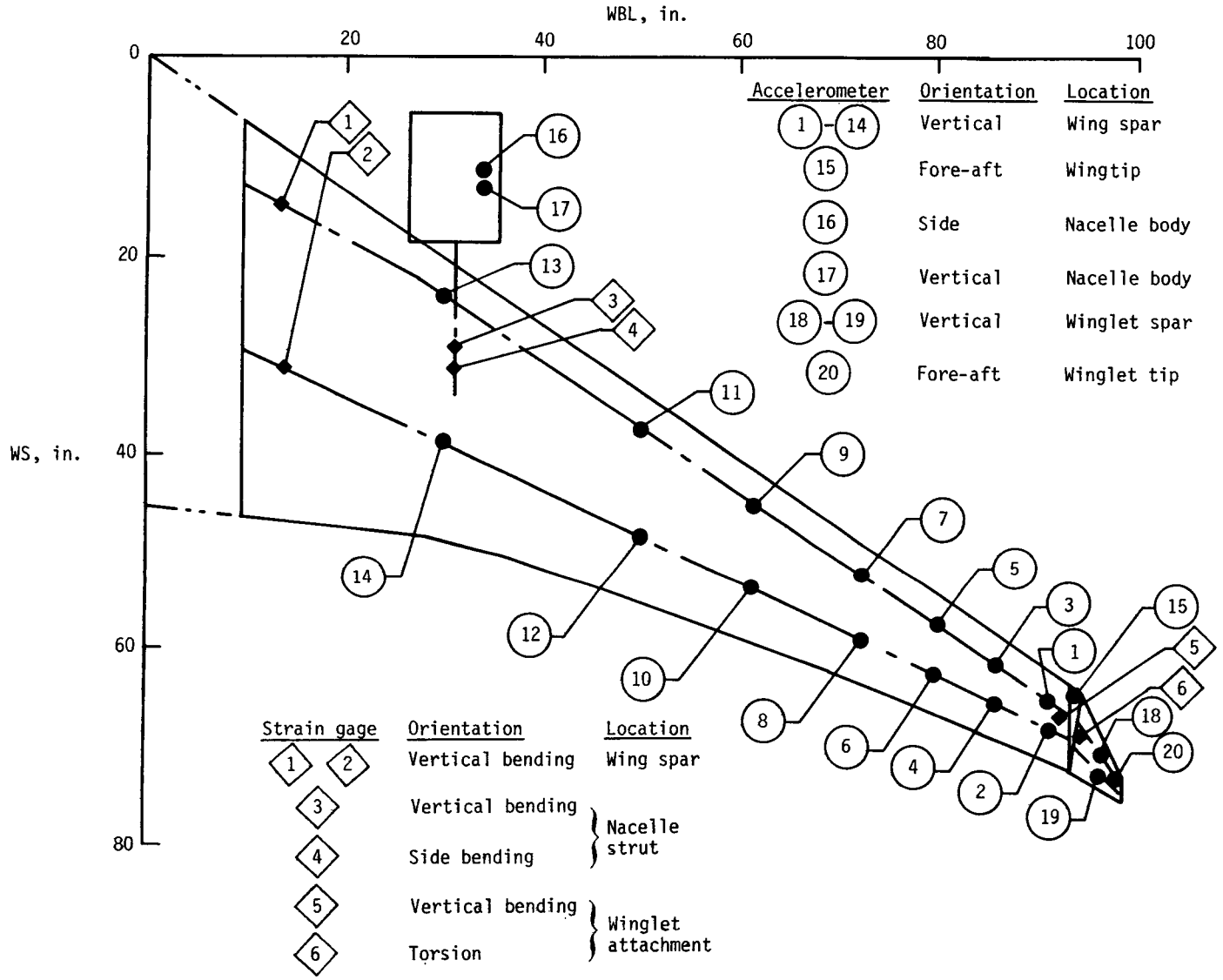

(c) Instrumentation on transonic model.

Figure 3.- Concluded.

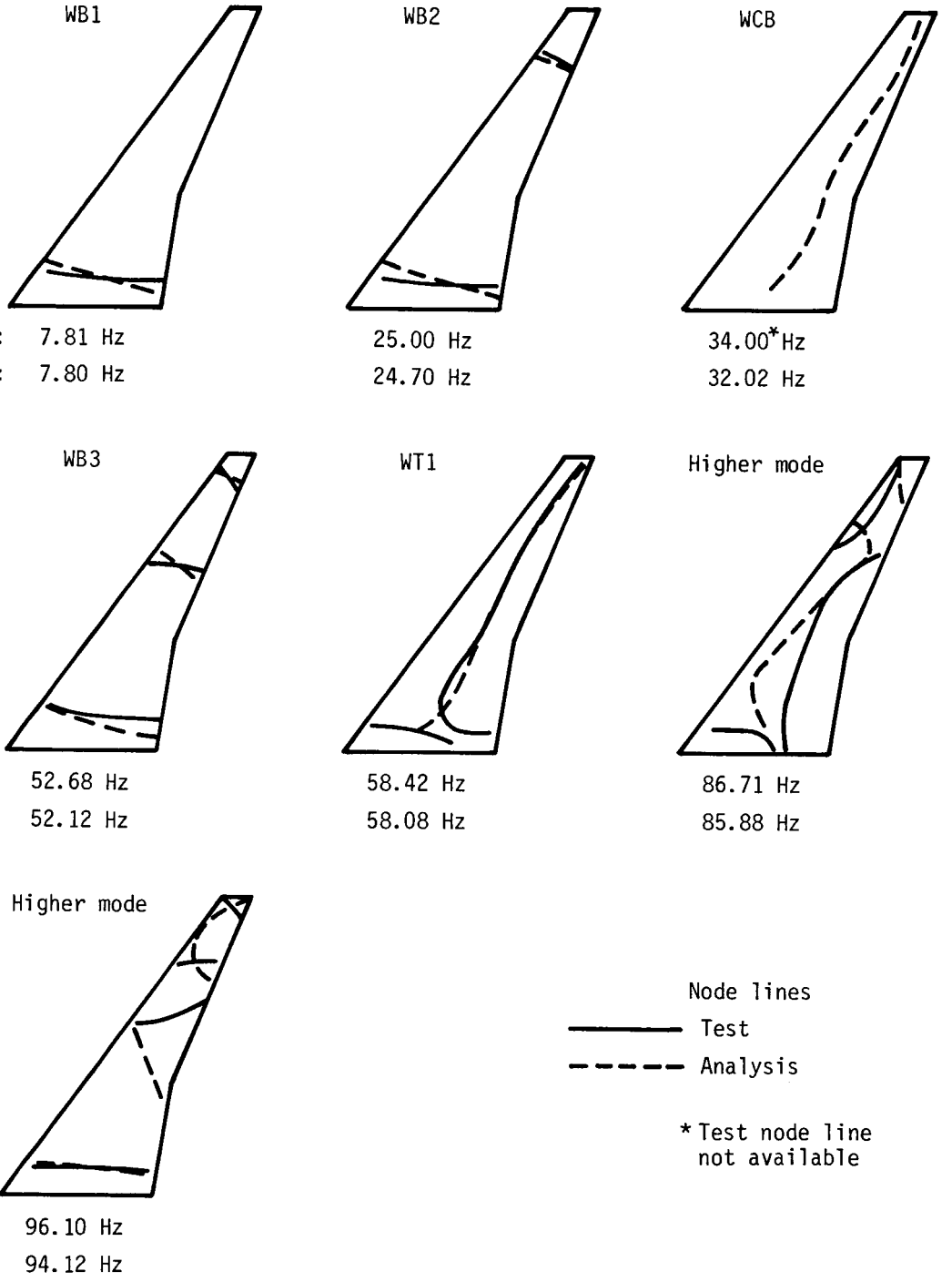

Figure 4.- Measured and calculated vibration frequencies and node lines of transonic-model configuration used for analytical stiffness modification. Configuration: no nacelle/empty wing/nominal tip.

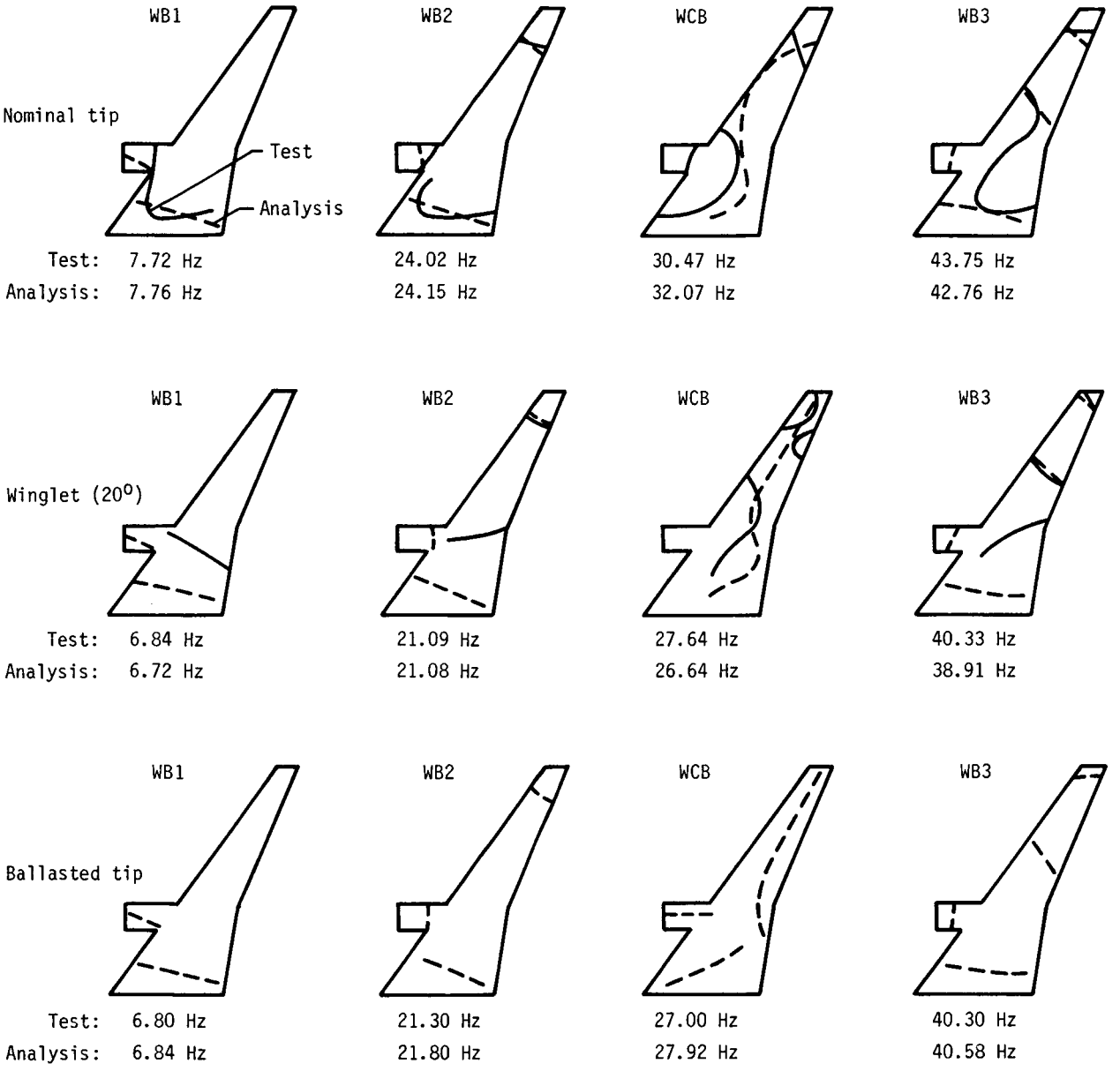

(a) Primary wing-bending modes.

Figure 5.- Measured and calculated vibration frequencies and node lines of transonic model for configuration with nominal nacelle/empty wing/ different wingtips. Test node lines not reduced for ballasted-tip configurations.

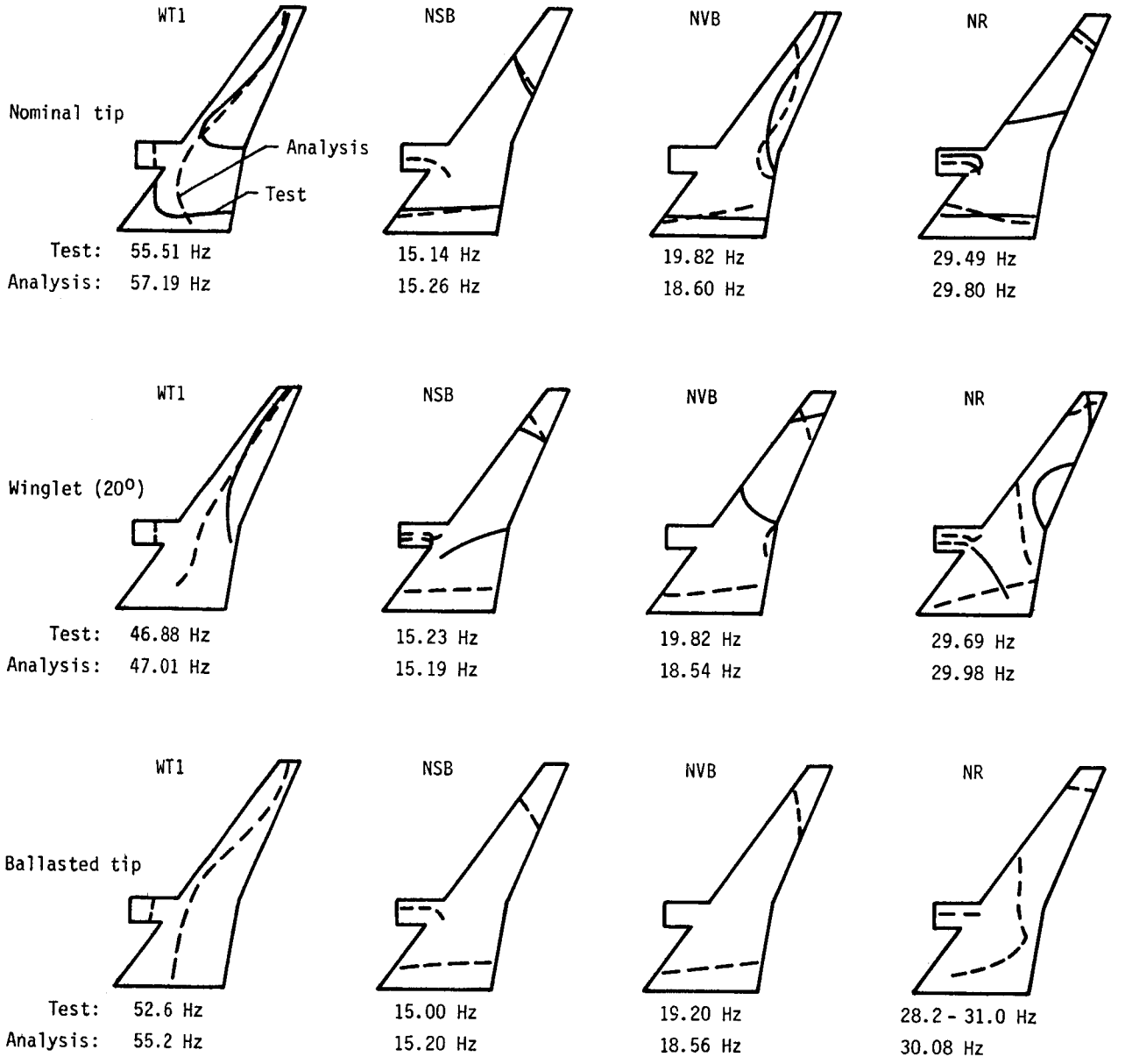

(b) Wing torsion and nacelle modes.

Figure 5.- Concluded.

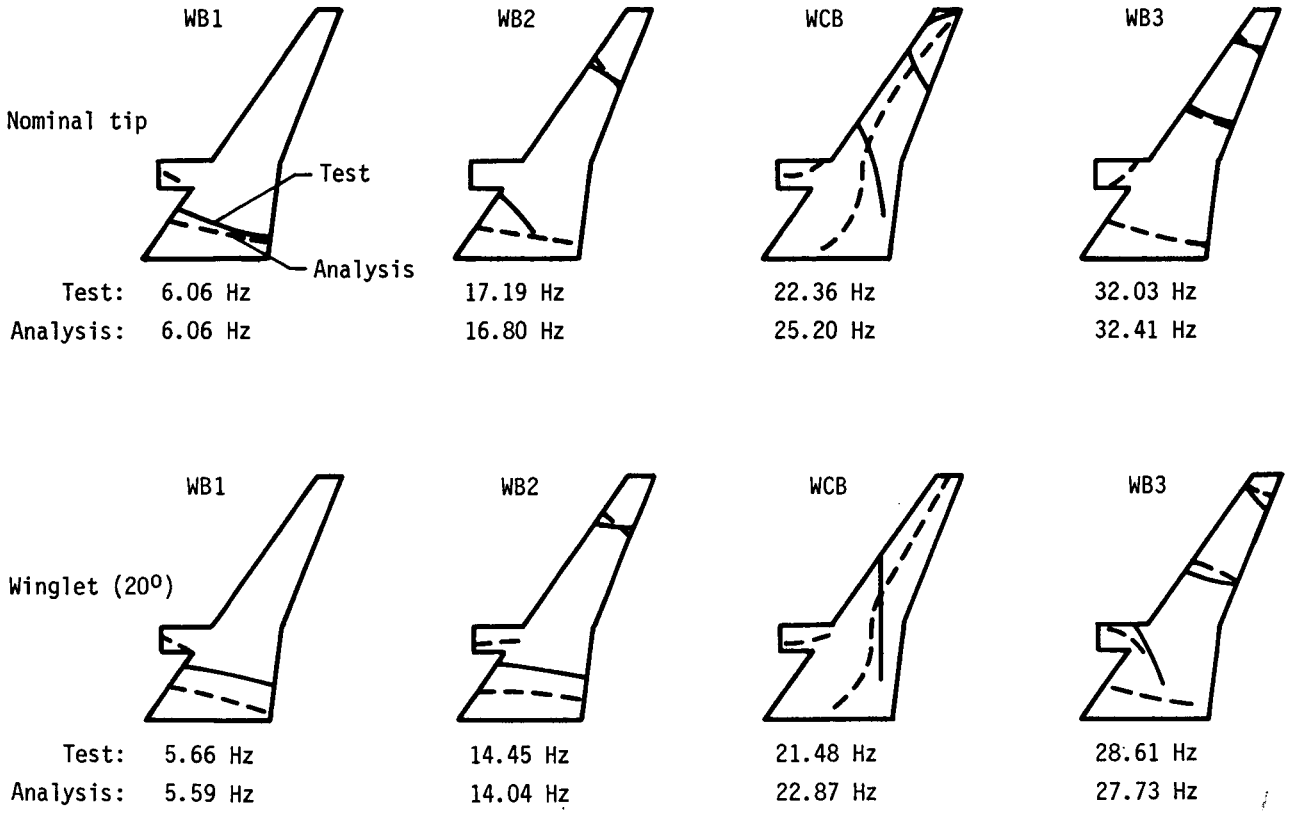

(a) Primary wing-bending modes.

Figure 6.- Measured and calculated vibration frequencies and node lines of transonic model for configuration with nominal nacelle/full wing/different wingtips.

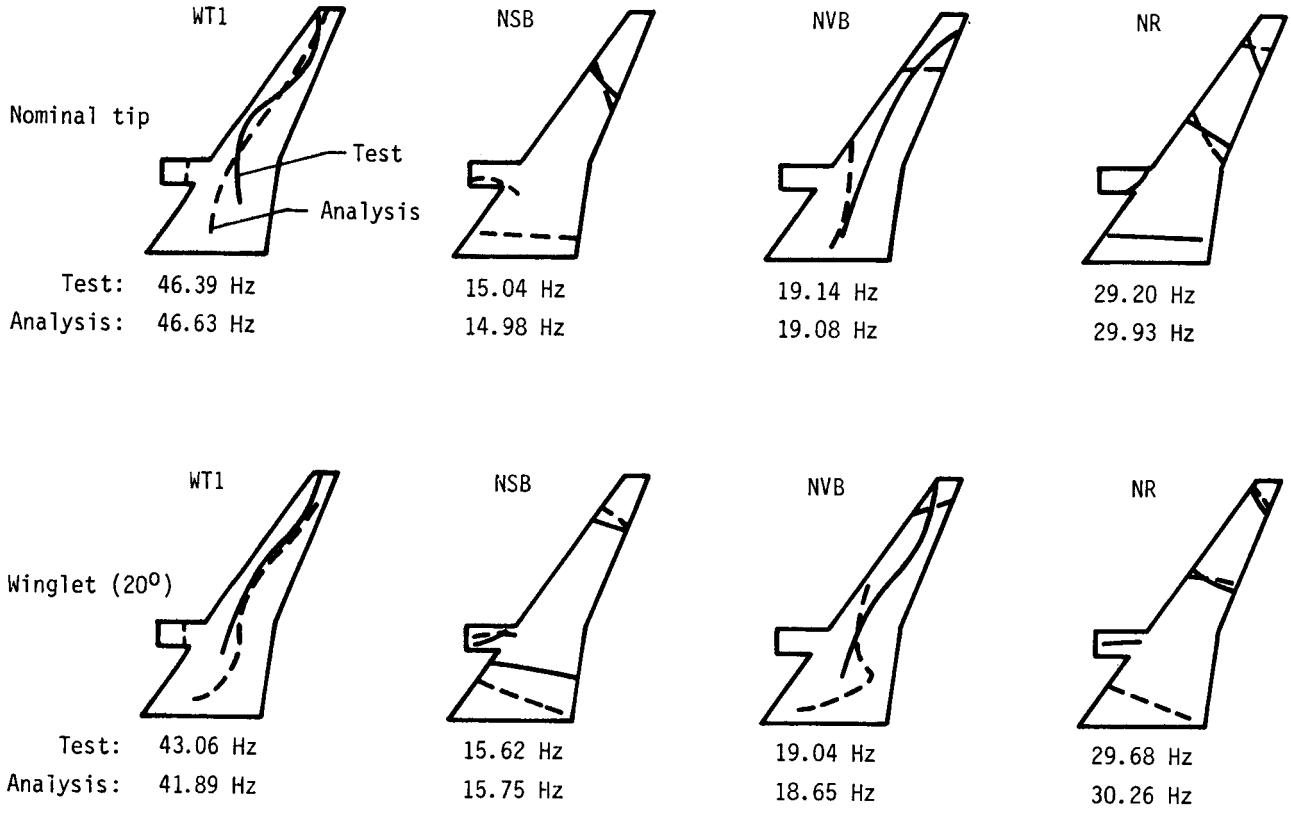

(b) Wing torsion and nacelle modes.

Figure 6.- Concluded.

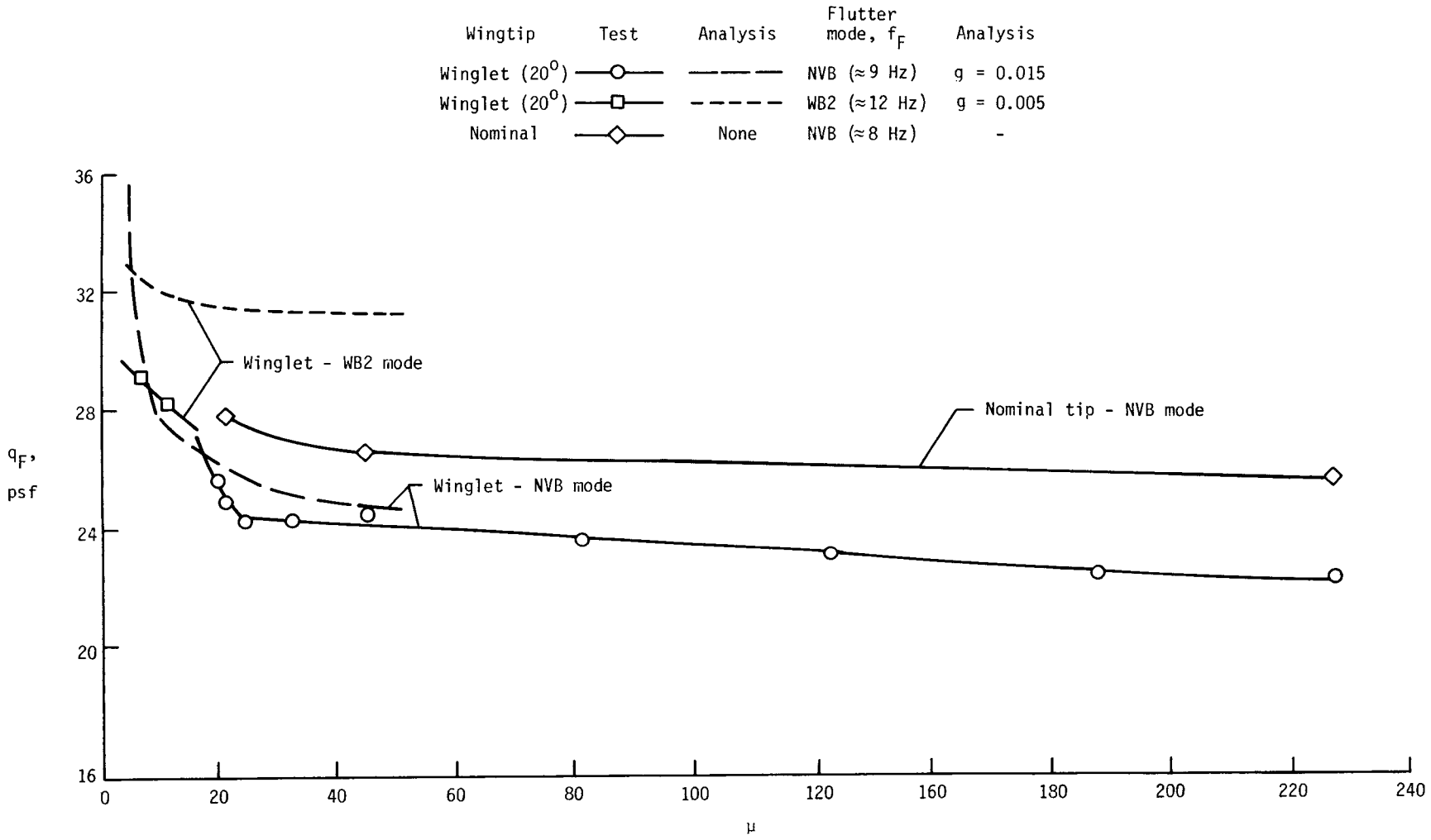

(a) Mass-density-ratio effects on q_F.

Figure 7.- TDT test-analysis correlations for low-speed model for configuration with nominal nacelle/empty wing/nominal tip or winglet (20°).

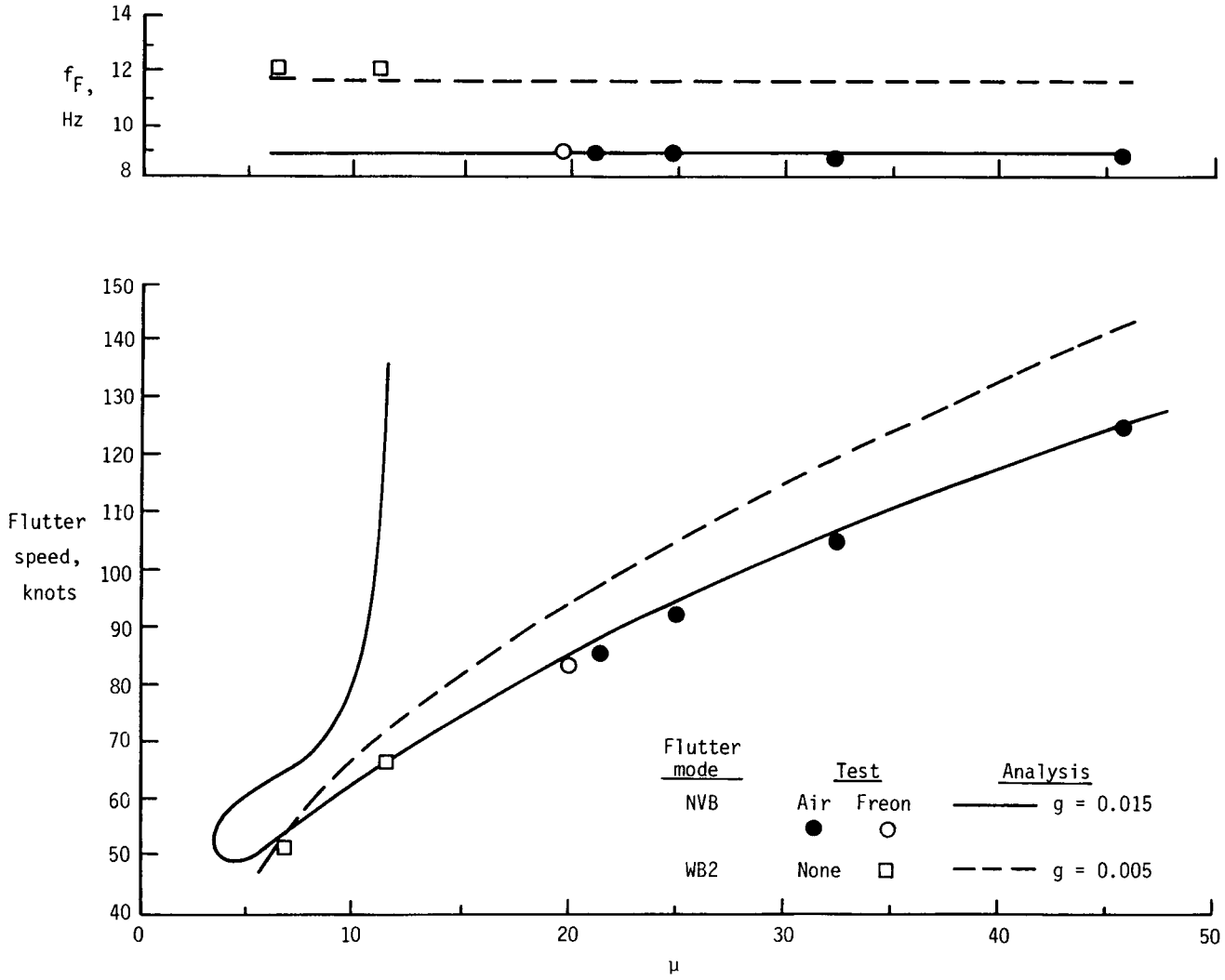

(b) Mass-density-ratio effects on flutter speed and frequency for winglet (20°) wingtip.

Figure 7.- Concluded.

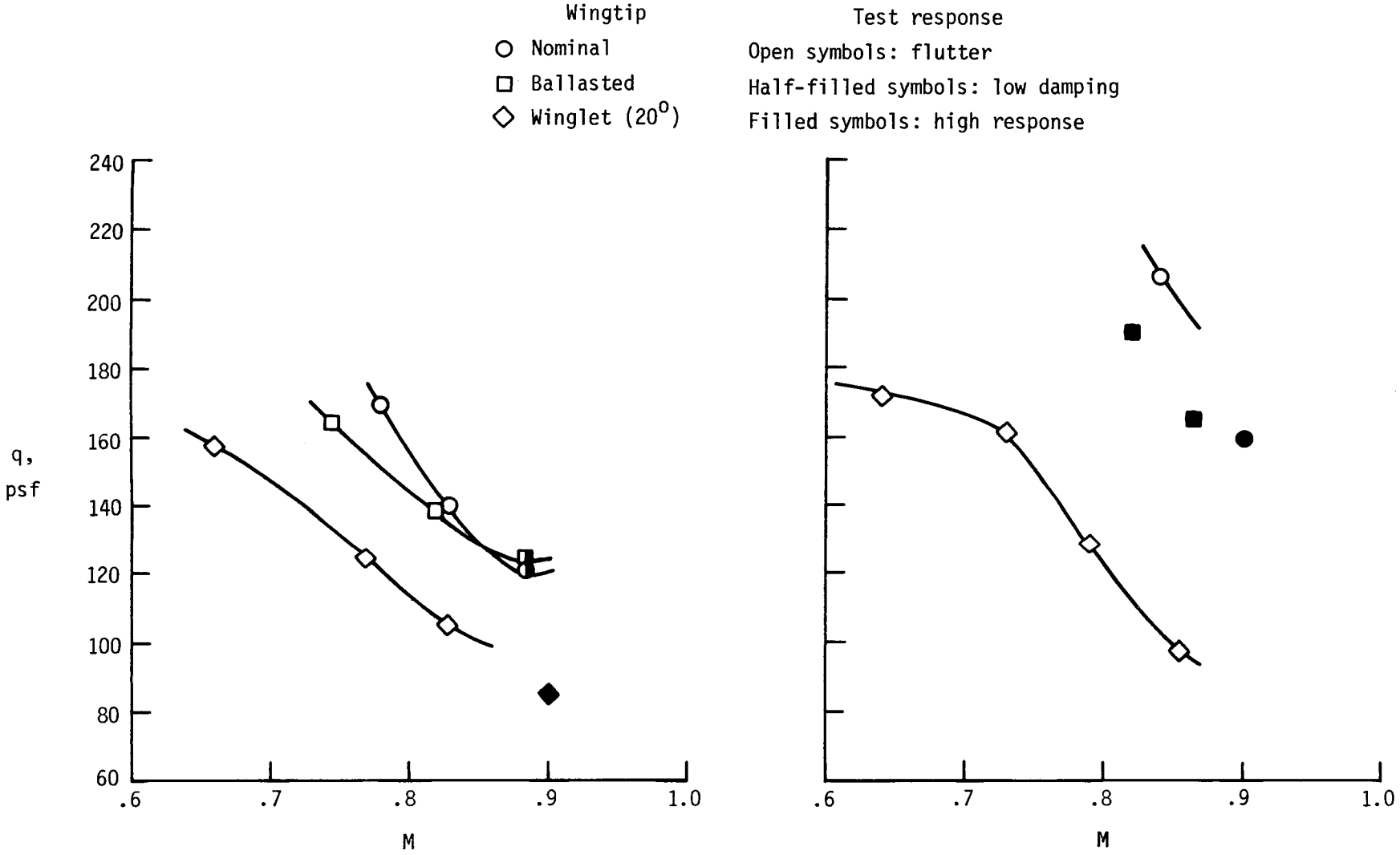

(a) Nominal nacelle/empty wing/different wingtips. (b) Nominal nacelle/full wing/different wingtips.

Figure 8.- Transonic test results showing wingtip effects on transonic-model configurations.

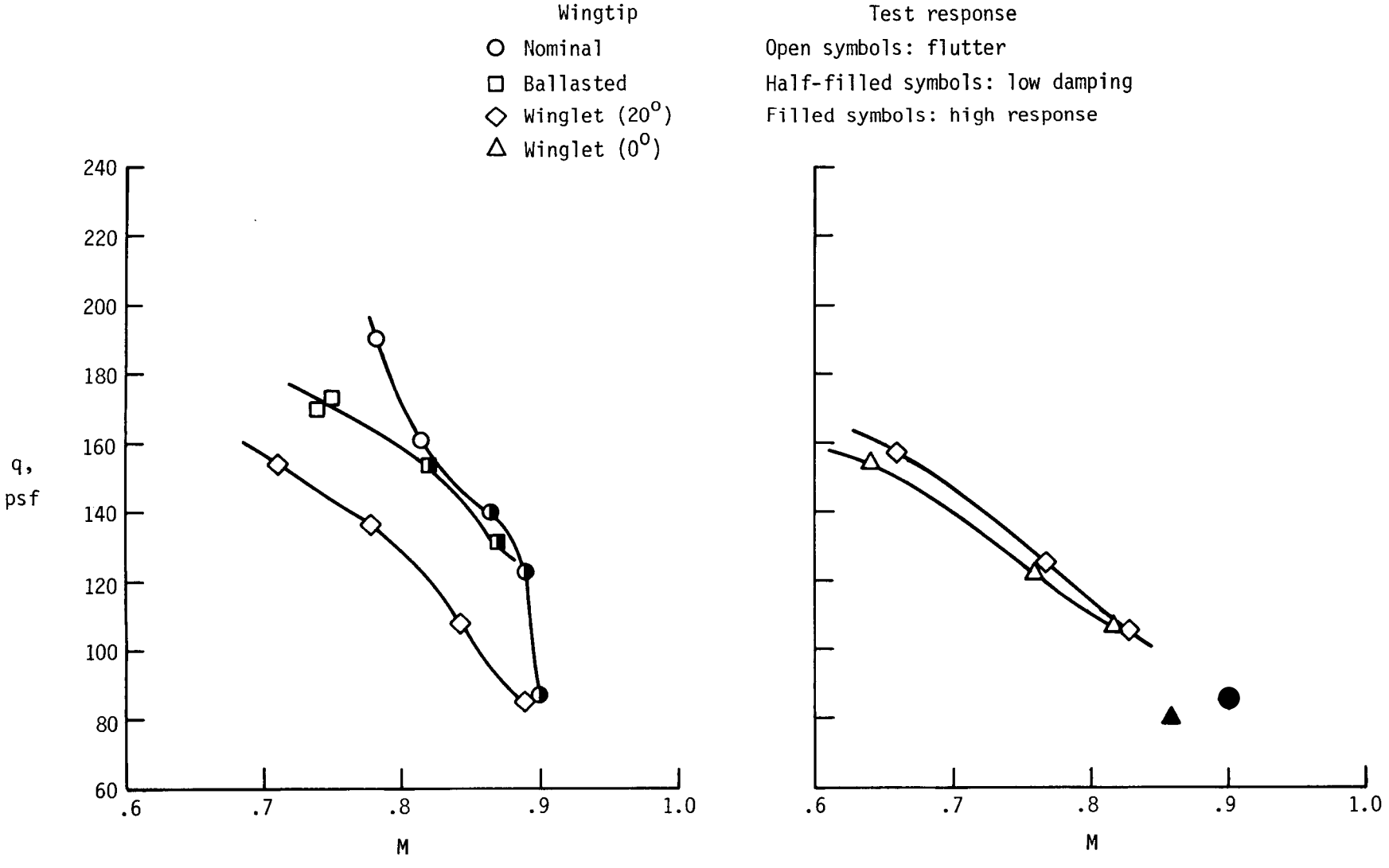

(c) Soft nacelle/empty wing/different wingtips.

(d) Nominal nacelle/empty wing/winglet (20° and 0°).

Figure 8.- Concluded.

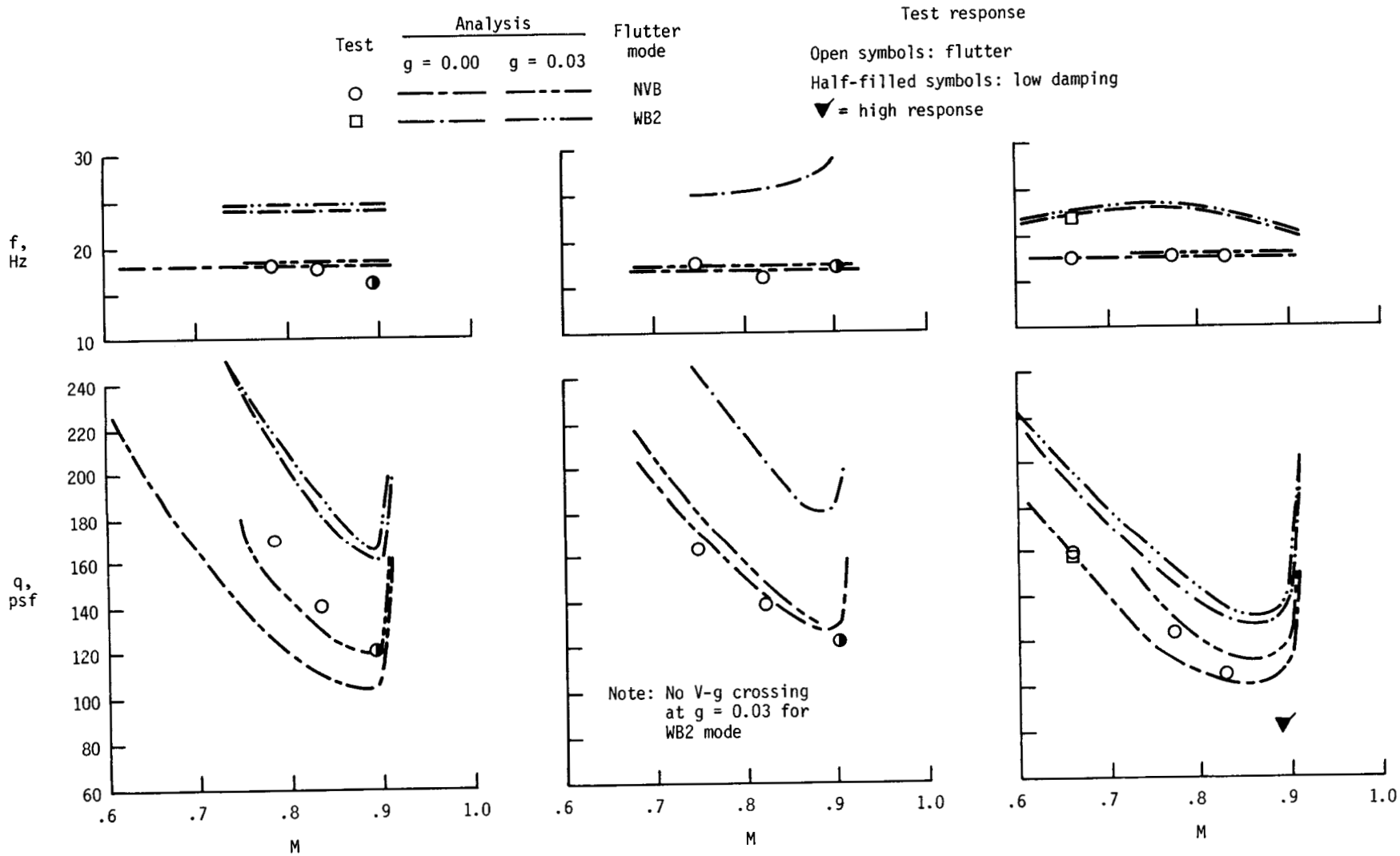

(a) Nominal tip.

(b) Ballasted tip.

(c) Winglet (20°).

Figure 9.- Transonic test-analysis correlations for configuration with nominal nacelle/empty wing/different wingtips.

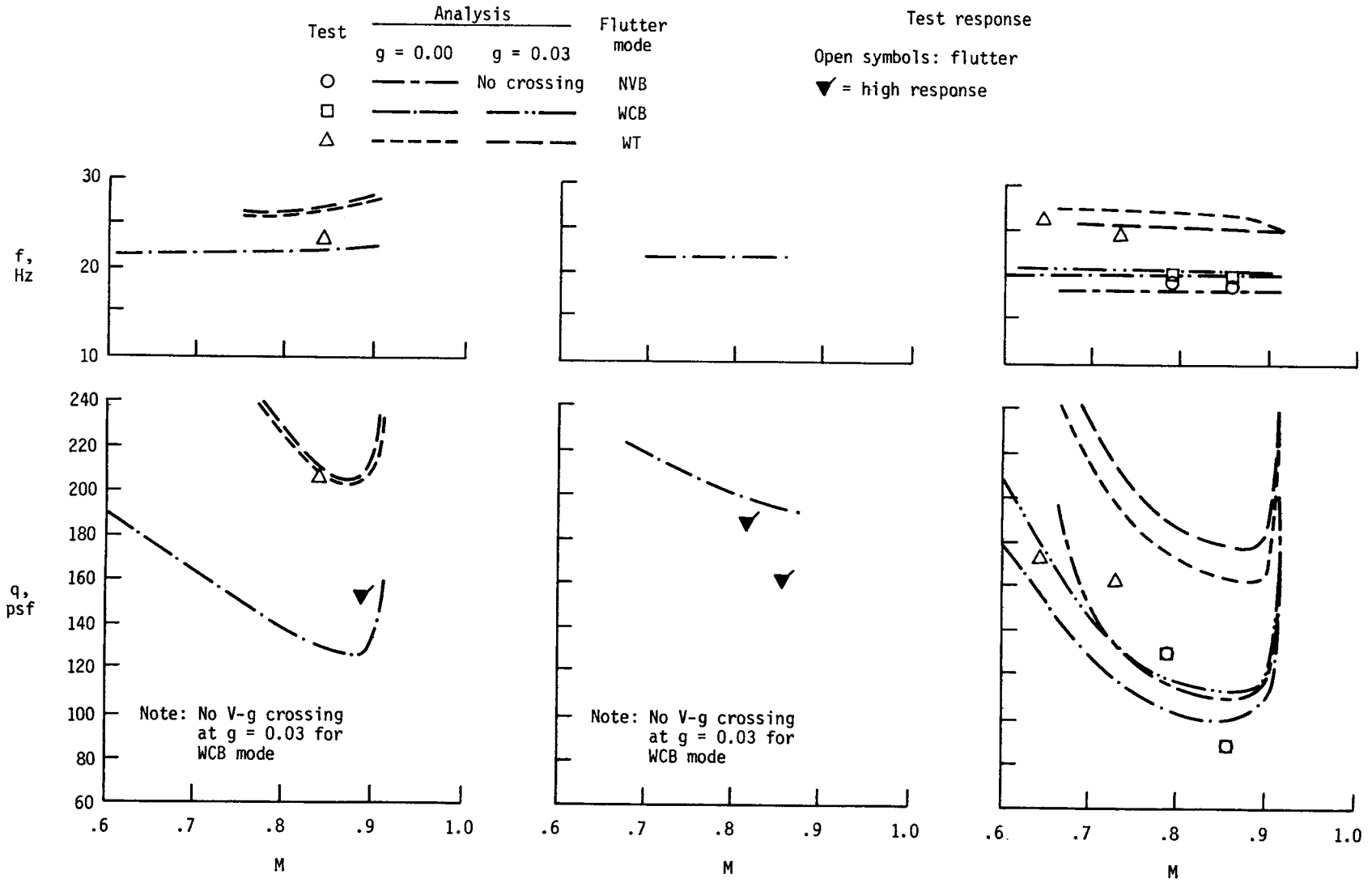

(a) Nominal tip. (b) Ballasted tip. (c) Winglet (20°).

Figure 10.- Transonic test-analysis correlations for configuration with nominal nacelle/full wing/different wingtips.

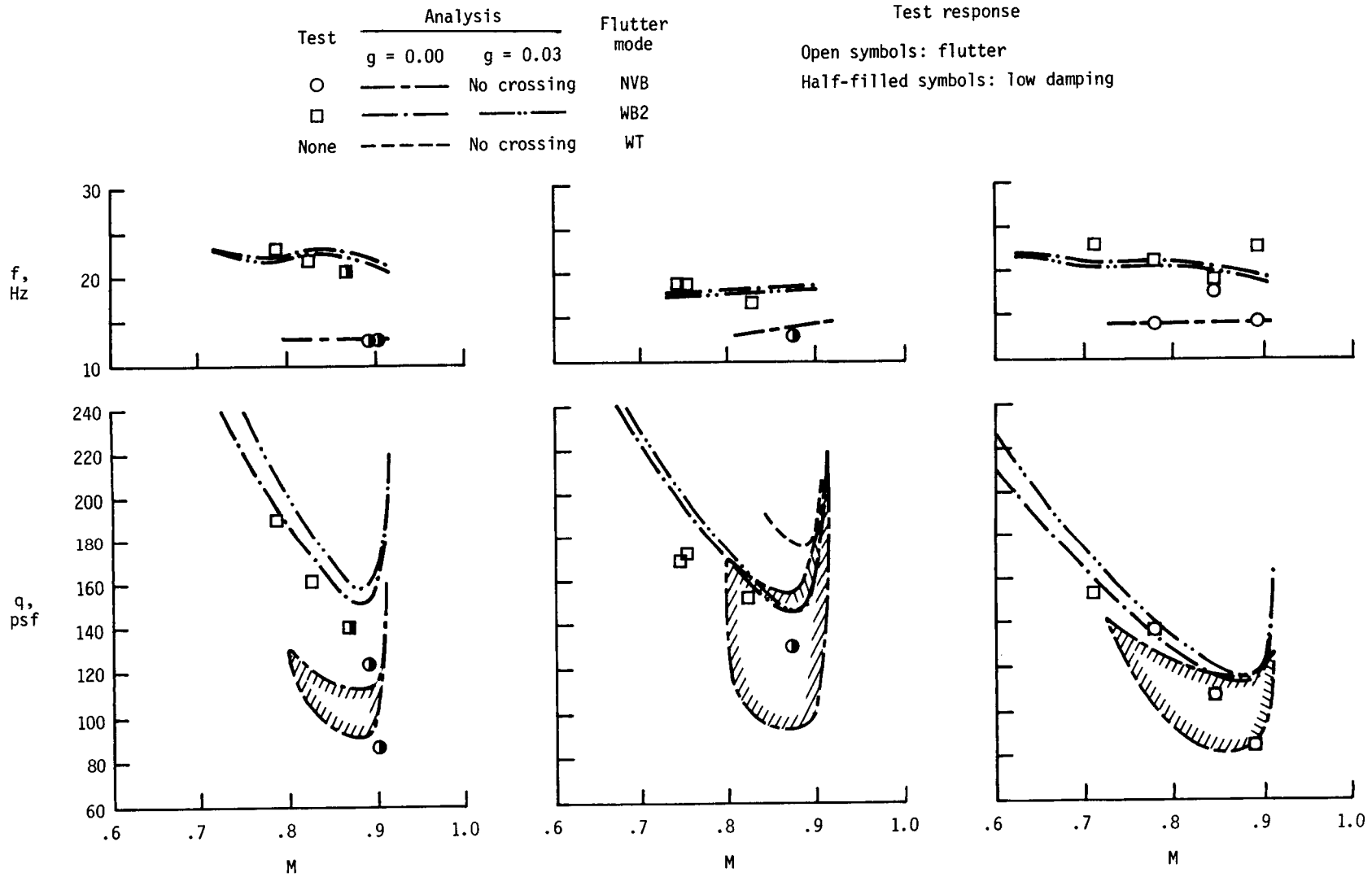

(a) Nominal tip. (b) Ballasted tip. (c) Winglet (20°).

Figure 11.- Transonic test-analysis correlations for configuration with soft nacelle/empty wing/different wingtips.

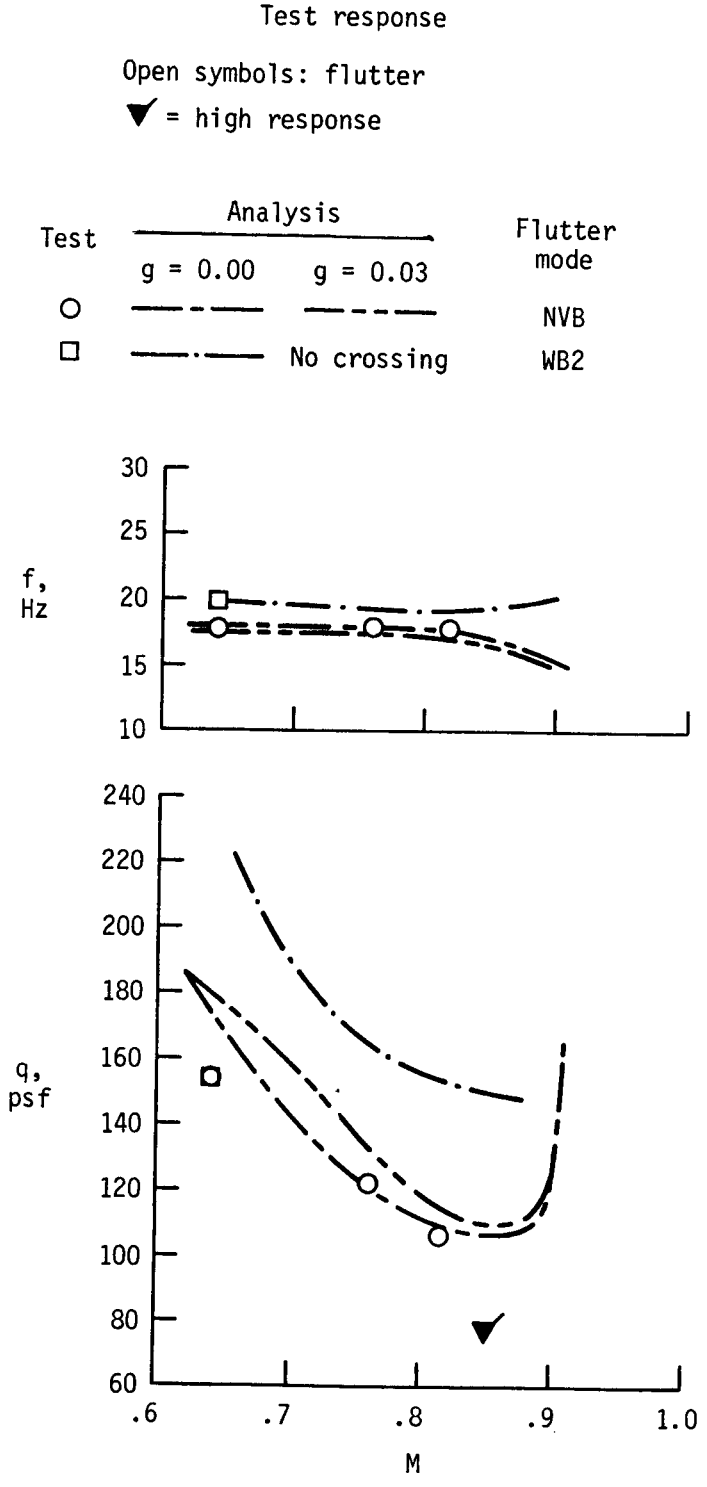

Figure 12.- Transonic test-analysis correlation for configuration with nominal nacelle/empty wing/winglet (0°).

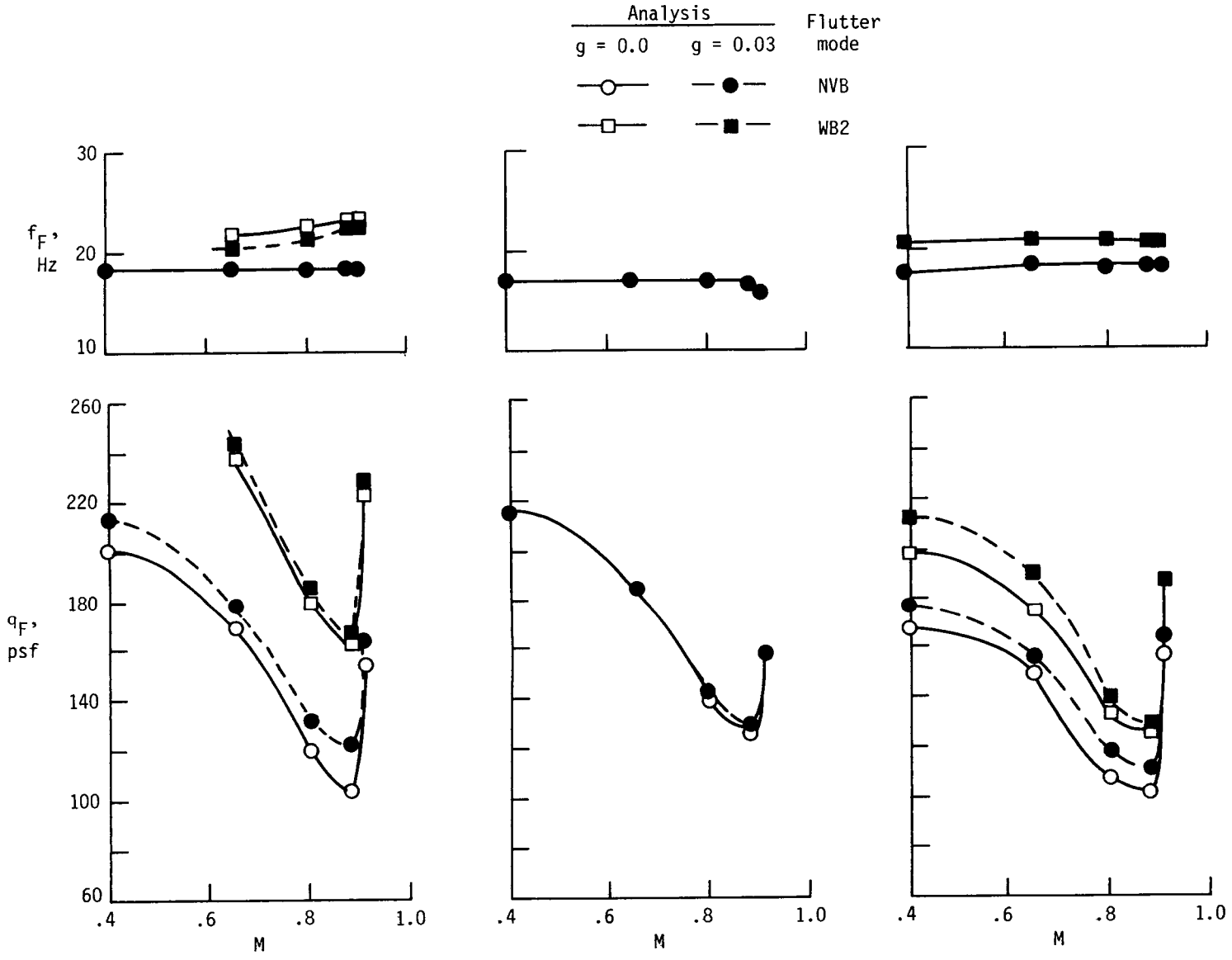

(a) Nominal tip. (b) Ballasted tip. (c) Winglet (20°).

Figure 13.- Analytical effect of M on q_F of critical flutter modes at constant density (ρ = 0.00111 slug/ft^3). Transonic-model configuration; nominal nacelle/empty wing/ different wingtips.

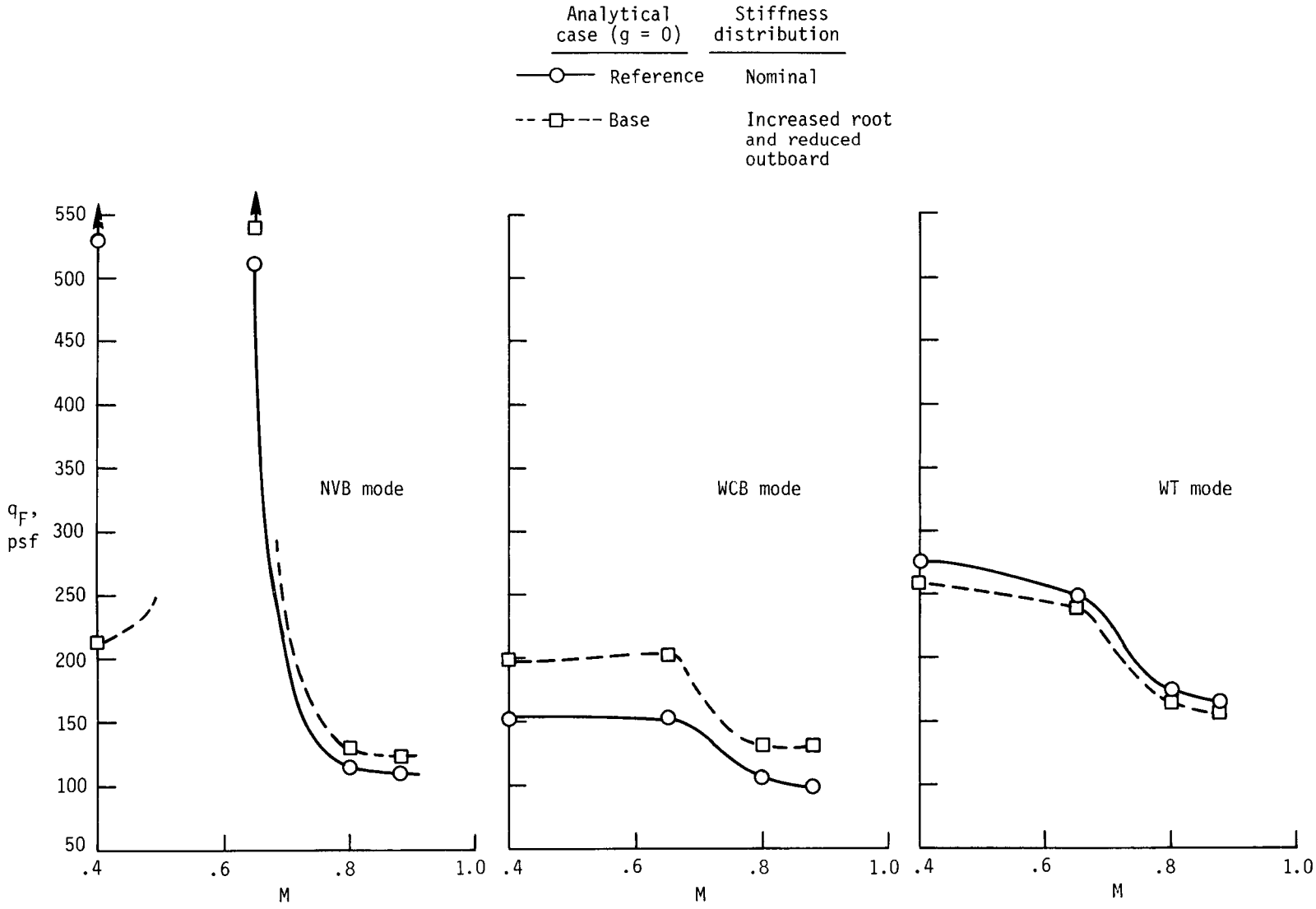

(a) Effect of variations in wing chordwise-bending stiffness.

Figure 14.- Analytical sensitivity of q_F for flutter critical modes to parameter changes. Transonic-model configuration; nominal nacelle/full wing/winglet (20°).

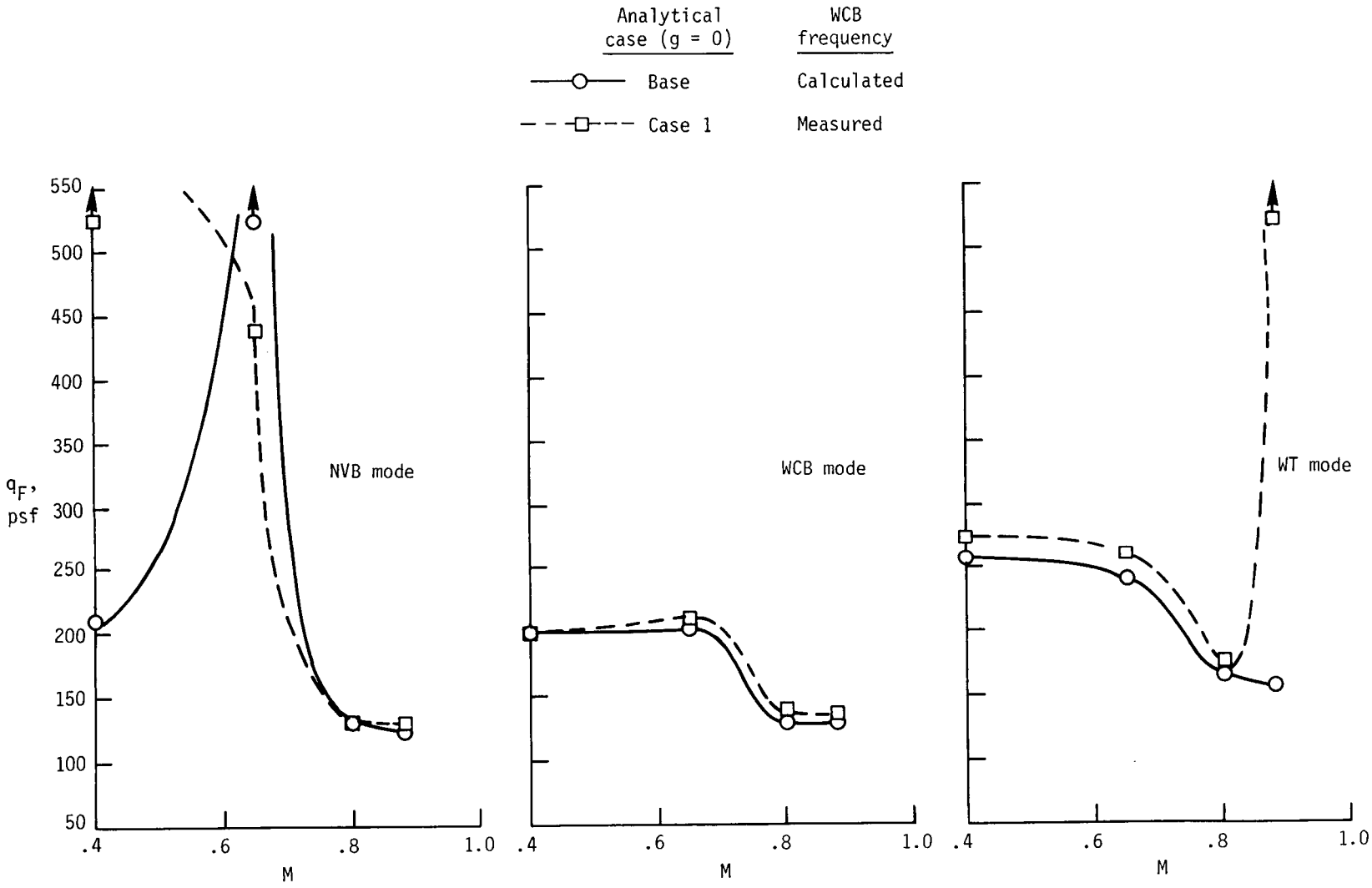

(b) Effect of tuning vibration-mode frequencies.

Figure 14.- Continued.

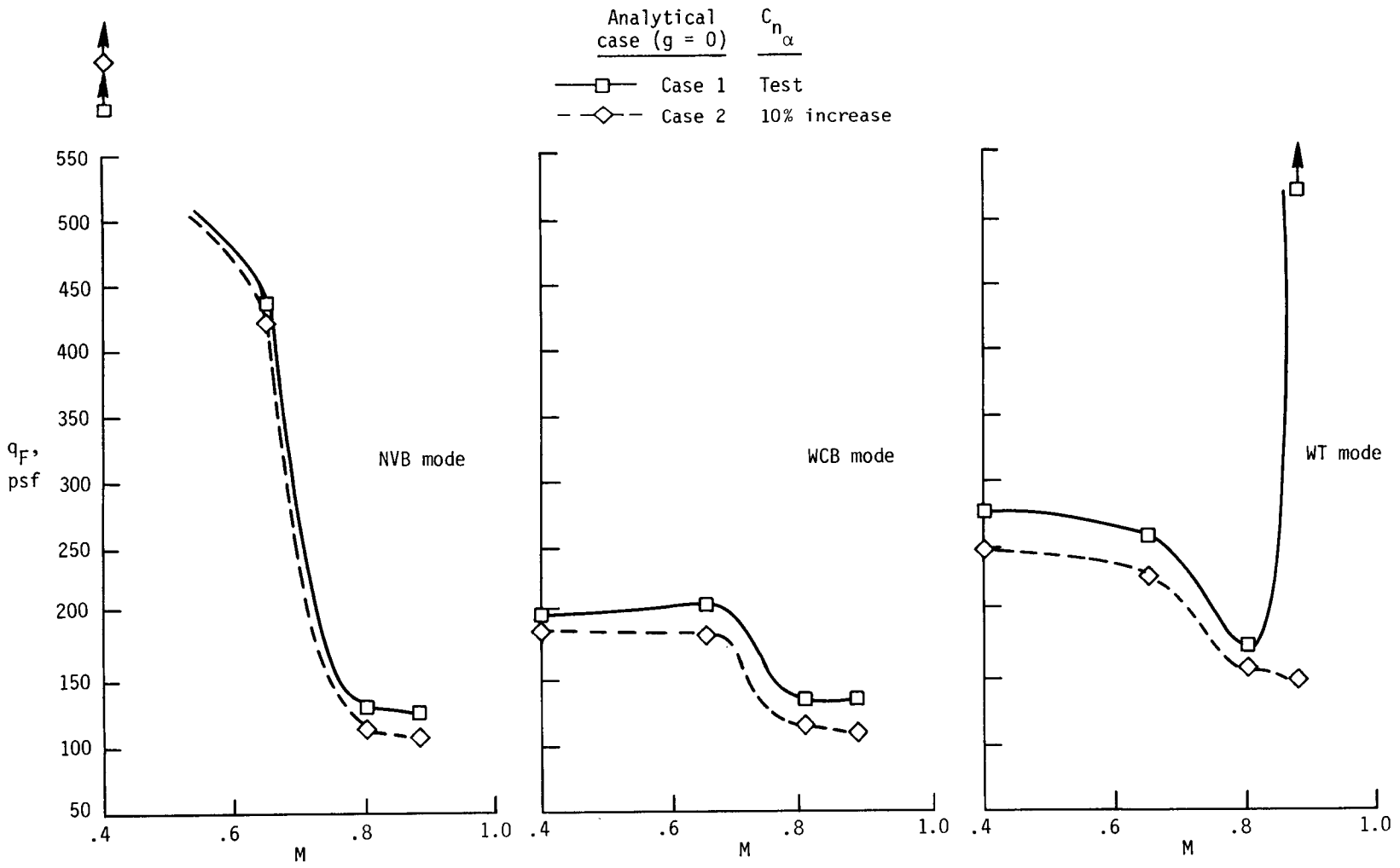

(c) Effect of increasing C_{n_α} by 10 percent.

Figure 14.- Continued.

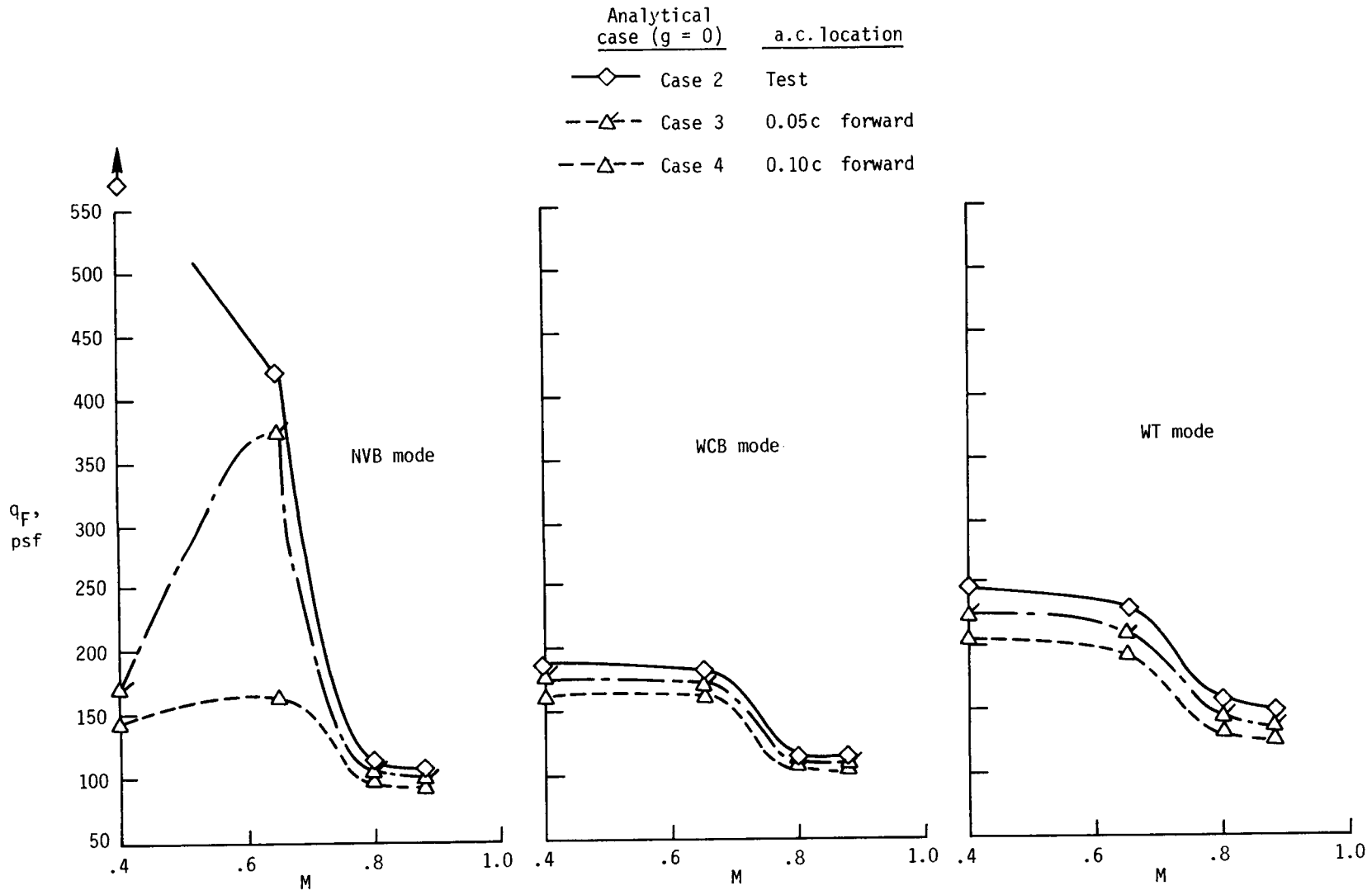

(d) Effect of moving a.c. location forward on wing chord.

Figure 14.- Continued.

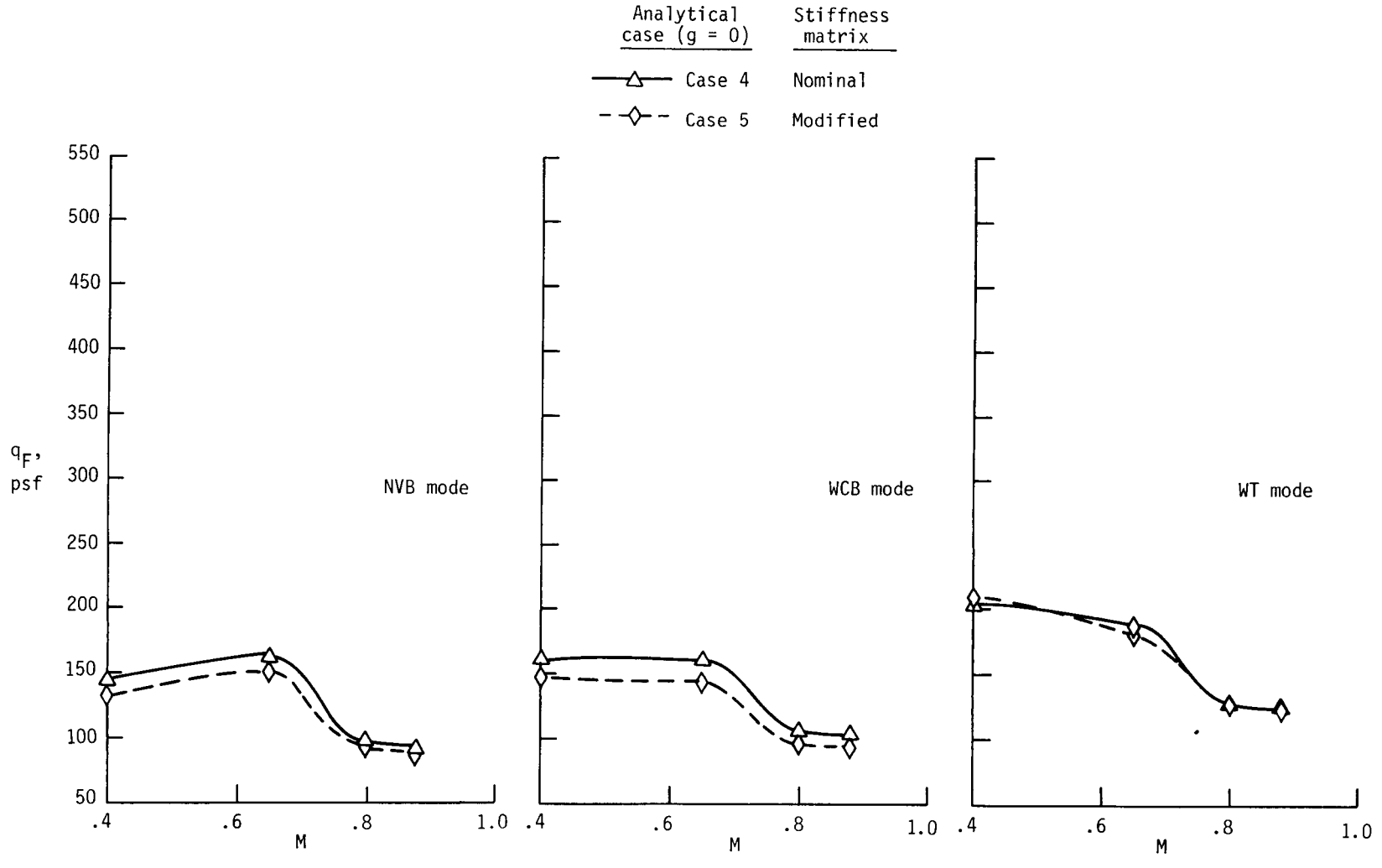

(e) Effect of stiffness matrix modification.

Figure 14.- Continued.

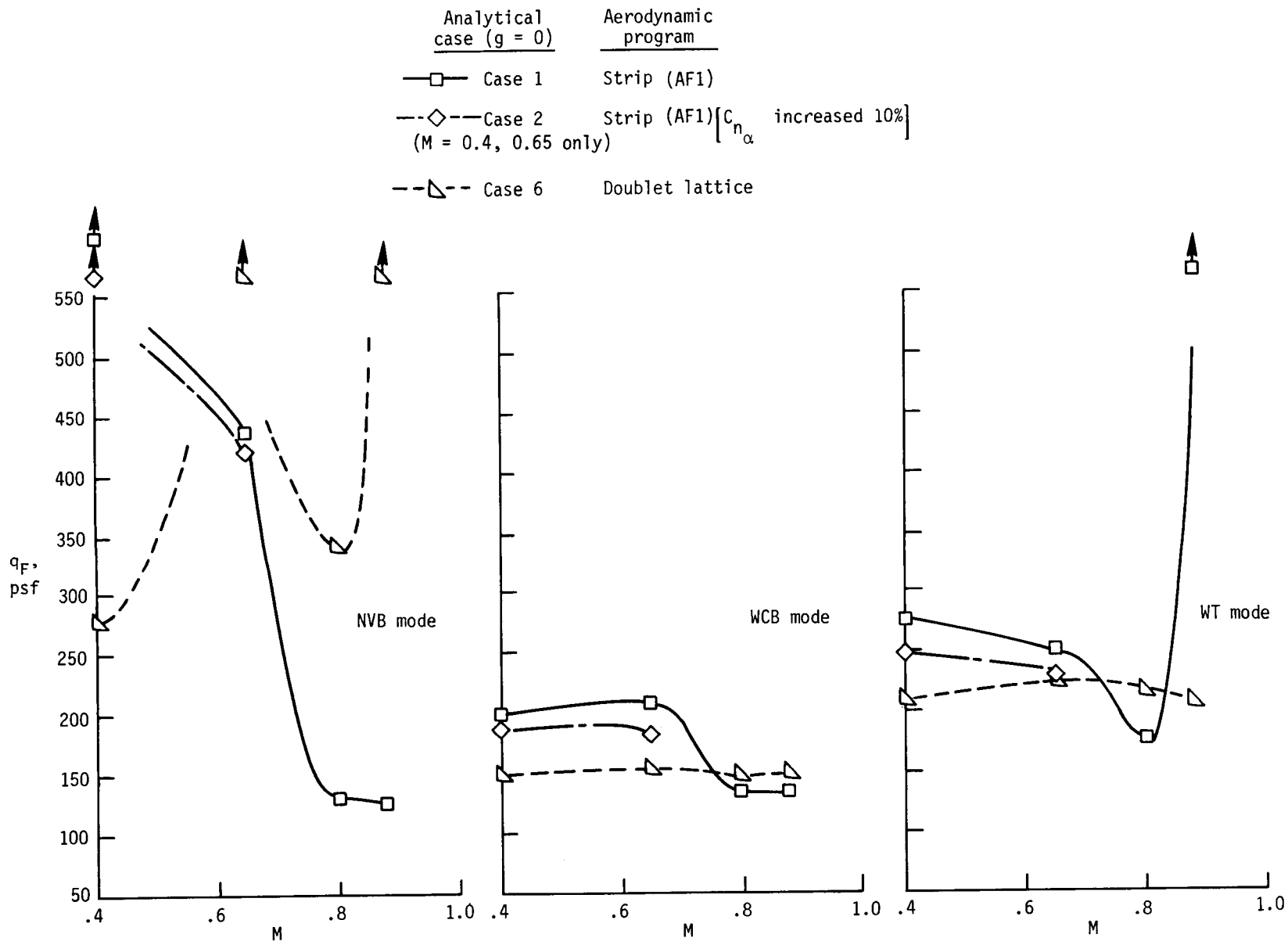

(f) Effect of using theoretical doublet-lattice aerodynamics.

Figure 14.- Concluded.

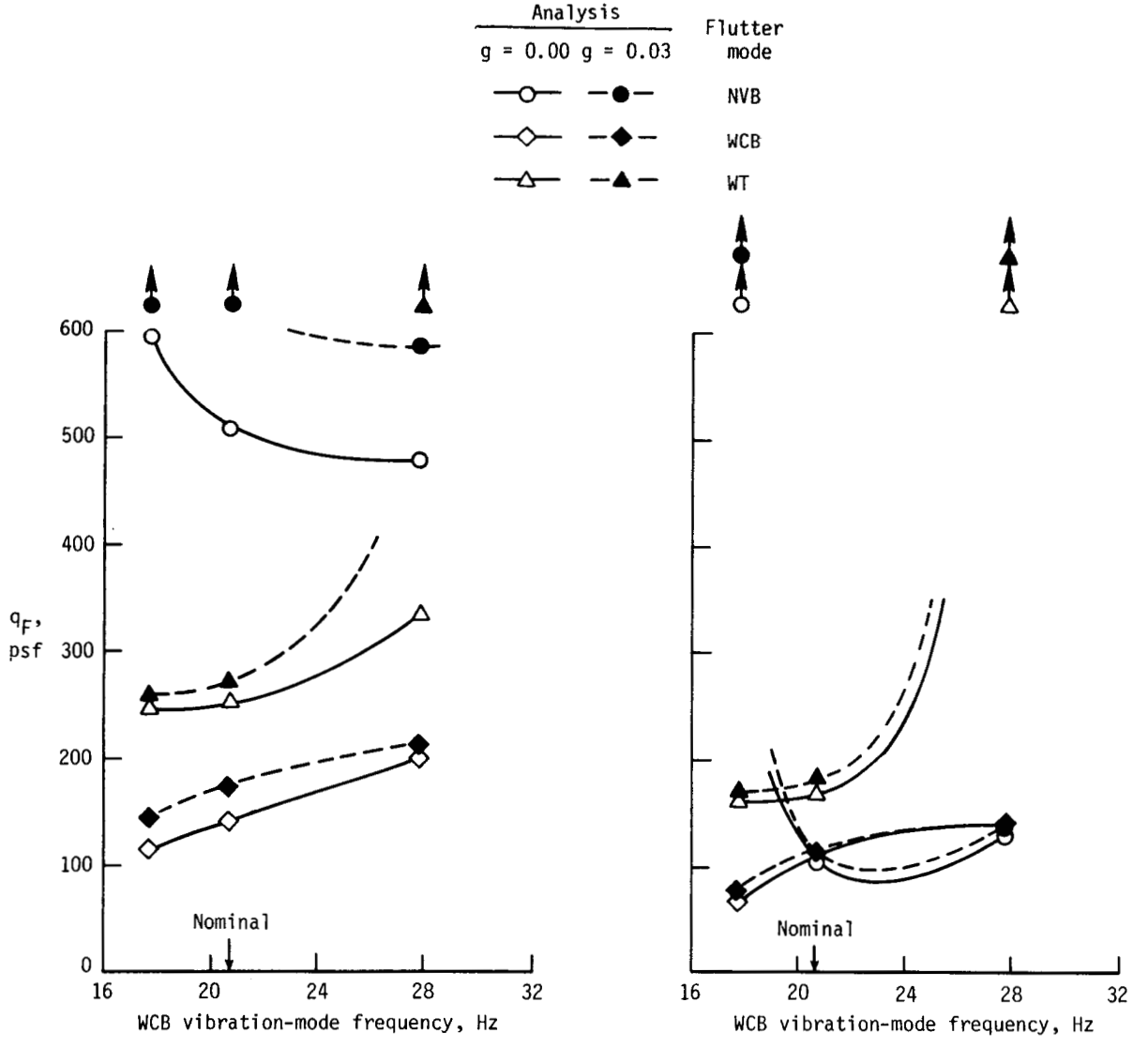

(a) M = 0.65; ρ = 0.00350 slug/ft^3. (b) M = 0.88; ρ = 0.00111 slug/ft^3.

Figure 15.- Analytical effect on q_F of varying frequency of wing chordwise-bending vibration mode. Transonic-model configuration; nominal nacelle/full wing/winglet (20°).

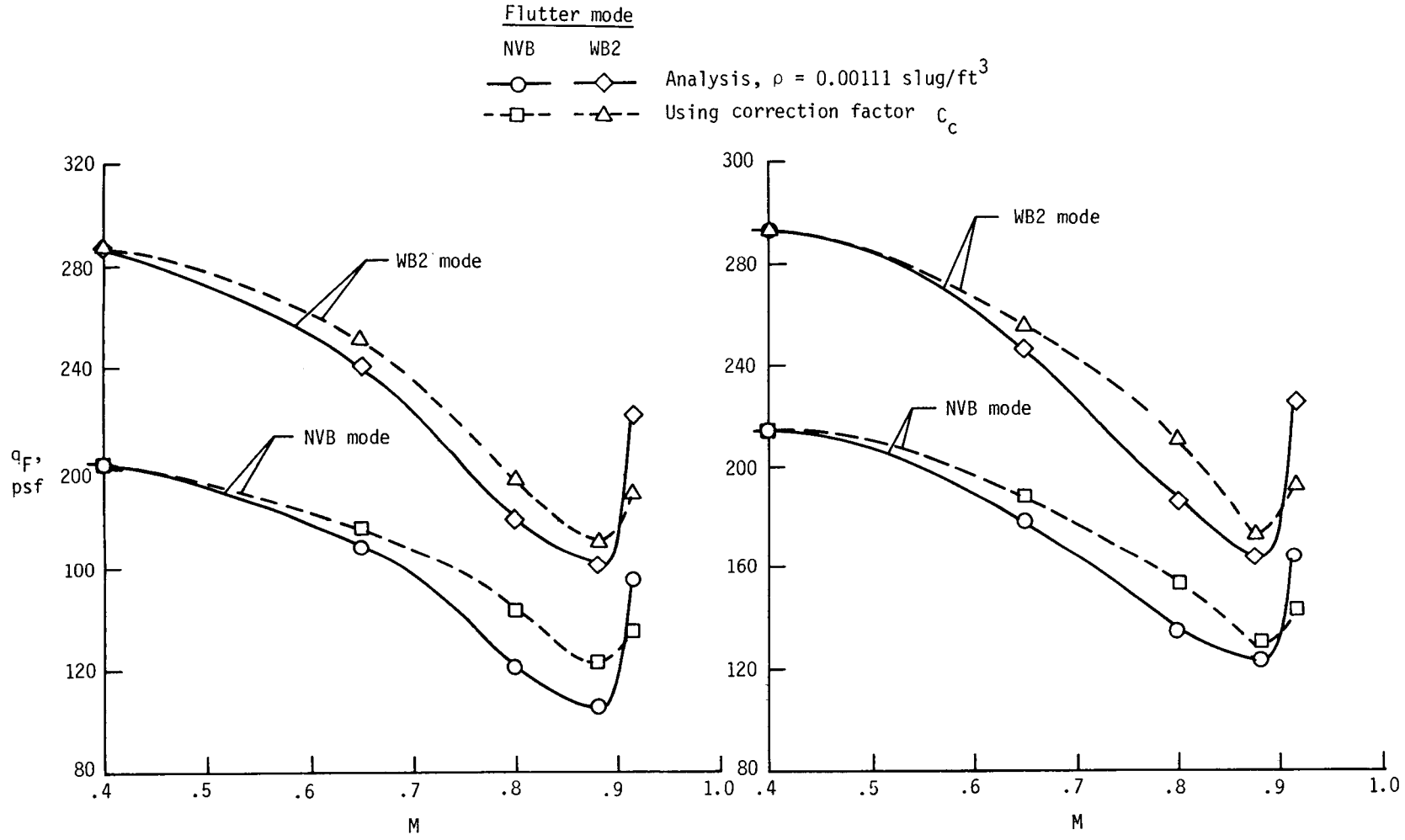

Figure 16.- Flutter boundaries determined by analysis and by using compressibility correction factor C_c. Transonic-model configuration; nominal nacelle/empty wing/different wingtips.

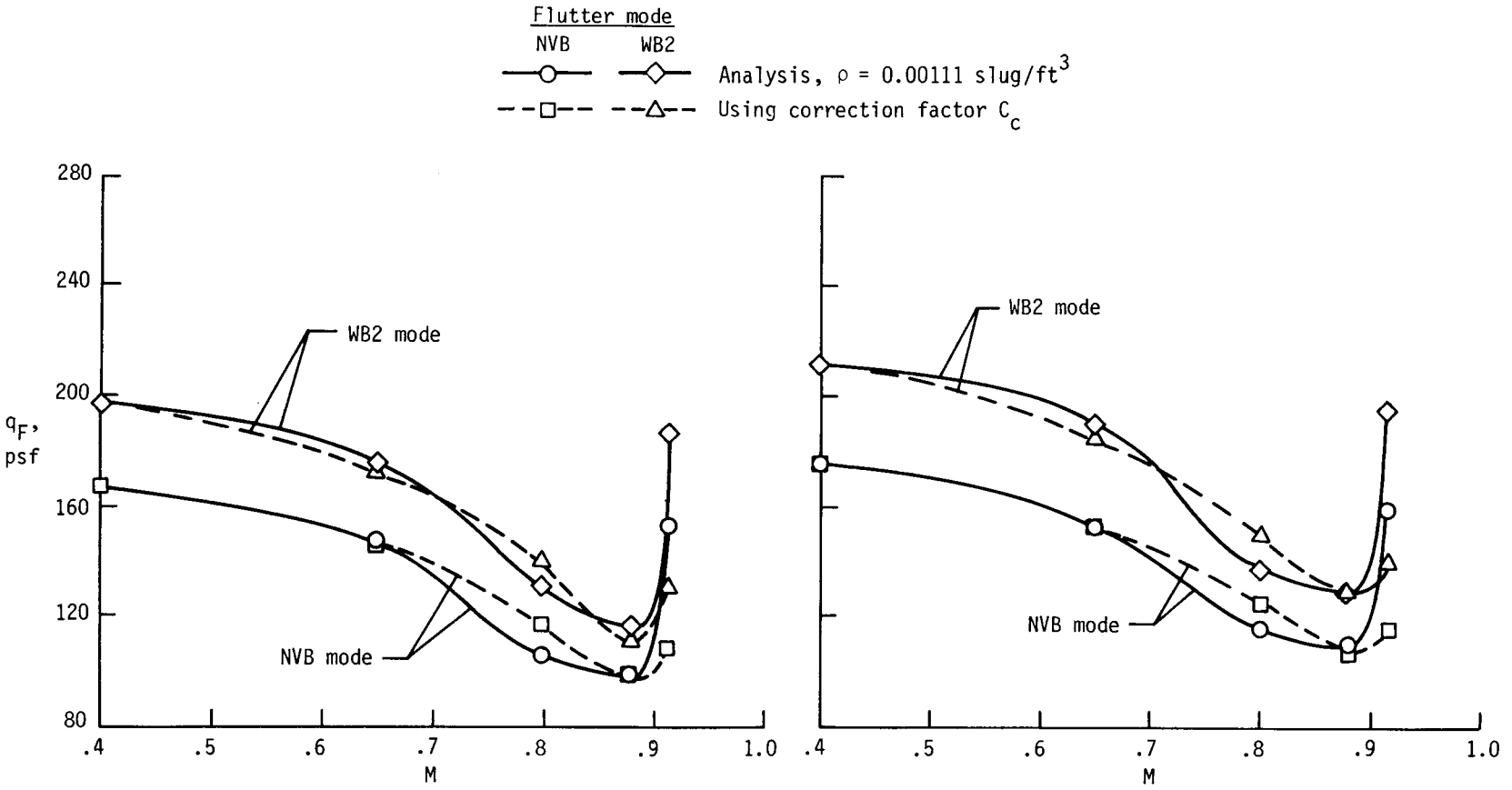

(c) Winglet (20°), g = 0.00.

(d) Winglet (20°), g = 0.03.

Figure 16.- Concluded.

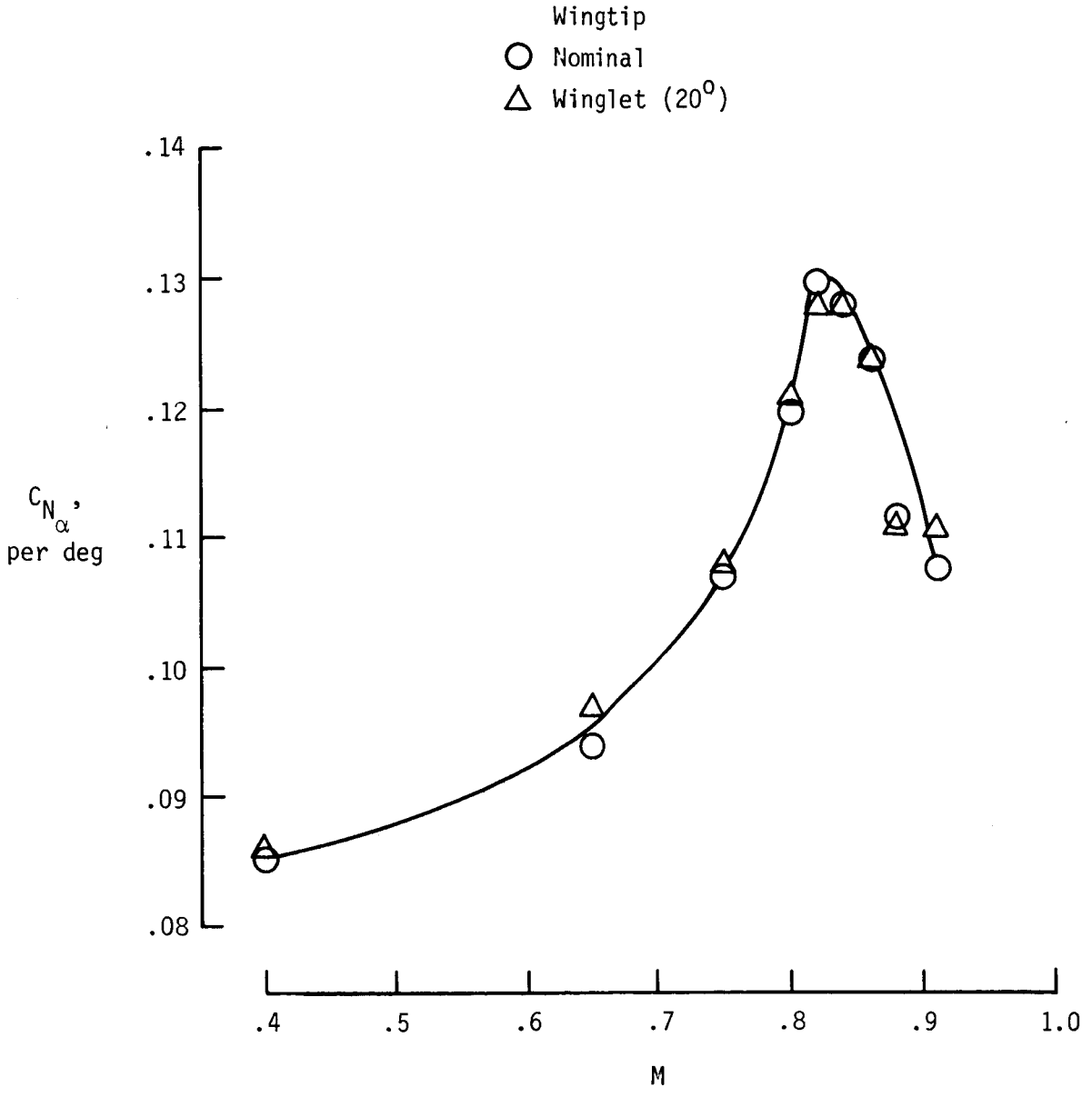

Figure 17.- Measured Mach number variation of total normal curve slope of semispan wing with nacelle.

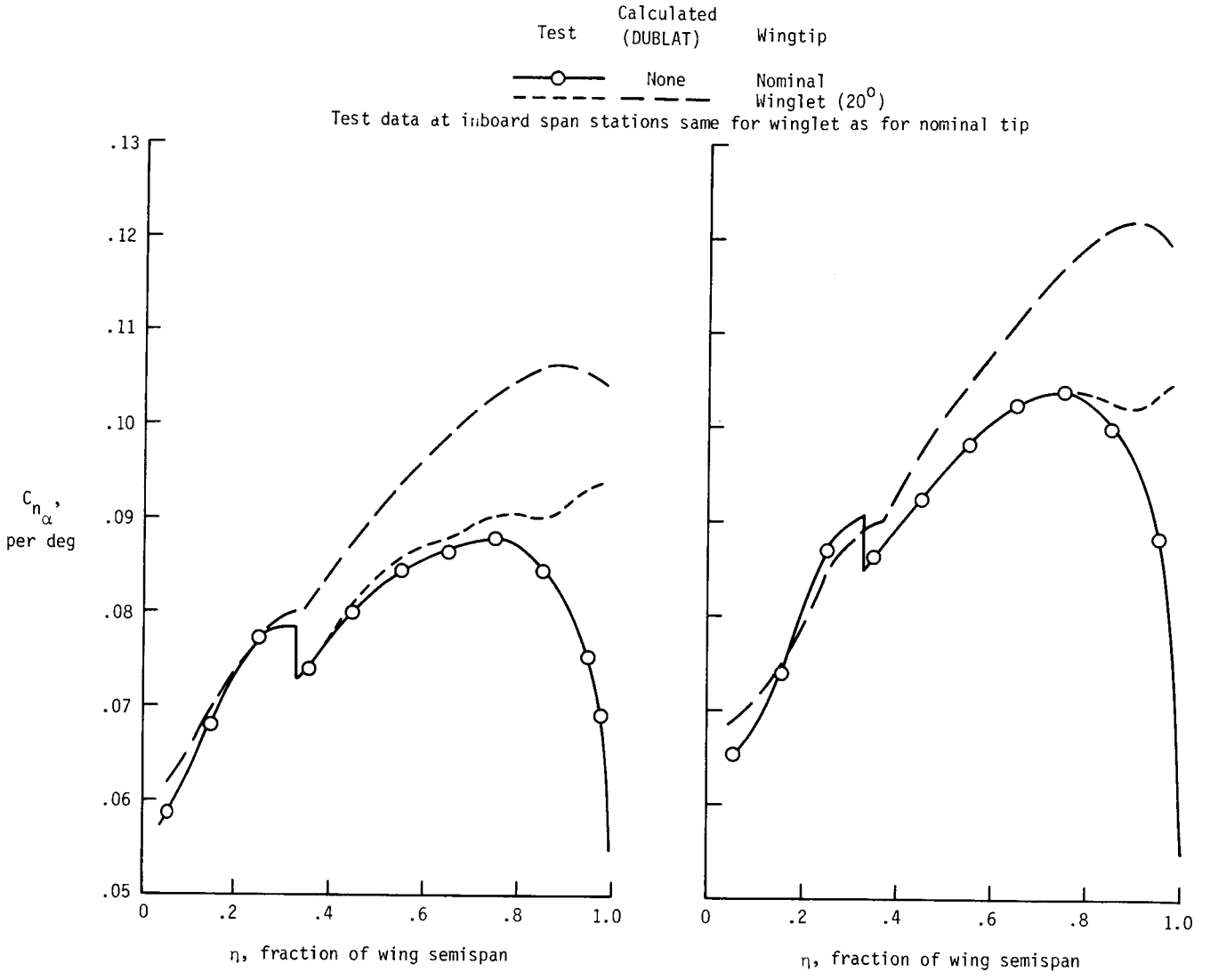

(a) M = 0.40.

(b) M = 0.65.

Figure 18.- Measured and calculated distributions of normal curve slope for wing with nacelle.

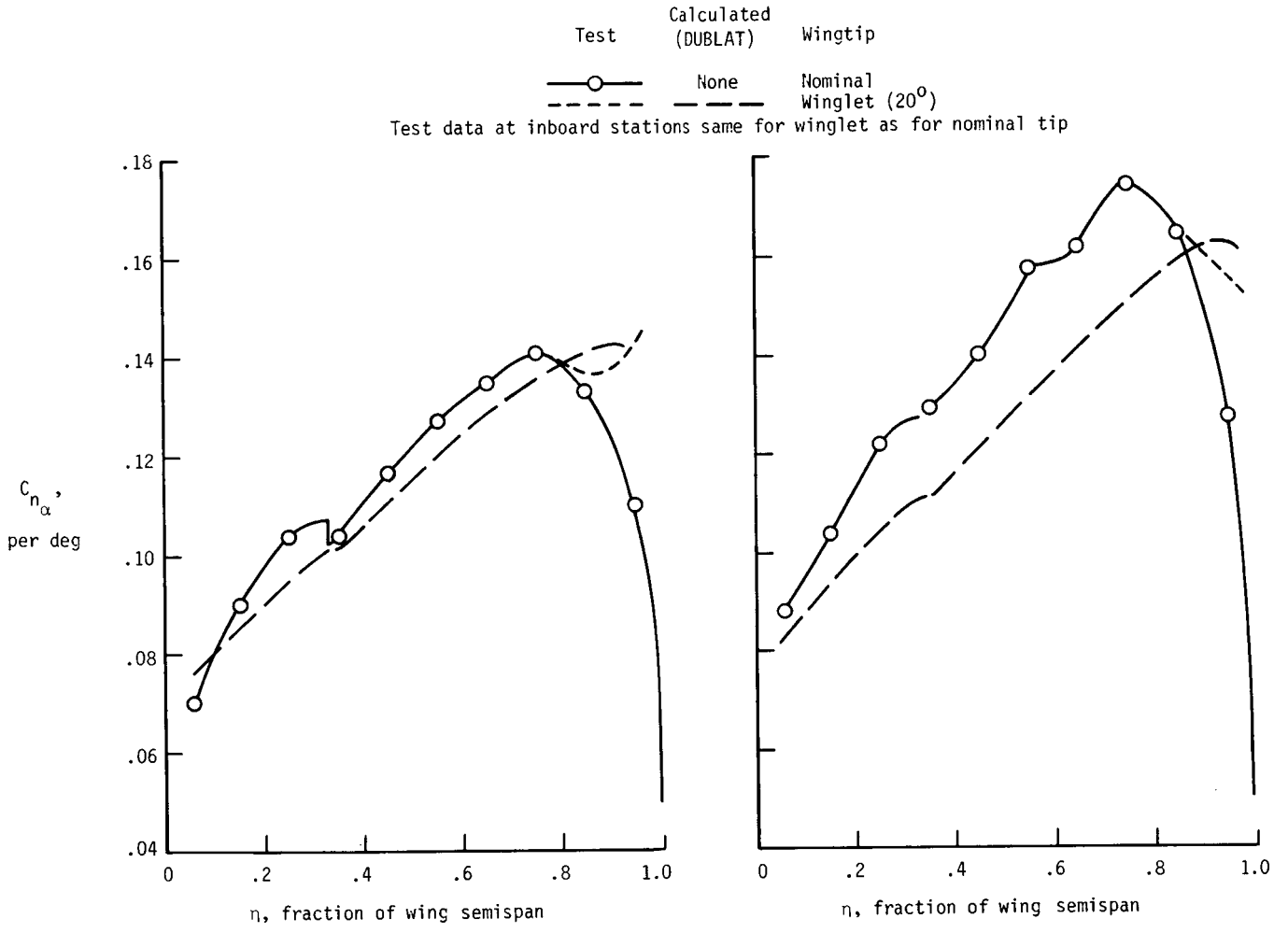

(c) M = 0.80.

(d) M = 0.88.

Figure 18.- Continued.

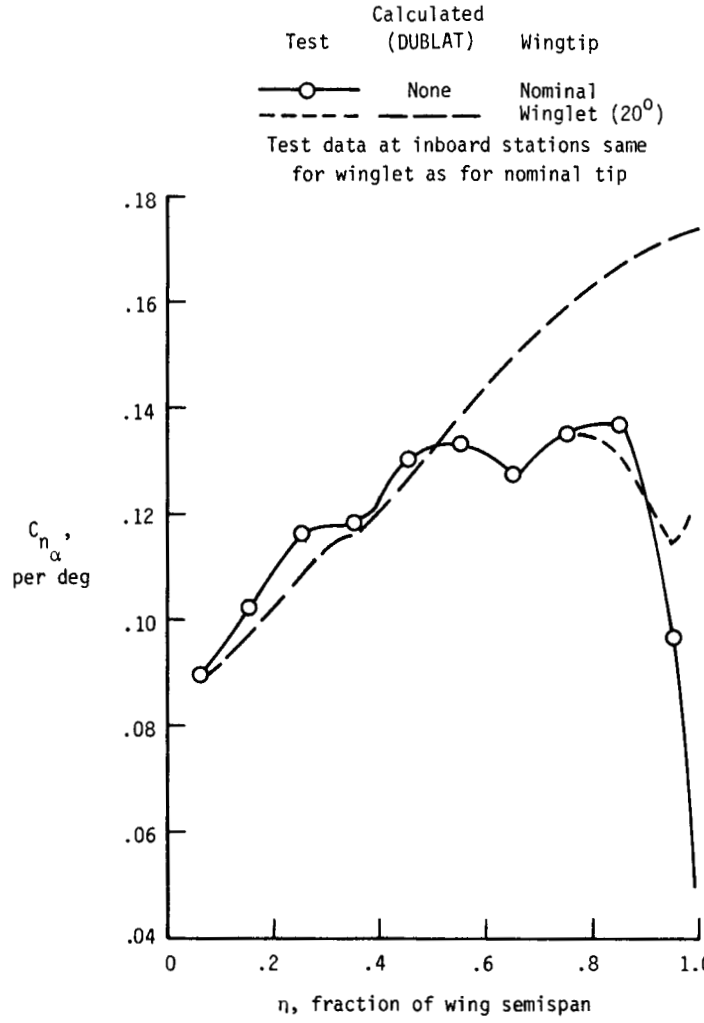

(e) M = 0.91.

Figure 18.- Concluded.

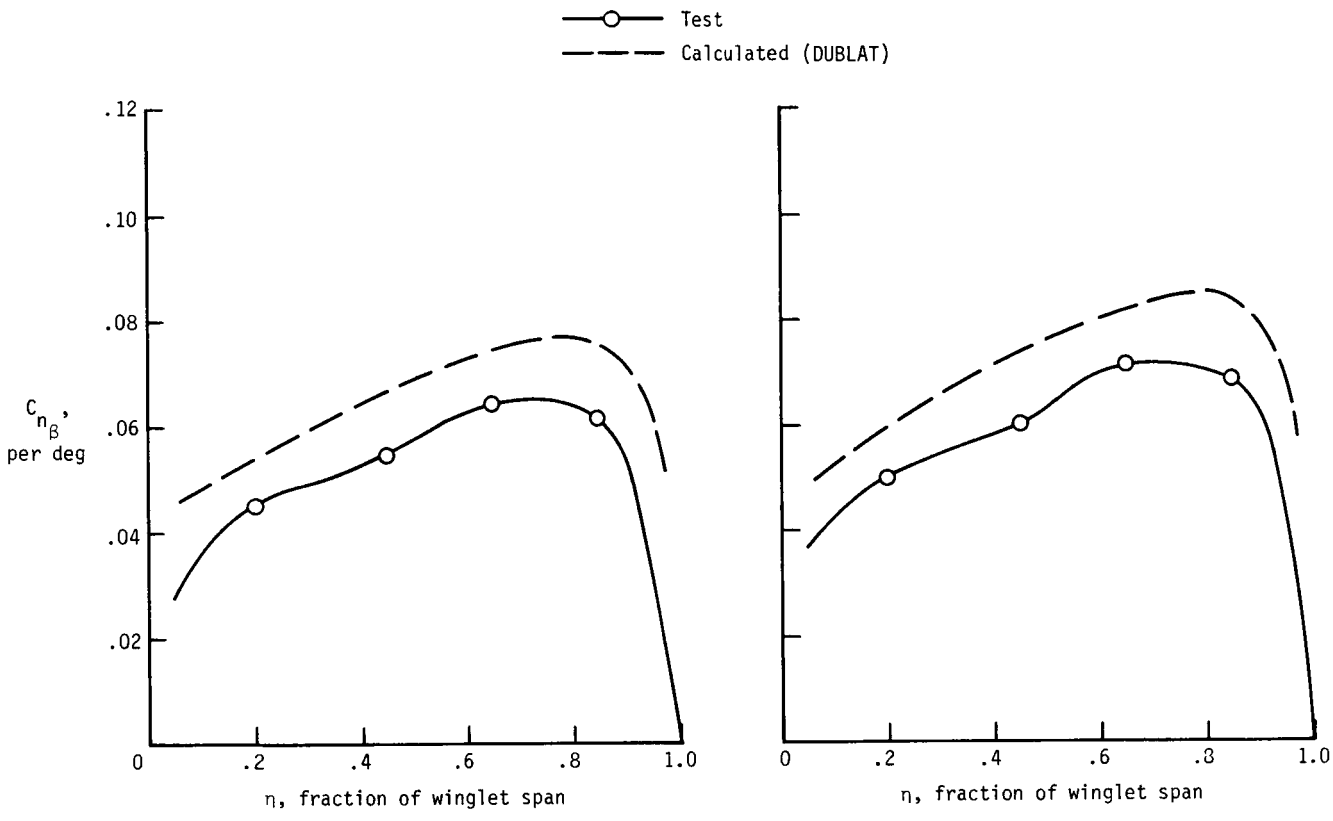

(a) M = 0.40.

(b) M = 0.65.

Figure 19.- Measured and calculated distributions of winglet normal curve slope. Winglet (20°) is attached at wingtip to wing with nacelle.

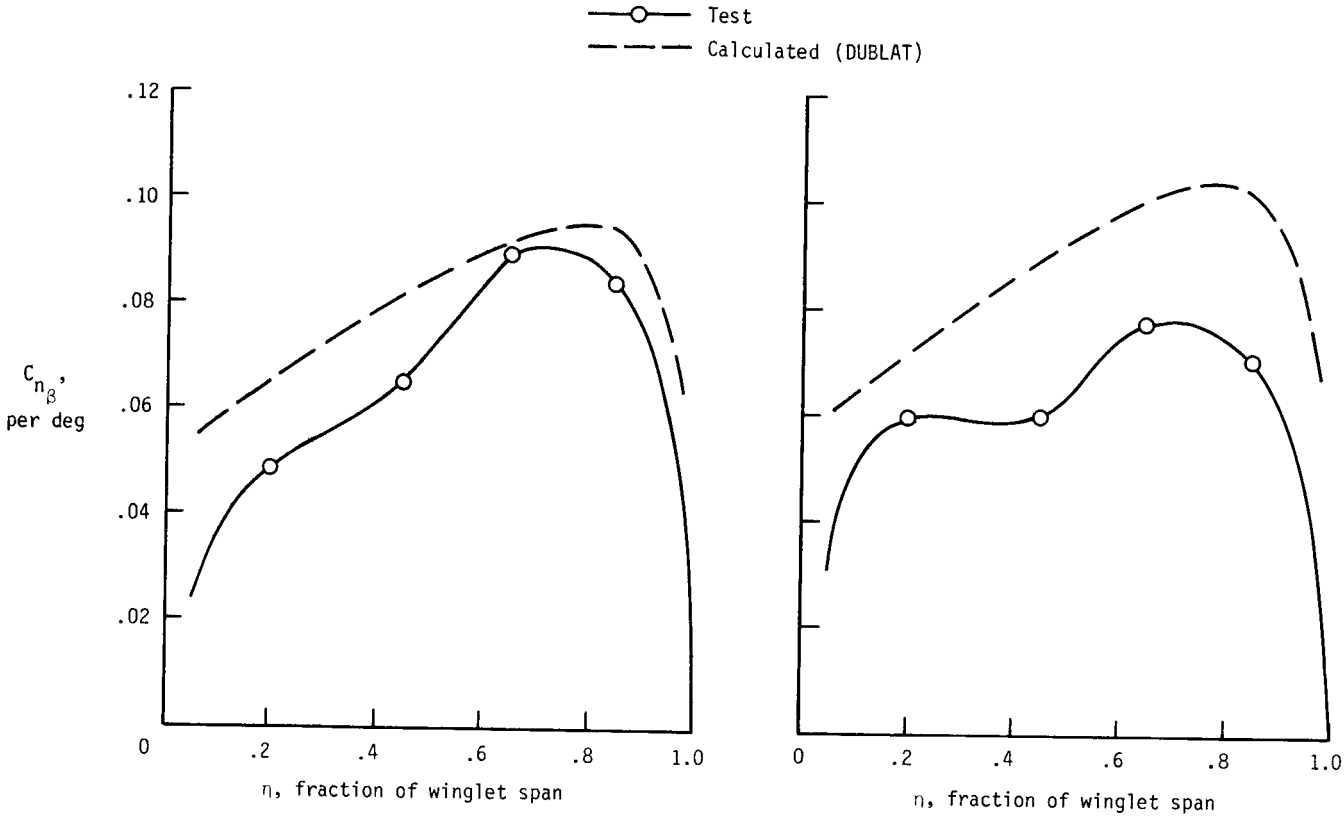

(c) M = 0.80.

(d) M = 0.88.

Figure 19.- Continued.

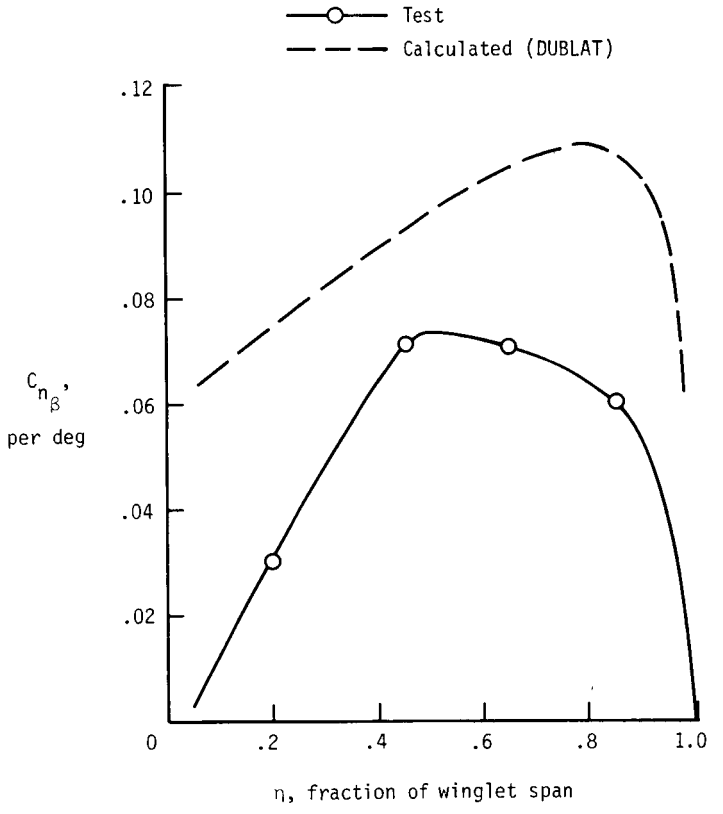

(e) M = 0.91.

Figure 19.- Concluded.

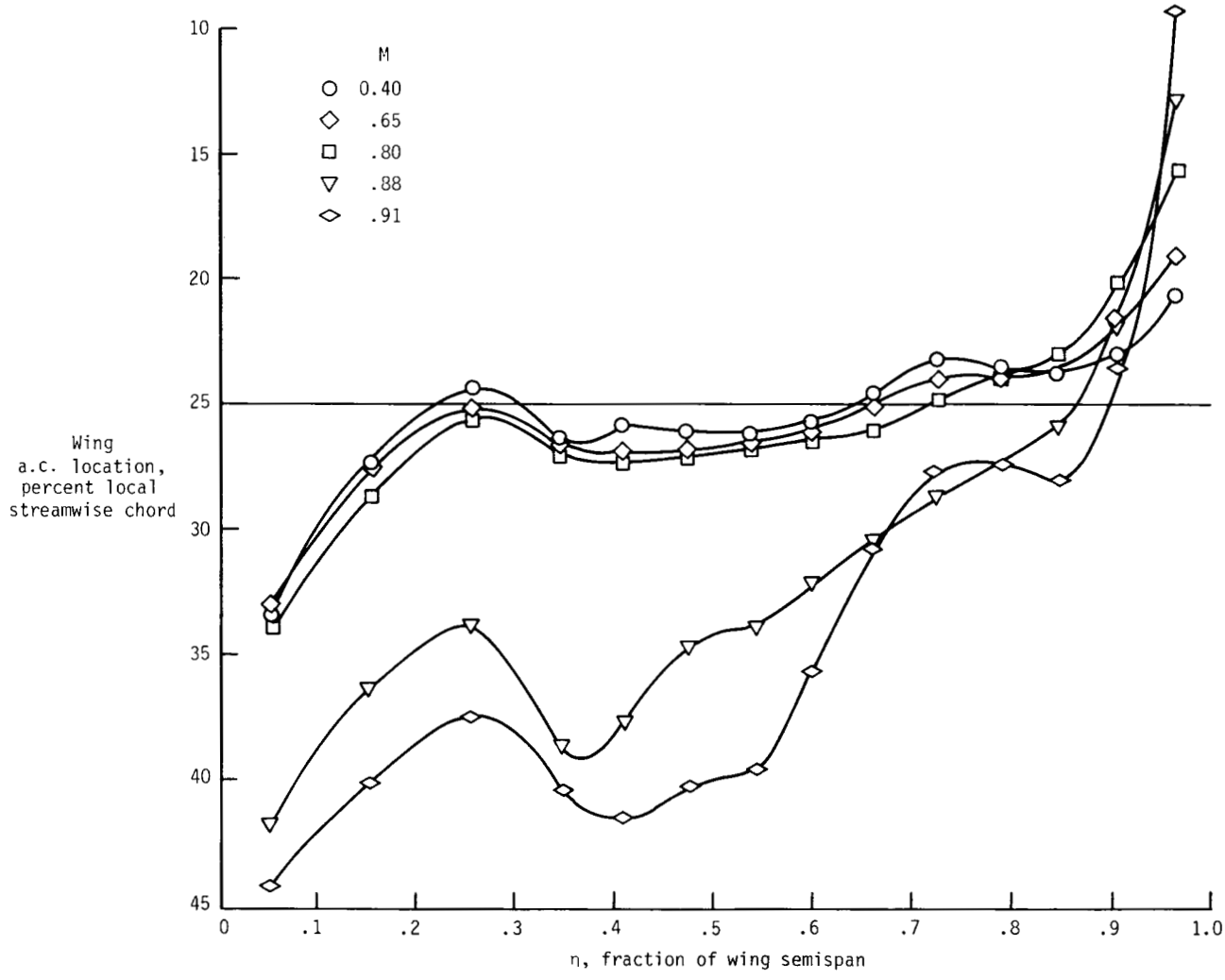

(a) Wing with nominal tip.

Figure 20.- Measured distributions of a.c. location of wing or winglet for wing with nacelle and different wingtips.

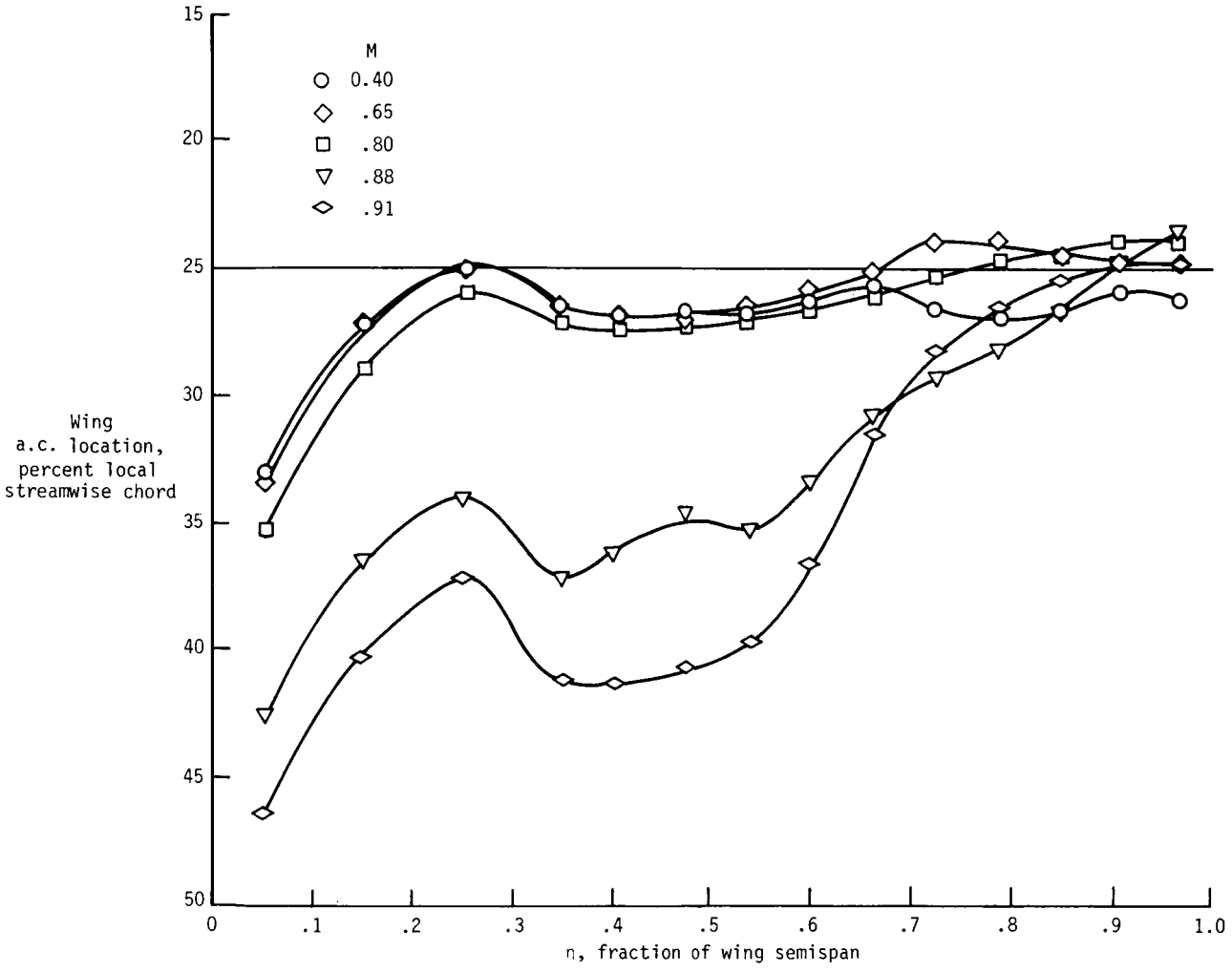

(b) Wing with winglet (20°).

Figure 20.- Continued.

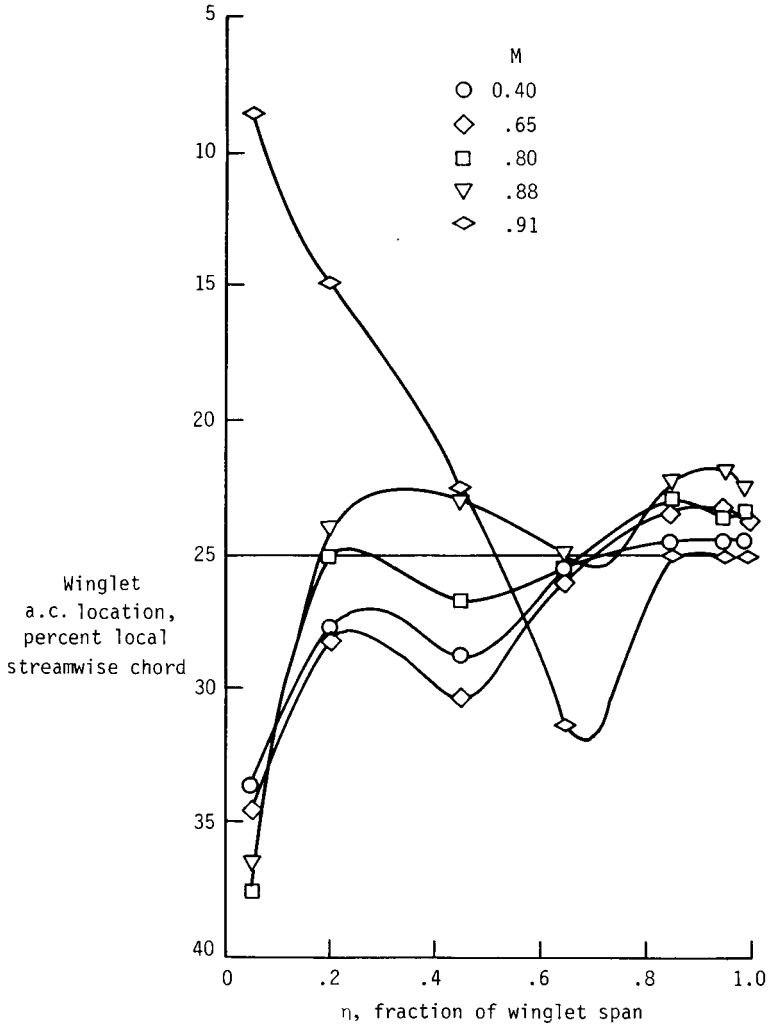

(c) Winglet (20°).

Figure 20.- Concluded.

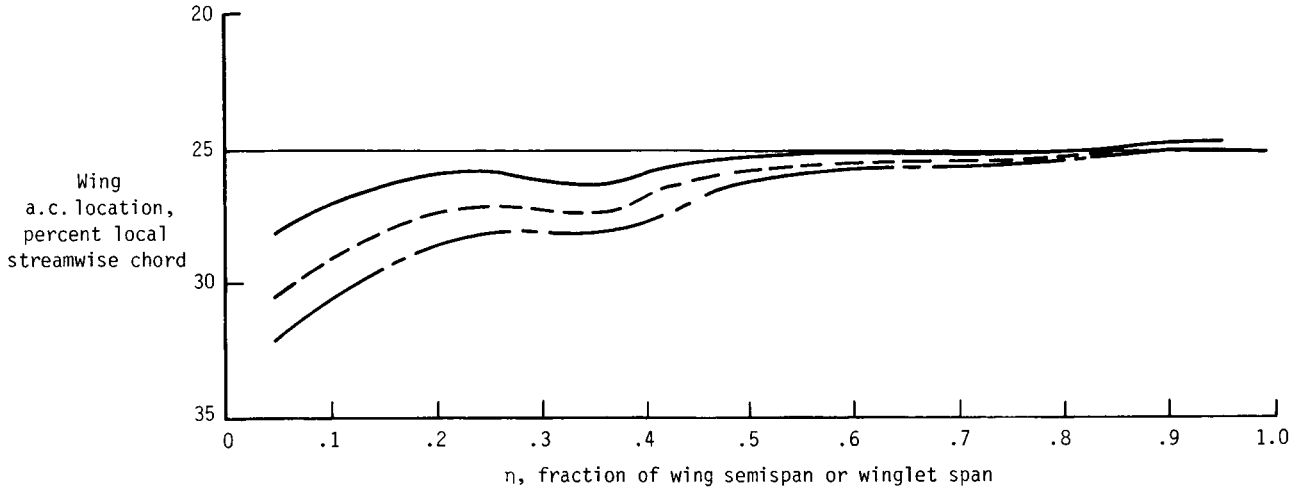

(a) Wing with winglet (20°).

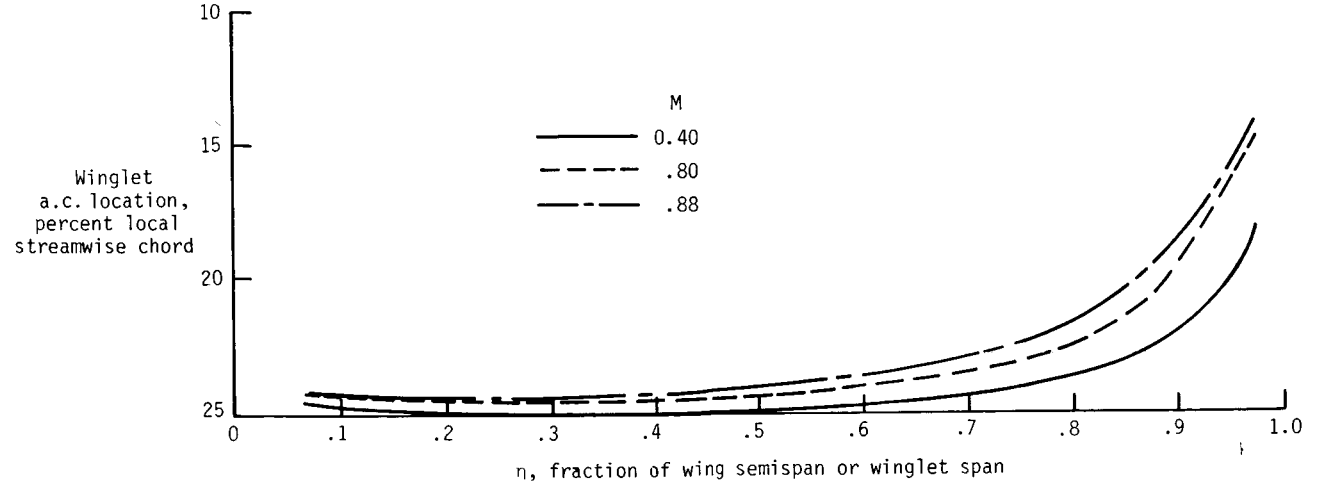

(b) Winglet (20°).

Figure 21.- Calculated (DUBLAT) distributions of a.c. location of wing or winglet for wing with nacelle and winglet (20°).

Standard Bibliographic Page

1. Report No.	2. Government Accession No.	3. Recipient's Catalog No.
NASA TP-2627		

4. Title and Subtitle	5. Report Date
Effects of Winglet on Transonic Flutter Characteristics of a Cantilevered Twin-Engine-Transport Wing Model	December 1986
	6. Performing Organization Code: 505-63-21-02
7. Author(s): Charles L. Ruhlin, Kumar G. Bhatia, and K. S. Nagaraja	8. Performing Organization Report No.: L-16095
9. Performing Organization Name and Address: NASA Langley Research Center, Hampton, VA 23665-5225	10. Work Unit No.
	11. Contract or Grant No.
12. Sponsoring Agency Name and Address: National Aeronautics and Space Administration, Washington, DC 20546-0001	13. Type of Report and Period Covered: Technical Paper
	14. Sponsoring Agency Code

15. Supplementary Notes

Charles L. Ruhlin: Langley Research Center, Hampton, Virginia.
Kumar G. Bhatia and K. S. Nagaraja: Boeing Commercial Airplane Company, Seattle, Washington.

16. Abstract

A transonic model and a low-speed model were flutter tested in the Langley Transonic Dynamics Tunnel at Mach numbers up to 0.90. Transonic flutter boundaries were measured for 10 different model configurations, which included variations in wing fuel, nacelle pylon stiffness, and wingtip configuration. The winglet effects were evaluated by testing the transonic model, having a specific wing fuel and nacelle pylon stiffness, with each of three wingtips, a nominal tip, a winglet, and a nominal tip ballasted to simulate the winglet mass. The addition of the winglet substantially reduced the flutter speed of the wing at transonic Mach numbers. The winglet effect was configuration-dependent and was primarily due to winglet aerodynamics rather than mass. Flutter analyses using modified strip-theory aerodynamics (experimentally weighted) correlated reasonably well with test results. The four transonic flutter mechanisms predicted by analysis were obtained experimentally. The analysis satisfactorily predicted the mass-density-ratio effects on subsonic flutter obtained using the low-speed model. Additional analyses were made to determine the flutter sensitivity to several parameters at transonic speeds.

17. Key Words (Suggested by Authors(s))	18. Distribution Statement
Flutter Winglets Transonic effects Aeroelastic	Unclassified - Unlimited Subject Category 39

19. Security Classif.(of this report)	20. Security Classif.(of this page)	21. No. of Pages	22. Price
Unclassified	Unclassified	76	A05

For sale by the National Technical Information Service, Springfield, Virginia 22161

NASA-Langley, 1986